Aalto University
School of Chemical
Engineering

**Tim Bernard Bellers**

# DEVELOPMENT OF THE EXPERIMENTAL METHOD FOR A NEW ATTACHMENT TIMER APPARATUS AS A DIAGNOSTIC TOOL IN MINERAL FLOTATION STUDIES

Master´s Programme in European Mineral Engineering Course (EMEC)

Master's thesis for the degree of Master of Science in Technology submitted for inspection, Espoo, 23rd of August, 2017.

Supervisor Assist. Prof. Rodrigo Serna

Instructor Nóra Schreithofer, D.Sc.(tech)

**Author** Tim Bernard Bellers

**Title of thesis** Development of the experimental method for a new attachment timer apparatus as a diagnostic tool in mineral flotation studies

**Degree Programme** European Mining, Minerals and Environmental Programme (EMMEP)

**Major** European Minerals Engineering Course (EMEC)

**Thesis supervisor** Assist. Prof. R. Serna

**Thesis advisor(s) / Thesis examiner(s)** N. Schreithofer, D.Sc.(tech)

**Date** 23.08.2017 **Number of pages** 106 **Language** English

## Abstract

This work describes the development and proof of concept testing of the prototype of the new Automated Contact Time Apparatus (ACTA), as a diagnostic tool in mineral flotation studies**.** By bringing bubbles into contact with a particle bed and determining the probability of particle attachment, ACTA allows for the characterisation of flotation systems. The main aims of this work were to further develop the first prototype of the instrument, to create the experimental procedure for performing particle-bubble attachment time studies with the device for different flotation related systems of interest, and to provide proof of concept of the device and the experimental method.

As part of this thesis work, several changes have been made to the original ACTA hardware components, operating software code, and functionality, to achieve a suitable experimental performance. An experimental method was developed concerning the preparation of the samples and their treatment prior to measurements and after their completion. The setup was tested by performing measurements on model systems, consisting of both pure and mixed samples of quartz and chalcopyrite particles. The expected trend of increasing attachment probability with increasing contact time was observed in two experiments with chalcopyrite particles. This indicates that the applied experimental method and the improvements made to the device have been a step in the right direction.

It is expected that the knowledge obtained with this work will serve as a basis upon which the improvement of ACTA can continue towards its eventual use as a practical and reliable measurement tool in mineral flotation-related studies.

**Keywords** Flotation; Induction Time; Bubble-Particle Interaction; Attachment Probability; ACTA

# Preface

This thesis work is the final proof of competence for obtaining my Master of Science degree from Aalto University, Wroclaw University of Science and Technology and University of Miskolc.

I would like to thank my supervisors, Rodrigo Serna, Jan Drzymala, and Ljudmilla Bokányi for their advice and their comments on my work. In addition, I would like to offer my special thanks to Nóra Schreithofer for all the advice she has given me throughout the course of this thesis. I am also very grateful to Markus Aspiala for teaching me how to operate ACTA and for his invaluable help in the process of getting ACTA operational. Furthermore, I want to thank my colleagues at the office and the EMEC programme, my friends, and my family, all of whom have provided support and advice without which I would never have completed this work.

Tim Bellers

Nieuwegein, The Netherlands

23rd of August, 2017

# Table of contents

# 1. Introduction

## 1.1 Background

Recently, an experimental attachment timer setup was developed at the Research Group for Mineral Processing and Recycling of the Department of Chemical and Metallurgical Engineering at Aalto University School of Chemical Engineering (Javor et al., 2016). This device, herein named Automated Contact Time Apparatus (ACTA), is the focus of this thesis and is described in detail in Section 3.1. In flotation studies results are often hard to predict, as flotation is a complex process in which several sub processes play important roles (Nguyen et al., 1998) and many of the parameters are interrelated (Kawatra, 2011). Models and laboratory experiments can help with this, but are far from ideal. Problems often arise when results obtained from laboratory-scale experiments are applied to the systems of an actual flotation plant due to scale-up issues and unforeseen interactions between materials and chemical compounds. As there are many factors influencing flotation, recreating the exact conditions of a flotation system in a laboratory-scale experiment can prove problematic (Bıçak et al., 2012). The best way to predict changes in flotation circuits would therefore be to perform all experiments in actual process liquid. However, if water taken from a flotation circuit has been stored for longer than a few hours, it has in practice become unusable for experimentation (Levay et al., 2001). As the liquid is stored or transported, time passes. Due to temperature changes, microbiological factors and the continuation of kinetic reactions, changes occur in the concentration of dissolved oxygen and chemicals as well as in the pH and Eh levels. As a result, the properties of the liquid are different from that of the initial process water, effectively invalidating any experiments performed in the aged process liquid. Unfortunately, experimenting solely in fresh process liquid is practically impossible, as one would have to be permanently on site. This is difficult for researchers working for example at academic or other research institutes that are located far from mineral processing plants. To be able to use experimental results to predict the response of full-scale flotation systems, a practical and reliable way to perform in-situ experiments with process waters is needed. As will be described in Section 2.2, one promising method for predicting flotation results is measuring the attachment time. Unfortunately the common methods for measuring attachment time, described in Section 2.3, are often neither practical in operation nor are they easily transported to a flotation plant. One of the aims pursued with the new ACTA setup is to address this lack of a reliable and transportable diagnostic tool for use in flotation related studies.

## 1.2 Objective of the work

The main objectives of this thesis are improving the functionality and user friendliness of the first prototype of the ACTA experimental setup, the development of a standard experimental procedure for performing particle-bubble attachment time studies with the device for different flotation related systems of interest, and providing proof of concept of the device and the experimental method.

The aim is to show that the results obtained with ACTA while using the developed experimental procedure will accurately and reproducibly depict well known trends, such as the increase in attachment probability when the contact time between a bubble and hydrophobic particles is increased (Ye et al., 1989). This trend is also expected with increasing ratios of hydrophobic to hydrophilic particles in solid particle mixtures. Obtaining such trends would simultaneously work as

proof of concept of the prototype device as well as validation of the experimental procedure. If this were achieved, a solid basis would be created for future research projects using ACTA as a measurement tool in flotation studies both in the laboratory and on-site.

## 1.3 Scope of the Work

Details regarding the original concept of the device and the design, assembly and installation of the first ACTA prototype as well as the first set of experiments showing the device can separate hydrophobic from hydrophilic particles can be found in the works of Javor et al. (2016) and Aspiala et al. (2017).

The present work will describe the process of further development and initial testing of the first prototype of the ACTA experimental setup. This process required familiarisation with the experimental setup and with the National Instruments™ LabVIEW® coding language by which the device is operated. It included the creation of LabVIEW programs and the optimisation of existing code for general device operation, addition of functionality, and the integration and operation of new components. Also included was the task of improving the operability of the device by the addition and assembly of new hardware components. In addition, this thesis consisted of attempts at obtaining further proof of concept of the applicability of ACTA as a diagnostic tool for detecting the effects of changes in water quality and reagent concentrations on flotation performance by performing measurements on model systems. These experiments would simultaneously serve to test the operating limits of the device. Furthermore, this work will detail the iterative process of developing the ACTA experimental procedure and its experimental validation by testing the reproducibility of the results. The obtained experience and know-how on the device operation and its experimental method were subsequently applied by advising in the development of new parts, updates, and future experimental possibilities and were also summarized in the form of a 'user manual' for use by future researchers.

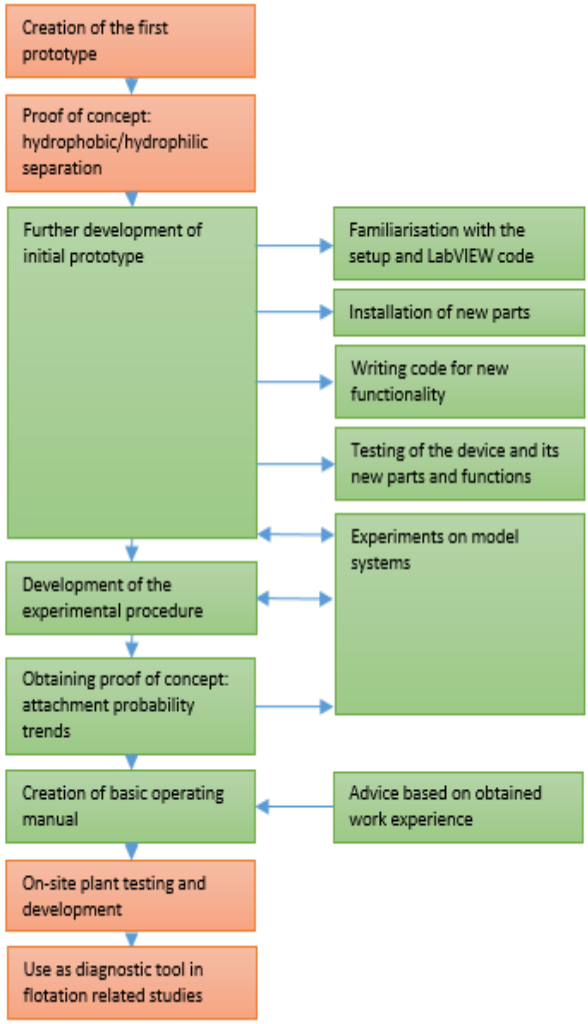


*Figure 1: Left column: Scope of the thesis (green) shown in the grander scope of ACTA development (red). Right column: Summary of the main tasks performed as part of the respective steps in the left column.*

Due to time constraints, further design work as well as tests with more complicated and more realistic model systems to prove functionality beyond the initial proof of concept discussed in Section 1.2 are left for future research. Similarly, using ACTA to perform in-situ tests at real flotation

plants as well as any changes to the experimental procedure that are necessary to make this happen are also outside of the scope of this work. An attempt was made to create an automated particle-detection program with LabVIEW or MathWorks MATLAB® but after several attempts, it became clear that solving this problem required a separate project. Although the initial attempts made will be described in this work, no solutions are included.

Figure 1 summarizes the thesis scope and its position within the larger process of ACTA development.

## 1.4 Structure of the work

Chapter 2 is a literature review of several topics of importance. Section 2.1 details the basic concept and importance of flotation as well as the collision between particles and bubbles. In Section 2.2, the process of particle-bubble attachment and how it has historically been researched is described. Section 2.3 summarizes the main methods currently used for measuring the attachment time while Section 2.4 elaborates on the various parameters that influence attachment time and the flotation of minerals.

Overall, the work done during this thesis can be split into 6 main stages of development and experimentation. In chronological order these are, the preparation work stage, the 1$^{st}$ experimental round, the 2$^{nd}$ experimental round, the maintenance break, the 3$^{rd}$ experimental round and the attempted 4$^{th}$ experimental round. The work done on the various parts of this thesis was iterative in nature. The development of the experimental method was heavily dependent on experience obtained during the first rounds of experiments and their results. The results in turn depended on the method and the capabilities of ACTA during the respective experiments. Due to the continuous changes made to both the procedure and the device itself, several iterations of both the machine and the experimental procedure have existed over the course of this thesis.

For this reason, a chronological format is chosen for Chapters 3 and 4. Chapter 3 describes the part of the thesis that is related to the improvement of the device. Section 3.1 will introduce ACTA, explaining its features and operating principle. Sections 3.2 and 3.3 contain a chronological summary of the most important modifications that were made to ACTA over the course of this thesis, and the issues encountered along the way. In the various subsections, there are descriptions of device components and features that should give a more detailed view of ACTA, expanding on the general information given in Section 3.1. Chapter 4 in turn details the development of the experimental procedure. Most of the changes to the procedure were implemented as a result of problems that were encountered during the trial experiments. These issues and the attempts made to solve them will also be described. Section 4.1 details the preparation of the solid mixtures. Section 4.2 covers the subject of preparing the samples for the ACTA measurements. The chosen measurement settings are detailed in Section 4.3 while the procedure for measuring the mass of the collected solids is covered in Section 4.4.

Although the information has been divided over two chapters, the developments described in there should be viewed as having occurred parallel or interwoven. The reason for splitting this into two chapters is that the combining of this information would lead to an incomprehensibly cluttered narrative. The iterative nature of the work means that although the focuses of Chapters 3 and 4 are on the development of the device and the experimental method respectively, a certain level of result analysis and discussion is necessary to explain the subsequent changes made to the

procedures and the device. As a consequence of this format there is in Chapters 3 and 4 on occasion made mention of trends or findings that are not shown until later chapters. Whenever possible, special mention of this is made for the readers' convenience. An attempt is made however to keep the experimental results to a minimum, only detailing what is relevant to show the reasoning behind the changes that were made.

Concerning the experimental results, there has been a lot of variance in the data that has been obtained. Several interesting trends and findings are only visible from the 'big data' sets that result from combining the results of all the various trials and real experiments. A description of the combined data of various experiments is therefore also necessary but does not fit well within the chronological format of Chapters 3 and 4. Excessive discussions and summarizing of data there would detract from the chapters' respective focuses on the device and experimental method. Most of the information regarding the measurement results is therefore saved for Chapters 5 and 6. Section 5.1 gives a description of how the data is processed while Section 5.2 lists the various possible sources of measurement error. The results of the performed experiments and in-depth discussions regarding their validity can be found in Chapter 6.

Chapter 7 contains the concluding remarks on this thesis while Chapter 8 details suggestions for future work, research, and device updates.

# 2. Literature Review

## 2.1 Froth flotation

Froth flotation is commonly used in the field of minerals processing for the concentration of valuable minerals from ores. It also has applications in treatment of wastewater, de-inking of paper waste, recovery of oil from tar sands and coal processing. In this work, the focus will be on froth flotation as it is used in the minerals processing industry. In froth flotation ore is beneficiated by the selective separation of desired mineral particles from undesired waste materials. This separation is based on the differences in surface properties between various groups of minerals and is generally achieved by selectively hydrophobizing the desired mineral particles by controlling the physico-chemical and hydrodynamic conditions. Bubbles are then created and mixed in a diluted mineral slurry. Hydrophobic particles colliding with the bubbles have a higher chance of attaching to them than hydrophilic ones. The bubbles and any attached particles then rise to the surface, where a froth phase is formed, which contains a higher concentration of hydrophobic particles than the feed. This froth is then skimmed off and the concentrate is directed to further processing. This process is depicted schematically in Figure 2. Flotation is a process that is governed by many factors with a high degree of interrelation, making prediction of result difficult (Kawatra, 2011). Flotation plants often rely on knowledge from the operators who know from experience what works and what does not. Over the years, a lot of research has been performed to gain a better understanding of the flotation process and the factors governing it. One of the most important factors, if not the most important one, is the process of how particles and bubbles attach to one another. This will be described in detail in Section 2.2. Before that however, it is prudent to take a short look at the entire process of particle bubble collection and at the process preceding that of possible attachment, namely the collision of particles and bubbles. These subjects will be discussed in Sections 2.1.1 and 2.1.2 respectively.

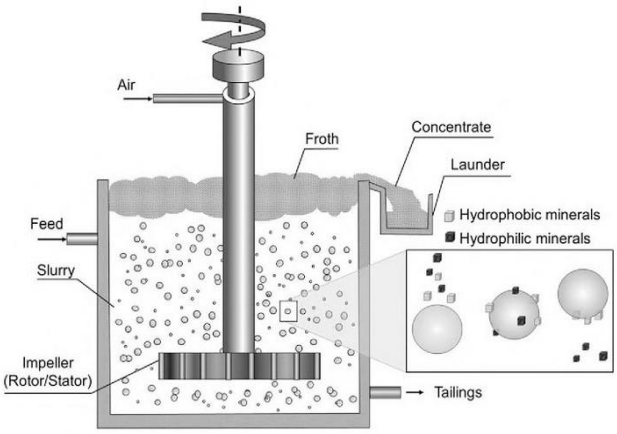


*Figure 2: Schematic depiction of a basic froth flotation process.* (Wills and Finch, 2016)

### 2.1.1 Particle-Bubble collection

In essence the collection of particles with bubbles in flotation depends on three separate processes, namely collision, attachment and detachment (Nguyen and Schulze, 2004). Initially particles have to collide with bubbles in a manner that allows for close enough contact. If particles are in contact with bubbles for a sufficiently long time, the attachment process will occur, which is described in more detail in Section 2.2. The key to particle-bubble collection is that during the attachment process a sufficiently strong connection is formed between particle and bubble that prevents subsequent detachment as a result of the kinetic energy acting on it due to the dynamic conditions in a flotation cell (Ralston et al., 1999b). Each of these steps has their own impact on the probability for a particle to be collected by a bubble during the process of flotation. The efficiency of collection is often defined as in Equation 1 (Newcombe and Ralston, 1994; Ralston et al., 1999b). In Equation 1, $E$ is the collection efficiency of a particle and a bubble, $E_c$ is the efficiency of collision, $E_a$ is the

efficiency of attachment and $E_s$ is the efficiency of stability of the system comprising the bubble and attached particles.

$$E = E_c * E_a * E_s \qquad \text{eq.1}$$

Derjaguin and Dukhin (1960) used this classification of the collection efficiency to create a model for particle-bubble capture consisting of 3 zones, in each of which a different type of force is dominant. This model is shown in Figure 3 and the active forces are from outside to inside, hydrodynamic forces, interfacial forces, and capillary forces governing the stability of the attached bubble and particle. It must be mentioned that in reality neither these zones, nor the three processes are truly so well defined but rather they gradually overlap with one another. However, the forces dominating the three processes are independent of one another. This means that each of the dominant forces (hydrodynamic, surface and capillary) only significantly influences one process. For example, the surface forces are too short-ranged to affect the collision process. This means it is justified to split the entire collision into three parts according to Equation 1 for easier study and modelling. (Nguyen and Schulze, 2004; Ralston et al., 1999b)

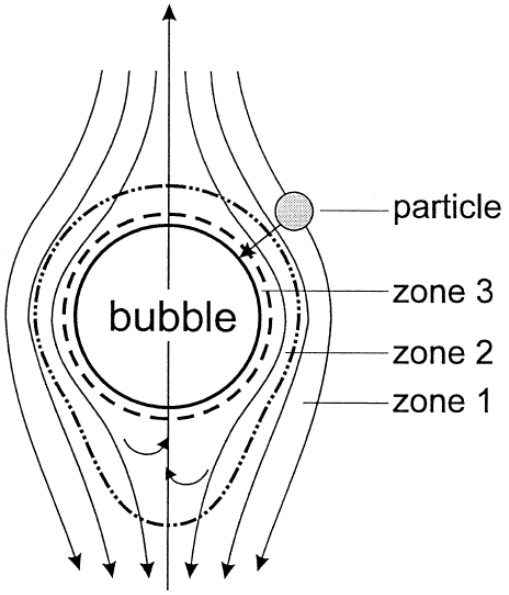


*Figure 3: Zones of interaction between a bubble and a particle as defined by* (Derjaguin and Dukhin, 1960)*. Dominating forces of influence for the various zones are as follows. (1): Hydrodynamic. (2): Interfacial. (3): Caplilary.* (Derjaguin and Dukhin, 1960)

The focus of this thesis lies on the process of particle-bubble attachment, while collision and detachment are for the most part outside the scope of this work. However, it seems only natural to provide some information about the moments just preceding the process of attachment. Furthermore, the concept of contact time is vital in understanding the overall attachment process. As the contact time is dependent on the type of collision interaction occurring between a particle and a bubble a short summary of the collision process will be given in Section 2.1.2.

### 2.1.2 Particle-bubble collision and the contact time

The collision between particles and bubbles during froth flotation is one of the main factors determining whether attachment will take place and has therefore been studied the most of the three processes described in Section 2.1.1. The way a particle and a bubble collide has a profound influence on their time of contact and on the efficiency of collection. As was mentioned above, the contact time is an important concept in the process of particle bubble attachment. Simply stated, the contact time is the time during which a particle and a bubble are in contact, independent of whether particle-bubble attachment actually occurs (Ye and Miller, 1989). In essence it is the time available for particle-bubble attachment to occur, which means it is the time during which the particle and bubble are sufficiently close together to allow attachment to occur before they move apart again (Ye et al., 1989). In the zoned model by Derjaguin and Dukhin (1960) shown in Figure 3,

the contact time would be the time a particle spent in the space between the bubble surface and the outer edge of zone 1 (Ye and Miller, 1989).

Commonly a collision between a bubble and a particle is categorised as either an 'impact interaction' or a 'sliding interaction' (Albijanic et al., 2010; Nguyen and Schulze, 2004; Schulze, 1992; Schulze et al., 1989), both of which are shown schematically in Figure 4. The contact times for these types of impact are named respectively the 'collision contact time' and the 'sliding contact time' (Albijanic et al., 2010; Nguyen and Schulze, 2004). In an impact interaction a particle comes into contact with the bubble surface with high momentum and at a near perpendicular angle, resulting in strong deformation of the bubble surface and short contact times. In the case of sliding interaction the particle essentially slides along the bubble surface, causing no significant bubble surface deformation generally resulting in longer contact time. Both are extreme cases, with true interactions most likely being somewhere in between. Schulze (1992) and Schulze et al. (1989) have found sliding interactions to be significantly more effective for the overall collection efficiency. It can also be expected that in a real flotation system the sliding interactions are more common as a result of the system hydrodynamics and the bubble and particle geometries (Verrelli and Albijanic, 2015). For both types of interaction, multiple models exist, each attempting to describe the exact interactions but for the sake of brevity these won't be described. A comprehensive summary can be found in the work of Nguyen and Schulze (2004).

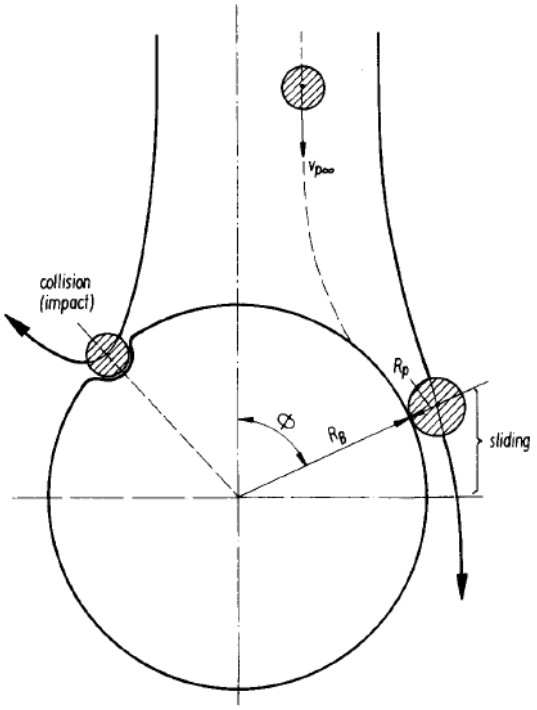


*Figure 4: Schematic overview of the two extreme cases of bubble-particle collision. Left: Impact interaction. Right: Sliding interaction.* (Schulze et al., 1989)

The collision contact time is generally much shorter than the sliding contact time due to the fact that the particle bounces away from the bubble again as a result of the strong deformation of the surface (Ralston et al., 1999a). This often leads to repetitive collisions between the particle and the bubble until the interaction becomes a sliding interaction (Albijanic et al., 2010). As the sliding interaction is longer, likely to be more common, and found to be more effective for the overall efficiency of collection it is usually the sliding contact time that is used as the contact time in the modelling of attachment efficiency.

## 2.2 Particle-bubble attachment

As mentioned earlier, there are many vital processes in froth flotation. The most important one is the attachment of particles to bubbles. This process results in the separation of hydrophobic particles from hydrophilic ones. By changing the surface properties of minerals and bubbles, the selective separation of materials can be achieved. The attachment of particles and bubbles is a process in which many complex phenomena play a role, not all of which are well understood (Nguyen et al., 1997, 1998). The explanation that is currently most accepted is that the process of

particle-bubble attachment consists of three subsequent steps, which are described by various authors such as Nguyen et al. (1997), Gu et al. (2003) and Albijanic et al. (2010). This three-step process is detailed in the following section.

### 2.2.1 Overview of the process

When a particle and a bubble are close enough, a so-called wetting thin film is formed. This film consists of a thin layer of liquid between the gas-liquid and liquid-solid interfaces of the bubble and the particle, respectively. As stated in Section 2.1, bubble and mineral surface properties are the driving force behind the attachment occurring in froth flotation. This is so because the stability of the wetting thin film in this situation depends upon the surface forces between the bubble and the particle. If the sum of surface forces is repelling, no attachment will take place. In case of an attractive sum of surface forces, water will drain from the thin film as the distance between the particle and the bubble gets smaller until it reaches a so-called critical thickness. At this point, the film will rupture and a nucleic hole with a critical radius is formed. The formation of this nucleic hole results in a three-phase contact line (TPCL) where previously there were only two-phase contacts (liquid-gas and liquid-solid). The gas-solid contact area will then increase as the TPCL expands until it reaches the minimum radius needed for the wetting perimeter to be stable. At this point, the particle is stably attached to the bubble. The process of bubble-particle attachment is illustrated in Figure 5.

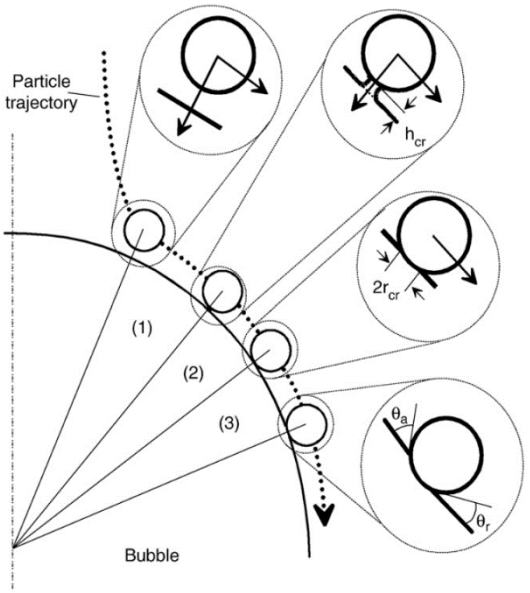


*Figure 5: The three steps that are currently understood to make up the process of particle-bubble attachment. 1: Thinning of the liquid film. 2: Film rupture and formation of the nucleic hole. 3: TPCL expansion and formation of a stable wetting perimeter.* (Albijanic et al., 2010)*, adapted from* (Nguyen et al., 1998).

The time it takes for the wetting thin film to drain to the critical thickness is called the induction time ($t_i$). Together with the time it takes for the thin film to rupture and form the TPCL nucleus ($t_r$) and the time during which the nucleus expands until a stable wetting perimeter has been formed ($t_{TPCL}$) these steps describe the total time it takes for this entire process of wetting thin film draining, rupture, TPCL formation and the TPCL expansion to occur. Therefore the sum of these three times is defined as the attachment time ($t_{att}$) as is shown in Equation 2.

$$t_{att} = t_i + t_r + t_{TPCL} \qquad \text{eq.2}$$

All three of these steps need to take place for the particle to be attached to the bubble and therefore attachment will not occur if the contact time is lower than $t_{att}$ (Albijanic et al., 2010; Evans, 1954; Verrelli et al., 2011).

Stechemesser and Nguyen (1999) report $t_i$ and $t_{TPCL}$ to be of the same order of magnitude (around 20 ms) and therefore equally important to the particle bubble attachment. However, Wang et al. (2005) and Rao and Leja (2004) report $t_i$ is the controlling step, whereas other authors such as Krasowska and Malysa (2007a) and Radoev et al. (1990) claim $t_{TPCL}$ is the dominant factor in determining the process kinetics. In light of these various points of view it is very well possible that the relative importance of the steps varies from situation to situation. This too might be contributing to the general lack of knowledge and conflicting information on the subject. In any case, the time for the rupture of the liquid thin film to take place ($t_r$) is generally around 1 ms and therefore much shorter than the time scales for $t_i$ or $t_{TPCL}$ and is therefore often ignored in explanations of the process and attempts to model it (Albijanic et al., 2010).

It is important to note here the difference between the concepts of attachment time and induction time. In current terminology, the attachment time is a larger concept encompassing the induction time. However, in many publications the term induction time is used in cases where the phenomenon being described is the attachment time (Dai et al., 1999; Gu et al., 2003; Ralston et al., 1999b). This practice is rooted deep in scientific literature and extends to the naming of equipment used for measuring attachment time. It is not always clearly stated which definition of the term is being used. This can cause difficulties for the reader, as it is often hard to determine whether or not the authors refer solely to the film draining time $t_i$ or if they include $t_i$ or $t_{TPCL}$ in their particular definition. In such cases, context and the publications that are being referred to must be used to get a correct interpretation. Some authors go so far as to state the film thinning time is being 'mistaken' as induction time (Rubinstein, 1995).

As far as it was possible to determine based on the conflicting information, it seems the cause of this interchangeable use of terms lies in the fact that when the term *Induktionszeit* was coined by Sven-Nilsson (1934), it was in reference to the minimum contact time necessary for attachment to occur between a particle and a bubble ($t_{att}$). At that time, this was assumed to be the time required for thinning of the liquid film to a critical thickness at which it will rupture spontaneously ($t_i$). When later the TPCL expansion and film rupture were recognized to be of importance, induction time ended up being used as a term to refer to both the time necessary for the entire attachment process as well as the time of the individual step of film thinning, which until that point had been synonymous. Since then both definitions have been in use and only recently have authors started indicating more clearly which definitions they are using in their publications, suggesting that in the near future, an end might come to this confusing practice.

This explanation for the issue stems from the fact that between various authors there is no consensus on the original definition of induction time by Sven-Nilsson (1934). The experiments performed by Sven-Nilsson factually measured the time of particle-bubble attachment including, although it was perhaps unknown at the time, $t_R$ and $t_{TPCL}$. In accordance with this, Nguyen Van (1993), Verrelli and Albijanic (2015) and various other authors state that Sven-Nilsson's induction time was defined as the minimum contact time required for attachment. Nguyen et al. (1998) and Gu et al. (2003) however, state Sven-Nilsson referred to the time needed for film thinning, which is more in line with the currently used definition of the term. This heavily contributes to the difficulties surrounding the subject and is perhaps caused by the fact that the original paper was written in German. As a result, it is likely that many authors are simply relaying the definition as they have found it in other papers.

To make matters worse the rupture time has only in 1997 been proposed as a separate step and is much shorter than the other two steps as has been stated above. It is therefore often, especially in older publications, not recognized as a separate step or is omitted completely from summaries of the process and attempts at modelling it. Due to the habit of rather arbitrarily grouping $t_r$ with $t_i$ and $t_{TPCL}$ or omitting it altogether, some publications mention only two distinct time intervals when discussing attachment time. Others do mention three but have included particle approach as the third time scale rather than rupture time (Rao and Leja, 2004).

Adding to the general confusion, various authors use different names when referring to the three fundamental steps. In this work the names will be used as described by Albijanic et al. (2010), which have been stated in the above explanatory section and equation 1. An exception is made for the methods and devices described in Section 2.2. Even though many of them measure attachment time, they are still commonly known as induction time apparatus and will therefore be referred to as such.

### 2.2.2 Attachment time research history

The interest in particle-bubble attachment time goes back decades and is well justified. Much is still unknown about the factors governing froth flotation. The results of changes made to a process can be entirely unexpected. Prediction of the results of flotation processes is hard and sometimes lacks scientific basis. With increasing demands on the efficiency and profitability in the process industry rises the need for actual understanding of the process and the factors governing it. The three sub-processes making up the attachment time are dependent on the many different surface properties of both particle and bubble, usually influenced by the physicochemical properties of the flotation system. The two sub-processes that are commonly considered most important are $t_i$ and $t_{TPCL}$ and it is currently not known which of the two is dominant in determining the attachment time. Both processes are much studied in their own right, but it is in a real flotation experiment near impossible to determine such parameters as film thickness, induction time and TPCL expansion. In comparison, the combination of the three fundamental steps is relatively easily measured and has been done so for decades (Sven-Nilsson, 1934). It is therefore in practice the attachment time that researchers turned to in their attempts to gain more insights into the factors governing the flotation process and to accurately predict its results.

Before the term induction time was first used, the thinning of the liquid film had already been recognized as a potential way of researching the froth flotation mechanism by Frumkin (1933). Frumkin also predicted that the liquid film between bubble and particle could rupture due to it potentially being thermodynamically unstable (Hubbard, 2002). The process of liquid film thinning was further investigated by Derjaguin and Kusakov (1937) whose experimental results proved the presence of various surface forces operating on the liquid film. At that time, those surface forces were undefined and all together called the disjoining pressure. This disjoining pressure is currently understood to comprise a multitude of phenomena and can be either negative or positive. In case of a negative disjoining pressure, such as is present on hydrophobic surfaces, the thin liquid film between particle and bubble becomes unstable and starts thinning quickly before rupturing. Among the phenomena making up the disjoining pressure and thus influencing the film thinning process and consequently flotation itself are structural forces such as attraction by hydrophobic interaction or oppositely, repulsion by hydrophilic interaction, electrostatic forces such as double-layer forces and electrodynamic interactions such as molecular and Van der Waals forces (Nguyen et al., 1997).

It is however Sven-Nilsson (1934) who is generally credited as being the first to recognize the important role of attachment time in controlling the flotation kinetics. He postulated that a minimum time of contact between bubble and particle was necessary for attachment to occur, the *Induktionszeit*. Aside from first using the term induction time, his experiments in which a captive bubble was pressed against a polished mineral surface showed the influence of various concentrations of chemicals such as potassium xanthate on the attachment time. Various other methods of measuring attachment time were devised in the years after the initial experiments by Sven-Nilsson, the details of which will be described in Section 2.3.

It took until the study of Eigeles and Volova (1960) for the real value of attachment time to become apparent and more widely accepted. Their systematic study revealed a number of interesting facts that clearly demonstrated the potential of the attachment time concept in predicting flotation results, which sparked interest in the phenomenon. In their work, they first demonstrated that measurements of the attachment time of mineral particles could indicate their level of hydrophobicity both in cases with and without addition of surfactants. The attachment time of particles was found to decrease with increasing concentration of collector, independent of mineral type. Induction time was also found to increase linearly when the size of the mineral particles increased and was found to exponentially decrease when temperature increased. From the latter, an estimation can be made of the activation energy necessary for bubble-particle attachment. Some of their results will be mentioned in more detail in Section 2.4.

Presently, several methods are available for measuring attachment time. Measurements of attachment time has been shown to be sufficiently sensitive for the detection of variations in the physical properties and chemical surface characteristics of pure mineral particles (Albijanic et al., 2010). Experiments with both pure minerals and real ore particles have led to numerous discoveries of mechanisms and factors influencing induction time and subsequently flotation itself, some of which will be explained in more detail in Section 2.4 (Albijanic et al., 2015, 2011). Thanks to recent research, it is now clear that there is a direct correlation between the results of attachment time experiments and flotation results. Lower attachment times result in higher flotation recovery (Albijanic et al., 2015, 2011; Jowett, 1980; Ye et al., 1989; Yoon and Yordan, 1991). With this knowledge, attachment time measurements can be used to clarify changes in flotation processes and when combined with knowledge about the flotation system and the material being floated it is possible to quantify flotation results. However, as deeper understanding of the attachment process is often still lacking, much of the research into attachment time and the models based on it thus far remains based on experimental data on attachment probability in combination with models on collision and stability of bubble-particle systems (Hewitt et al., 1995; Yoon and Mao, 1996).

### 2.2.3 Modelling of attachment time

With its fundamental role in the kinetics of the flotation process and its potential for flotation result prediction, it is unsurprising that many scientists have attempted to obtain a better understanding of the attachment time by devising various ways of modelling it. From these attachment time models scientists hope to gain more insight into the workings of froth flotation itself and the processes governing flotation. Another goal is to model the attachment time based on first principles and fundamental particle characteristics so theoretical models instead of empirical ones can be used to predict flotation results. Much like modelling flotation itself, modelling attachment time, has proven hard due to the many unknown aspects and the effect of factors that are hard to

measure (Albijanic et al., 2010; Hewitt et al., 1995; Li et al., 1987). The amount of models on attachment time is steadily increasing, but still insignificant when compared to the many models on particle-bubble collision (Dai et al., 1999; Nguyen et al., 1998).

Sutherland (1948) first showed it was possible to predict the probability of particle-bubble attachment based on a comparison of the contact time with $t_{att}$. His model proved that the attachment of bubbles and particles could be calculated and quantified with $t_{att}$ as a variable. To obtain these results, a drastic simplification of the complex bubble-particle attachment was needed and the model was therefore not always a good approximation of real flotation. Nevertheless, since then his model has been the basis of many later works that have attempted to improve it and make the models more applicable to a true flotation situation (Dobby and Finch, 1987, 1986; Finch and Dobby, 1990; Nguyen Van, 1993; Schulze, 1992; Yoon, 1991; Yoon and Luttrell, 1989).

Almost four decades after the paper by Sven-Nilsson, Scheludko et al. (1970) first investigated the importance of the TPCL expansion in the overall kinetics of the attachment process. Around 20 years later, the importance of TPCL expansion in the attachment process was well recognized. By then it was commonly accepted that the probability of particle attachment to a bubble depends on the probabilities of both film thinning and TPCL expansion (Crawford and Ralston, 1988; Hewitt et al., 1995; Schulze, 1992)

The potential importance of film rupture and nucleic hole formation was first mentioned by Scheludko et al. (1976). They stated that a possible energy barrier resulting from line tension might have to be overcome in the initial formation of a de-wetted area. This would particularly affect the flotation of fine particles. In the currently accepted three-step model that was proposed by Nguyen et al. (1997, 1998), the rupturing of the liquid film was eventually recognized as a separate step in the process between the film thinning and TPCL expansion. The proposition of this new approach was prompted by a comparison of new experimental results with the Sutherland modelling approach by Hewitt et al. (1995) and subsequently by Nguyen et al. (1997). They found that the models of that time failed to adequately describe the true situation for small particle sizes and it was noted that the models only took into account film thinning. They too stated that the rupturing of the liquid film may play a critical role in the flotation of fines and suggested a new model for calculating the particle-bubble attachment probability by multiplying the probabilities for the three sub processes. Up until that point, most models had oversimplified the situation by assuming the probability of attachment to be equal to the probability of the film thinning to its critical thickness, thereby not taking into account the influence of film rupture or TPCL expansion. It was shown that this approach usually resulted in over-estimation of attachment probabilities and reasoned that all three steps have to be considered to reach a proper description of the particle-bubble attachment process and to obtain qualitative prediction results.

### 2.2.4 Benefits over contact angle

A method that is often used for indicating particle hydrophobicity is the contact angle measurement. The theory of contact angles was first described in the early work of Young (1805). In contact angle measurements, a bubble is attached to a solid surface. The angle between the liquid-vapour interface and the solid-liquid interface is then measured through the liquid phase. Figure 6 depicts this schematically. The more hydrophobic the surface is the bigger will be the angle between the air-water and solid-water interfaces. Contact angle measurements have often been used in attempts to predict flotation performance. A benefit of contact angle measurements is that

the basic measurement is relatively easy to perform and can in principle be done without the purchase of specialized equipment. When compared to attachment time measurements however, it is not hard to understand why the latter is found to better indicate flotation behaviour (Nguyen et al., 1998). The contact angle is dependent on the surface chemistry of the system and will provide information on the particles' hydrophobic state but it is a purely thermodynamic measurement of an equilibrium situation (Albijanic et al., 2010; Yoon and Yordan, 1991). Froth flotation however is a kinetic process that depends on more than just the surface forces of particles and bubbles. A vital role is played by the kinetics (Ye et al., 1989) and the hydrodynamics of the system (Schulze, 1984). In attachment time measurements, the particle and bubble are brought closer together at a desired velocity and therefore the kinetic factor is taken into account in addition to the system's surface chemistry. Attachment time is thus a more appropriate indicator of real flotation behaviour than the equilibrium situation of the contact angle measurement (Eigeles and Volova, 1960; Wang et al., 2005; Ye et al., 1989). The attachment time measurement is also a much more sensitive indicator in general. Whereas the contact angle can vary between 0° and 180°, the attachment time can change over a range of several orders of magnitude, giving a much more nuanced indication of the effect of various changing parameters (Yoon and Yordan, 1991).

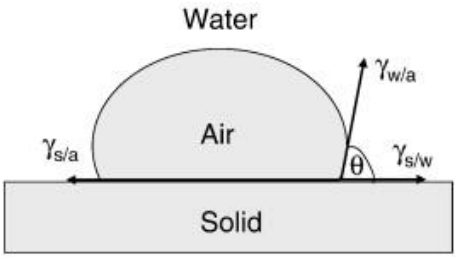


*Figure 6: Schematic representation of the contact angle between an air bubble and a solid surface. The angle between the air-water interface and the solid-water interface measured through the water phase, ϑ is named the contact angle* (Young, 1805). *Figure obtained from* (Chau et al., 2009).

Another factor to consider is that a polished mineral surface is often required for the bubble-mineral contact angle to be measured easily. This causes several problems. First of all, there might not always be a sufficient quantity of mineral available to create such a polished surface large enough for bubble attachment. Secondly, it has been proven that surface forces on polished mineral surfaces are vastly different than those present on actual mineral particles, indicated by the measured attachment times on polished surfaces being larger by a factor of at least 50 times when compared to those measured at a bed of particles (Ye et al., 1989). As will be described in Section 2.4.2 factors such as particle roughness (Krasowska and Malysa, 2007a, 2007b; Verrelli et al., 2014; Ye et al., 1989), shape (Dippenaar, 1982; Verrelli et al., 2014) and size (Eigeles and Volova, 1960) play a huge role in the probability of attachment. As the measurement of attachment time more easily allows the use of a bed of particle or even single mineral particles it is clearly a better, if still not an exact, approximation of the real flotation process than the measurement of contact angle on a polished surface. Various authors have proven that contact angle, although it is certainly a useful indicator, does not sufficiently represent the flotation performance. Flotation of mineral particles was found to occur even though the measured contact angles were close to zero, seemingly indicating hydrophilicity of the particles (Finch and Smith, 1972; Iwasaki et al., 1960; Lai and Smith, 1966; Smith, 1963). Additionally, in several experiments the contact angle measurements failed to accurately represent flotation of particles whereas the flotation behaviour was correctly represented by the attachment time measurements. This was shown for bitumen (Su et al., 2006) and coal particles (Ozdemir et al., 2009; Ye et al., 1989). Ye et al. (1989) used data from several other authors such as Laskowski and Miller (1984) and Miller et al. (1984, 1983) to demonstrate these apparent discrepancies between contact angle measurements and flotation efficiency.

## 2.3 Induction time measurement devices

There are many advantages to combining the complexities of froth flotation in one parameter, which can be used to indicate whether attachment will take place by a simple comparison with a flotation system's contact time. Consequently, it is no wonder that over the years various methods and devices have been developed to measure the attachment time. Using these devices, results have been obtained that provided experimental proof of the importance and potential of attachment time as an indicator in flotation result prediction. Additionally, these results gave rise to new theories and explanations for the various phenomena occurring during the process of particle-bubble attachment and consequently have led to a better understanding of froth flotation itself. Several methods for measuring the attachment time are currently in use, each with their own benefits and drawbacks. As has been stated in Section 2.2.1, the difficulties surrounding the naming of the particle-bubble attachment process extend to the naming of the measurement equipment. Many of the devices mentioned below are generally described as apparatus for measuring induction time. Keep in mind that the phenomenon being measured with them is in fact the attachment time, unless it has been specifically mentioned otherwise. However, the way the attachment time is measured and how exactly it has been defined vary between different methods. Attachment times measured with one method are not necessarily comparable to those measured with another. When reading literature it is important to have an understanding of these differences to know what is being presented by the respective authors. To that end the most commonly used methods will be described below.

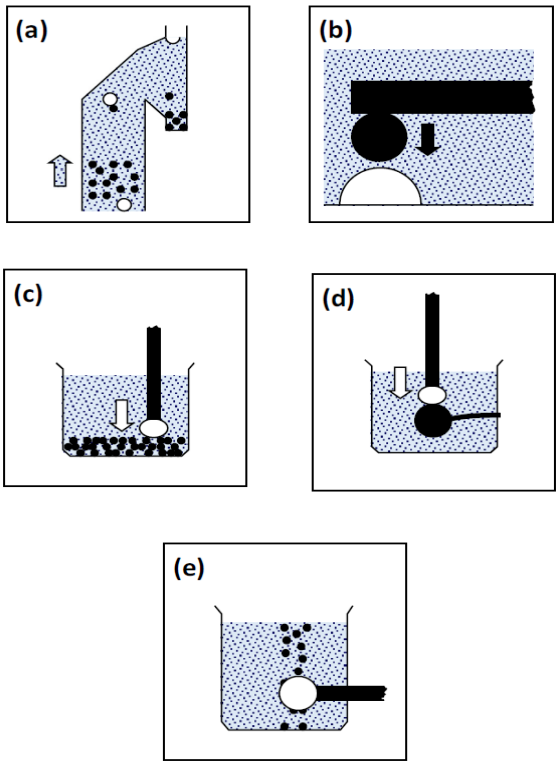


*Figure 7: Schematic representation of the five common attachment time measurement methods. a: Back calculation from Microflotation. b: Atomic Force Microscope. c: Induction Timer. d. Integrated Thin Film Drainage Apparatus (ITFDA). e: Milli-timer. White areas indicates the gas phase, while black indicates the solid phase and grey shaded parts indicate the liquid phase. The coloured arrows indicate motion of their respective phases.* (Verrelli and Albijanic, 2015)

The ideal attachment time measurement as described by Verrelli and Albijanic (2015) has three distinctive qualities. Firstly, the method would directly and unambiguously measure the attachment time. Secondly, the measurement would be easy to perform, fast, consistent and not need the use of expensive equipment. Thirdly, the measurement conditions would reproduce the most important sub-processes occurring in a true flotation experiment, resulting in data that can be directly interpreted and used for flotation processes in industry.

Although this ideal measurement is as of yet still non-existent there are five commonly used techniques for measuring the attachment time. The respective methods are: calculation of the attachment time based on Microflotation, Atomic Force Microscopy, the Induction Timer, the Integrated Thin Film Drainage Apparatus (ITFDA), and the Milli-Timer. A schematic representation

of the basic idea behind each of the techniques can be seen in Figure 7, but variations to the different devices depicted there are also possible.

### 2.3.1 Microflotation - Back calculation

In this method a microflotation experiment is performed. Afterwards the approximate contact time is calculated from the obtained results. In a microflotation experiment, a device resembling a Hallimond tube is used, in which an upwards fluid flow is created at such a velocity that a dilute bed of fluidized particles can be formed in the tube. Bubbles are then created at the bottom of the tube at such a rate that they pass one by one through the bed. At the top of the device, the bubbles reach the water level and once they burst, the collected solids settle in a separate compartment. From the amount of collected material the collection efficiency is calculated, which can then be used to calculate the approximate attachment time. For this calculation, a collision frequency model is necessary that describes how the two factors are related. The Generalised Sutherland Equation (GSE) developed by Dai et al. (1998) is often mentioned in this regard but several other options are also available (Ives, 2001; Jiang et al., 2010). As was described in Section 2.2.3, these models are often severely simplified. Certain factors might be left out, to be able to get a grip on the extremely complex attachment process. This means that any values calculated with this method will by definition be mere approximations of the true attachment time, although some of the models have in fact been experimentally validated, predicting collection efficiencies that correlate well with true experimental results (Dai et al., 1998). A benefit of back calculating from microflotation is that the bubble-particle motions and their way of coming into contact are natural, albeit occurring at a lower velocity than in actual froth flotation. Other benefits include the use of bubble and particle sizes that resemble those used in industry, low equipment cost and relatively short experiment times. However, different models will result in different calculated attachment times and it is important, for the estimation to be as correct as possible, that a model is chosen that applies to the used conditions such as particle size, concentration and fluid flow dynamics. Although an attachment time calculation can be made with this method, it is not ideal for this purpose due to the use of inherently simplified models. Other, more direct methods are better suited for this purpose. Microflotation in turn is best suited for determining the efficiency of attachment under certain conditions. These efficiencies can then be used to make comparisons and determine which conditions will yield optimal results. (Verrelli and Albijanic, 2015)

### 2.3.2 Atomic Force Microscope (AFM)

In this method, an Atomic Force Microscope (AFM) is used to bring a bubble and a solid material into close contact. This can be achieved either by moving a bubble closer to a solid particle (Butt, 1994; Ducker et al., 1994; Krasowska et al., 2011; Nguyen et al., 2003; Ozdemir et al., 2009) or oppositely, moving a solid surface against a bubble (Manor et al., 2008). The forces acting between the two surfaces are measured from the deflection of the sensitive cantilever (Wang et al., 2013). Note that while Figure 7b depicts the cantilever as the moving component, in some AFM devices a piezo stage on the bottom moves upward while the cantilever remains in place. Due to the bubble being able to deform, the measured forces cannot simply be plotted against the distance between the particle and the bubble although in very simple cases the distance as a function of time can be estimated from models (Verrelli and Albijanic, 2015; Wang et al., 2013). The attachment time is defined as the time between the point when hydrodynamic forces between the bubble and the solid are becoming visible, until the point of particle-bubble attachment. This point of attachment can be inferred from a jump in the measured forces occurring when the liquid layer breaks and the

bubble envelops the particle, forming solid-gas contact, and is quite well defined (Snyder et al., 1997). The exact starting point has to be chosen by the user, which leaves some room for ambiguity. It is possible that, like with the ITFDA described in Section 2.3.4, both the attachment time and induction time can be measured with this method but none of the reviewed papers make specific mention of this.

The speed of film drainage depends linearly on the applied pressure and therefore the attachment time measured with this method will depend on the approach velocity (Snyder et al., 1997). This velocity can be set by the user and will therefore have to be kept constant between various measurements if comparisons between results are to be made. The AFM is a device that works on a micrometre or even nanometre scale, with very small forces in the range of micro-, nano- or even picoNewton being measured (Ducker et al., 1994). The movement range of an AFM is generally below 20 µm so particle and bubble sizes are chosen at comparatively small scales. The maximum velocity with which the bubble is moved can be up to several micrometres per second and the device is set up in such a way that the motion is constricted to a head-on collision between bubble and particle. Clearly, none of these factors approximate an industrial flotation situation and therefore the results obtained with this method are not directly usable in industry. Another issue is that AFMs are extremely expensive devices that require trained operators, which limits the accessibility of the method. All in all this method is better suited for fundamental scientific research into the close-range forces governing the attachment process than it is for predicting industrial flotation results by way of measured attachment times. (Verrelli and Albijanic, 2015)

### 2.3.3 Induction Timer or Glembotsky device

In his pioneering publication, Sven-Nilsson (1934) first measured the attachment time by bringing a bubble into contact with a flat mineral surface and then removing it with a repeatedly oscillating movement. The time of contact between the surface and the bubble was known and could be varied. In each experiment, a contact time was set and the motion was repeated until the bubble first attached to the surface. The amount of contacts necessary for attachment to first occur (*n*), was then plotted in the form of 1/*n* against the respective contact time. This process was repeated for various other contact times. The attachment time was defined as the contact time where 1/n is 0.5, or *n* is 2. An example of the attachment time determination by Sven-Nilsson is shown in Figure 8 (top)

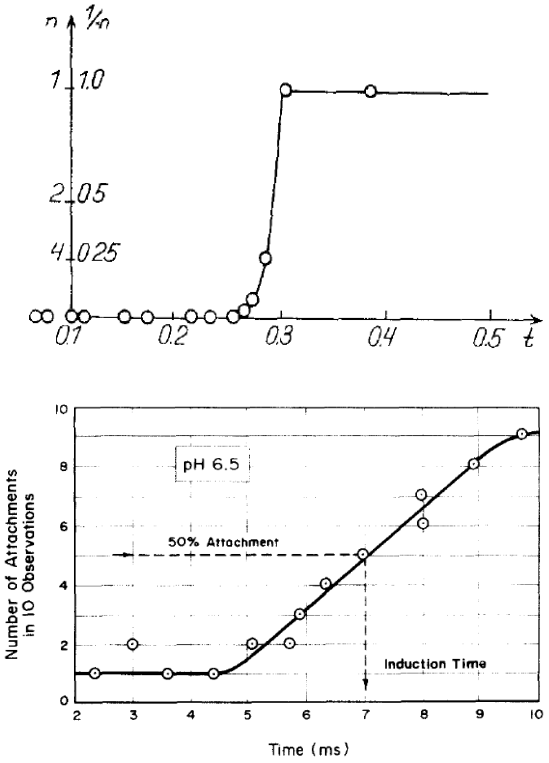


*Figure 8: Examples of the definition of induction time in the works of* (Sven-Nilsson, 1934) *(top) and* (Ye and Miller, 1988) *(bottom).*

Glembotsky (1953) further developed and perfected this method of measurement. In his device, the flat mineral surface was replaced by a bed of particles, which closer resembles a true

flotation experiment. A bubble is brought into contact with the top layer of the particle bed for a set amount of time. This process is repeated several times, each time in a different location on the bed. Whether or not bubble-particle attachment has taken place is counted. The definition of when bubble-particle attachment has taken place can vary between experiments. Attachment is commonly counted when the bubble picks up any particle (Verrelli and Albijanic, 2015), but a certain threshold amount of particles, or a percentage of the amount of particles present in the contact area are also possible (Eigeles and Volova, 1960). The statistical law of large numbers states that if the contact is repeated a large number of times, the frequency of bubble-particle attachment will approximate the true attachment probability for that specific contact time (Rasemann, 1988). Due to practical reasons, most notably the available time, most authors perform 10 attachments per variable (Albijanic et al., 2015, 2012, 2011; Gu et al., 2003; Yoon and Yordan, 1991), although some choose to use more, like Verrelli and Albijanic (2015) who use 20. This process is repeated for various contact times and the attachment time is then defined as the contact time at which the attachment probability is a certain predefined percentage. This percentage is generally chosen as 50% (Gu et al., 2003; Verrelli and Albijanic, 2015; Ye et al., 1989; Yoon and Yordan, 1991) but can vary between authors with some choosing to use a probability of 100% (Albijanic et al., 2011; Ozdemir et al., 2009). An example of this method of attachment time determination is shown in Figure 8 (bottom). The device Glembotsky developed and modified versions of it used by later authors, are occasionally referred to as Glembotsky devices, but more common is the term Induction Timer.

The Induction Timer and the above described method of attachment time determination have since been used by many other authors (Albijanic et al., 2015; Eigeles and Volova, 1960; Gu et al., 2003; Ye et al., 1989; Yoon and Yordan, 1991). Interestingly enough, the Induction Timer is more often mentioned in context with Eigeles and Volova (1960) than with Glembotsky (1953), even though the devices currently used more resemble the one used by Glembotsky than the one used by Eigeles and Volova, in which the particle bed rather than the bubble was the moving component. This is likely a result of the fact that the publication by Eigeles and Volova (1960) is widely known for being the first publication to deliver systematic and experimental proof of the importance and potential uses of the attachment time phenomenon, helping to put it on the map as an important concept. Figure 9 schematically depicts an attachment time measurement performed using an induction timer.

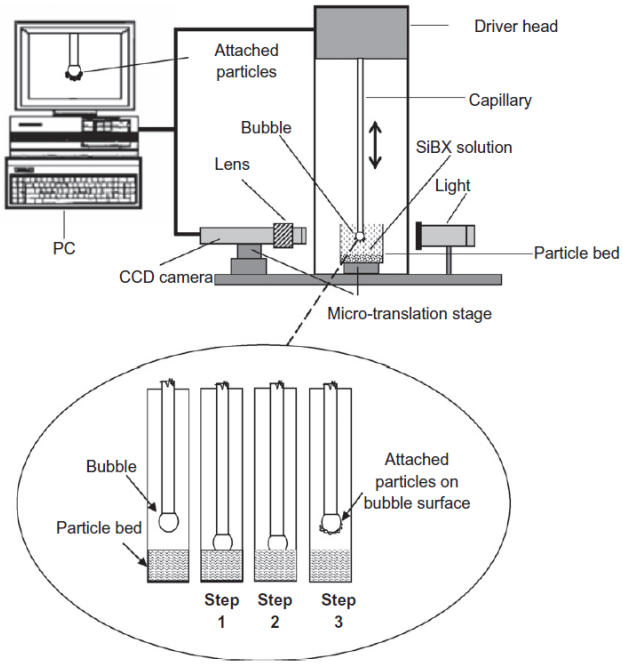


*Figure 9: Schematic representation of an induction timer (top) and the way it operates (bottom).* (Albijanic et al., 2012)

Induction timers are now commercially available and one of the most commonly used methods for measuring attachment time. The device allows control of the bubble motion parameters such as approach distance and velocity and cameras are used to view whether or not bubble-particle attachment has taken place. Both the measurement itself and the analysis of results can take multiple hours. The method has a strong dependence on the various parameters determining the bubble-motion, such as the speed of approach and retraction, approach distance and bubble compression (Gu et al., 2003), which is the distance the bubble is pushed 'into' the bed. Even though it is usually possible for a user to set these parameters, it can still be difficult to determine the exact force with which the bubble contacts the particles and the respective contact area. A change in any of the parameters will cause vastly different measurement results and therefore consistency and reproducibility is vital. With this large dependence on these user-set parameters and considering that many different devices have been used over the years, it is hard to compare data from one publication to another. Additionally, it can be questioned whether this method sufficiently approximates the real situation, considering the bubble movement is not quite natural as it only moves vertically and at a set velocity and neither is a bed of particles present in true flotation. In truth an attachment time obtained with this method will most likely not be the attachment time as it is in actual flotation. The method is nevertheless very useful for comparative studies. The exact parameters chosen are in fact not relevant as long as they remain the same over a series of experiments. In this case, the experiments show the relative ease of attachment of certain particles in certain environments and conditions. Comparisons of these results can then indicate situations and conditions that are likely favourable for flotation performance in the real system. Benefits of the method are that bubble and particle sizes can be chosen to mirror industrial flotation processes and it is even possible to test actual solid and liquid samples from industry, increasing relevancy of the results. (Verrelli and Albijanic, 2015)

### 2.3.4 Integrated Thin Film Drainage Apparatus (ITFDA)

The Integrated Thin Film Drainage Apparatus (ITFDA), described by Wang et al. (2013) combines features of both the AFM and the Induction Timer. Similarly to the Induction Timer a captive bubble is moved closer to a solid surface. Instead of a particle bed however, the bubble is moved closer to a glass sphere. This sphere is attached to a force sensor and the forces acting on its surface as the bubble approaches are measured. There are many resemblances between the ITFDA and the AFM method. Like the AFM, this device shows a directly measured force profile of the entire attachment process. The ITFDA measurements allows for the calculation of both the induction time as well as the total attachment time. It is therefore important to check which of the two times is being reported in a publication. Like with the AFM, the movement of the bubble is restricted to being one dimensional and results in a head-on collision between bubble and particle. It therefore does not well represent an actual flotation system. As with the AFM, the chosen approach velocity will significantly influence the attachment time value and should therefore be kept constant. The use of this method requires the need for specialized equipment and operators. The forces measured with this device are in scale of milliNewtons while the distances measured, including the size of the bubble and the glass sphere, are in the range of millimetres. All are therefore larger than the dimensions being investigated with the AFM method. While the size of the glass sphere, with 4.5 mm is significantly larger than the particle sizes in froth flotation this could be improved in later iterations, bringing the device closer to resembling industrial flotation conditions. Like the AFM, the ITFDA is better suited for researching the forces acting on bubbles and particles during the

attachment process, albeit on a larger scale than the AFM method, than it is for result prediction. (Verrelli and Albijanic, 2015)

### 2.3.5 Milli-Timer

With a Milli-Timer, particles are dropped on a captive bubble (Verrelli et al., 2011) as is schematically depicted in Figure 7e. The particles are free to slide along the bubble and can then either become attached or continue falling, very much resembling a real situation in froth flotation. Cameras are used to film the interactions. The attachment time is counted as the time between which a particle first touches the bubble and the point it becomes attached to the bubble. The point of initial contact is determined as the moment the particle first deviates from its original trajectory. As with the AFM and the ITFDA this means selecting the starting point requires some level of decision making by the user and therefore the attachment time is not completely unambiguously defined. If sufficiently sensitive video equipment is used, the actual moment of particle-bubble attachment can also be observed (Verrelli et al., 2011). Both particles and bubble sizes can be chosen to mirror conditions in industrial flotation processes. A downside of the method is that the contact between particles and the bubble is hard to govern. The particles are dropped and can from that point on no longer be influenced. The approach speed and angle of collision can be inferred from the video footage and from them the energy of impact can be calculated but they cannot be controlled as such. This means the influence of impact energy cannot be investigated using the Milli-Timer. Possible future addition of liquid flow may help with this and allow for the study of hydrodynamics as well as even better approximating a true flotation situation. Downsides of the method are the specialized equipment needed and the fact that it can take days to analyse all the filmed interactions. Of all the above-mentioned methods, the Milli-Timer is the only device resulting in a direct measurement of the attachment time. Microflotation and the Induction Timer are more suited for providing relative attachment efficiency while the AFM and Milli-Timer are more useful for researching forces, as their measured attachment times are completely dependent on the chosen speed of movement. (Verrelli and Albijanic, 2015)

## 2.4 Parameters influencing attachment time

As has been stated in Section 2.2, researching the attachment time is a practical way of studying the many parameters that influence the entire process of flotation. Over the years, various researchers have performed experiments on mineral particles, coal particles and bitumen droplets and have determined the dependence of the attachment time on several chemical and physical conditions. Through the bubble-attachment process these factors directly influence the results of real froth flotation processes. Although some parameters may have been mentioned in above paragraphs it is useful to have a clear list of some of the most important factors influencing the attachment time between a bubble and a particle. Additionally, summarizing these factors will give a clear overview of the kind of influences and conditions that have been studied with the use of attachment time measurements. As has been described in Section 2.3, many different ways of measuring attachment time are in use. Attachment times measured by one method are not necessarily the same as those measured by another but it would stand to reason that any general trends and observations measured with one method would hold for other methods as well. To remain within the scope of the thesis and for the sake of brevity this summary will describe the effects of various factors on the attachment time and to the causes of these effects, without going into too much detail about effects on general flotation and the interactions with other parameters. An example of this is the effect of ion concentration on collector adsorption. Although a change in

adsorption efficiency will technically change the attachment time and with it the effectiveness of flotation, this change in attachment time is actually the result of a change in the effective hydrophobicity of the particle surface, which is itself already discussed as a factor.

### 2.4.1 Bubble properties

*Effect of size & gas type*

The attachment time is dependent on the size of the bubble (Gu et al., 2003; Hewitt et al., 1995; Wang et al., 2005). It has been consistently observed that larger bubbles result in larger attachment times. In fact, Gu et al. (2004b) have measured a critical cut-off size. Hydrogen bubbles bigger than this cut-off size did not attach to bitumen droplets while those that were smaller did. The exact value of this critical diameter varied with other parameters such as temperature, water quality and ionic composition and the size of the bitumen droplet. Wang et al. (2005) reported that the effect of bubble size was more noticeable for large particles and attributed the increase in attachment time to a longer time of film drainage, caused by the larger contact area between bubble and particle. Hewitt et al. (1995) mention the same but attributes the shorter attachment time to a reduction of both film thinning and TPCL expansion time, as a thin liquid film of a smaller area both drains and ruptures faster (Fisher et al., 1992; Newcombe and Ralston, 1994).

From these findings, it can be inferred that for achieving optimal flotation, smaller bubbles are better suited than larger bubbles. Obviously this does not take into account any possible counteracting effects caused by other factors of influence when the bubble size is reduced, as this can only be measured when experiments are performed on real systems. Gu et al. (2004a) have researched the effect of the type of gas used for creating the bubble both in deaerated municipal water and in cleaned process water and have found that hydrogen gas results in shorter attachment times than does the use of oxygen. They state that the difference may be a result of the fact that oxygen molecules are more easily polarized. As they are more polar than hydrogen molecules, their interaction with the water molecules due to hydrogen bonding will be stronger, resulting in stabilisation of the thin liquid film, which in turn results in a longer attachment time.

*Effect of surface contamination*

The amount of time that has passed since the bubble has been created is also an important factor, which was already noticed by Eigeles and Volova (1960). The surfaces of aged bubbles have often become contaminated with surfactant molecules, such as the often-present frother chemicals (Nguyen, 1999). In the correct dosages, these chemicals improve flotation by promoting the formation of a stable froth phase and because the use of frothers results in smaller bubbles. There is also a downside to their presence however, as these molecules affect the surface tension of the bubbles as well as immobilize the gas-liquid interface. Both are bad for the attachment efficiency. Freshly made bubbles have a clean, highly active surface and therefore attach more easily to particles (Nguyen, 1999; Yoon and Yordan, 1991). For this same reason, it also matters whether or not the bubble is in motion and from which direction the particle collides. Collector molecules and other contaminants on a moving bubble may be pushed away from the front to the back side of the bubble, thus creating a ‘clean’ bubble surface at the front (Clift et al., 1978; Nguyen, 1999; Yoon and Yordan, 1991).

### 2.4.2 Particle properties

*Effect of hydrophobicity*

As flotation is a method that primarily separates materials based on differences in their hydrophobicity, this is perhaps the most obvious factor of influence. In their early systematic work, Eigeles and Volova (1960) found that materials that floated easily had much shorter attachment times than materials that were difficult to float. Nowadays the relationship between hydrophobicity and attachment time has been well established and it is understood that materials that float easily in fact do so because of their short attachment times (Albijanic et al., 2015, 2011; Jowett, 1980; Ye et al., 1989; Yoon and Yordan, 1991). With the important role that (hydrophobic) surface forces play in the process of particle-bubble attachment and consequently in flotation itself, it is unsurprising that anything altering the surface states of the particle (or the bubble for that matter) affects the attachment time. Extended exposure to oxygen in air and liquid causes contamination of the particle surfaces by both physical and chemical reactions, decreasing the hydrophobicity. This causes increased attachment time, which in turn causes lower flotation recovery (Somasundaran et al., 2000; Yoon, 2000). As with bubbles, the amount of time a particle has been submerged in liquid has an influence because the surface becomes contaminated by other compounds. Although not a specific topic of their research, the influences of particle surface purity and the effect of submergence time were also noticed by Eigeles and Volova (1960). As will be explained in Section 2.4.3 the pH of the solution can also affect particle hydrophobicity.

Particle hydrophobicity is an important parameter affecting the attachment time but it is certainly not the only one. As was mentioned earlier in Section 2.2.4, the surface forces on polished mineral surfaces are vastly different than those at the surface of mineral particles, which was demonstrated when Ye et al. (1989) measured attachment times that were at least 50 times larger than those measured at a particle bed. As the same mineral was used, this phenomenon can't possibly be explained by just the hydrophobic state of the material. There must therefore be other factors that influence the surface forces and attachment times.

*Effect of size*

In the science of minerals processing two of the most studied subjects in regards to flotation result predictions are the liberation of the minerals and the size of the mineral particles to be floated. Clearly, the importance of the amount of exposed mineral follows directly from the different levels of hydrophobicity of various minerals. That the size of a particle affects the attachment time has been known since the publication of Eigeles and Volova (1960) and has since been reconfirmed by many other authors. The attachment time increases logarithmically with increasing particle size. Eigeles and Volova (1960) attributed this to the fact that a larger attractive force is necessary to balance the bigger weight of a large particle. They reasoned that, as a larger attractive force is needed, it would take longer for all the forces to be balanced. They investigated the influence of $t_{TPCL}$, before coming to the conclusion that it must be due to an increased $t_i$. Yoon and Yordan (1991) also suggested an increase in film drainage time to be responsible for this observation, as displacing the water film on a bigger particle would take more time than it would on a smaller particle. In theory, this relationship results in better flotation for smaller particles. In reality, there is often an optimum size. Flotation recovery tends to decrease for very small particles, as flotation of fines is plagued by its own difficulties. Examples of this are the fine particles having less momentum, and being more easily affected by water chemistry and surface coatings (Pease et al., 2006). The details on the problematic flotation of fines are outside the scope of this work however. As was mentioned

in Section 2.2.2, it was in fact the illogical finding that for fine particles the calculated attachment times increased with decreasing particle size, while large amounts of theoretical and experimental evidence proved the opposite, that led to Hewitt et al. (1995) stating the ineffectiveness of the models of that time and to Nguyen et al. (1997) proposing the importance of the rupture and expansion of the TPCL in attachment efficiency modelling.

By examining different types of coal particles, Ye et al. (1989) and Ye and Miller (1988) later found that the extent to which the size affects the attachment time is in fact governed by the particles density. A plot of the measured attachment times against the size of the particles showed different slopes for particles with different densities as can be seen in Figure 10. A similar plot for various types of coal particles of roughly the same density but with different levels of hydrophobicity showed the same slope for all coal types, indicating that the hydrophobicity of the particles did not affect the slope of the line, as is shown in Figure 11. This indicates that although the attachment time certainly depends on particle hydrophobicity, the extent to which it depends on particle size is governed by density rather than hydrophobicity.

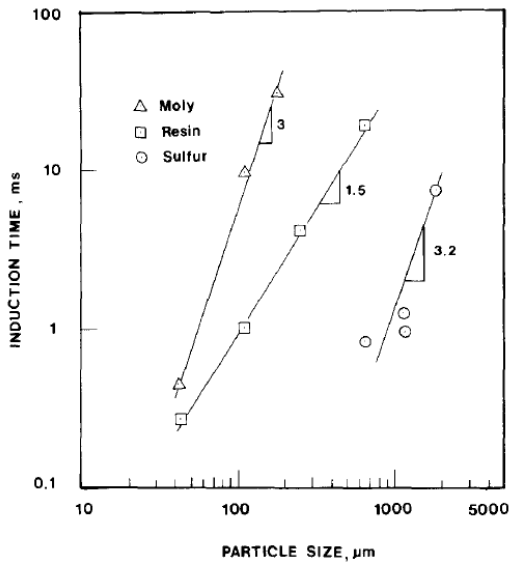


*Figure 10: Attachment time versus particle size plot for particles of different densities. Moly: Molybdenite (4.7 g/cm³). Resin: Fossil Resins (1.03 g/cm³). Sulfur: Elemental Sulphur (2.07 g/cm³). Please note that the induction time is actually the attachment time.* (Ye et al., 1989)

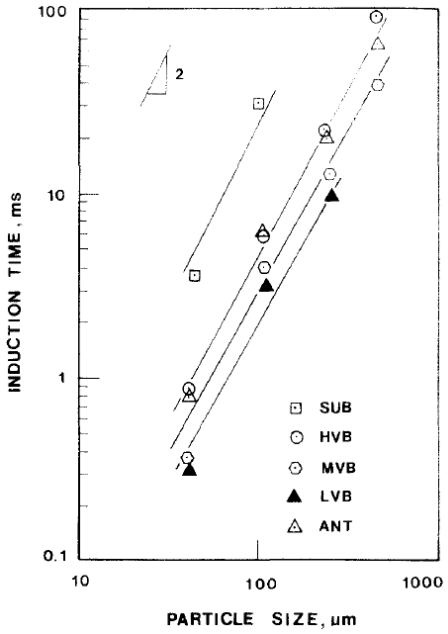


*Figure 11: Attachment time versus particle size plot for particles of various coal types of similar density (1.3 to 1.4 g/cm³). SUB: sub-bituminous. HVB: high-volatile bituminous. MVB: medium-volatile bituminous. LVB: low-volatile bituminous. ANT: Anthracite. Please note that the induction time is actually the attachment time.* (Ye and Miller, 1988)

*Effect of shape*

As can be seen in Figure 12 the shape of a particle can vary a lot, and often depends on the type of pre-processing that was done. The particle shape can influence the flotation behaviour of the particle. When Koh et al. (2009) performed flotation tests on both ground (angular) particles and on spherical particles they found that the results could be well correlated to the sphericity of the particle, with ground particles having markedly better flotation performances. Vizcarra et al. (2011) nuanced this discovery by finding that angular particles only float better than spherical ones in the case of collectorless flotation and other low-floatability situations. When a collector was used the influence of particle shape disappeared. Years earlier the effect of angularity had also been noticed by Anfruns and Kitchener (1977) who found that the shape of the particles heavily impacted the collection efficiency, with spherical particles having an efficiency of collection of merely 50% while that of angular particles was 100%. They attributed this to the fact that sharp edges and corners cause the thin liquid film to drain faster, resulting in faster overall particle-bubble attachment times. The effect of particle shape, hydrophobicity, and size on the film thinning time with regards to froth stability was researched by Dippenaar (1982). He found that angular galena particles with relatively low hydrophobicity may result in shorter induction times than hydrophobic glass spheres, seemingly confirming the assumptions of Anfruns and Kitchener (1977). Although Dippenaar (1982) showed shorter film thinning times for angular particles, his research was performed in the context of froth stability. In his research they placed a particle on a suspended water film with air on both sides, which does not much resemble a flotation situation. Verrelli et al. (2014) stated that for a long time the effect of particle angularity in flotation was more anecdotal than it was truly scientifically proven and that it was in fact still unknown which of the particle-bubble attachment sub processes were actually affected by particle shape. They proceeded to directly quantify the effect of particle shape on the attachment time by studying the interactions between a particle and a bubble using a Milli-Timer device. They found a shorter attachment time for angular particles than for round ones, thereby confirming the assumptions of Anfruns and Kitchener (1977), although they mentioned that a measurement of the effects of varying degrees of sphericity would be left for future work.

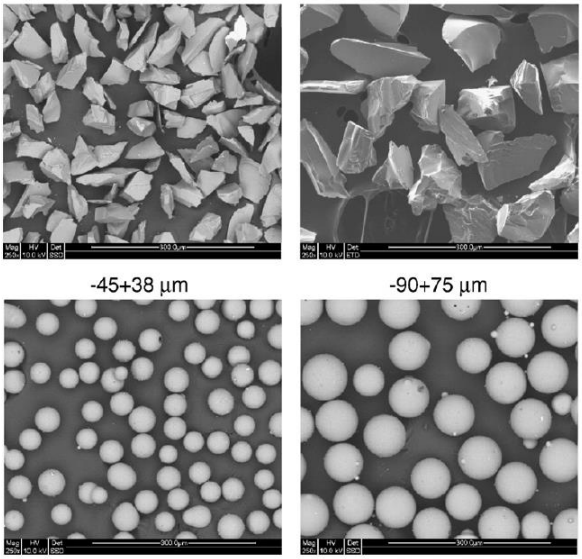


*Figure 12: SEM images of ground (angular) and spherical ballotini particles of two different size classes.* (Koh et al., 2009)

*Effect of surface roughness*

Another shape-factor, the surface roughness also impacts the attachment time as was shown by Krasowska and Malysa (2007b). They measured the time between bubble-solid contact and the formation of a TPCL that was large enough to prevent bubble detachment on various Teflon surfaces and found shorter times for rougher surfaces. Two possible reasons are given to explain this. The first is the fact that the asperities protruding from the material's surface effectively lower the thickness of the thin wetting film which therefore results in a more rapid attainment of the

critical rupture thickness. A TPCL would in this case first appear on the asperities, before spreading to the rest of the solid surface. The second is that on rough hydrophobic surfaces nanobubbles may be present that influence the long-range attraction forces and therefore make film rupture easier. The effect of surface roughness was also shown for fluorite surfaces by Zawala et al. (2008) who suspect the first reason to be the cause of their findings as the fluorite surface was determined to be quite hydrophilic.

Verrelli et al. (2014) state that this effective thinning of the liquid film due to protruding asperities occurs when the ridges are in the micrometre scale. Roughness on a smaller nanometre scale has however also been shown to have an effect. Oliver and Mason (1977) investigated the spreading of liquid over rough surfaces by using SEM. They found that sharp edges as small as 500 Å in height may significantly slow the spreading rate of the TPCL. These nanometre scale edges can therefore have an effect on the attachment time through $t_{TPCL}$.

### 2.4.3 Properties of the physical and chemical environment

*Effect of reagents*

In nearly all flotation processes, collectors are used to selectively increase the hydrophobicity of certain mineral surfaces. By increasing the hydrophobicity of mineral surfaces, these chemicals increase the strength of the bubble-particle interaction. Other types of chemicals called activators and depressants are used to respectively enhance or prevent the selective adsorption of these collectors onto specific mineral species or to render some of the particles hydrophilic. All these chemicals adsorb on the particle surfaces either physically or chemically and thus influence the interactions between bubbles and particles. Due to this change in the forces of interaction, the induction time changes and consequently so does the flotation response. It was in fact various concentrations of collector chemicals such as potassium xanthate that Sven-Nilsson (1934) used as the variable in the first ever published experiment measuring the *Induktionszeit*. Since then, many scientists have researched the influences of collector concentration on the attachment time both separately and combined with the effects of other influences such as temperature and ionic strength. Among them were Eigeles and Volova (1960) whose studies put attachment time on the map as an important phenomenon. However, the effect of flotation collectors on the attachment time is due to increased particle hydrophobicity. As the effect of hydrophobicity on attachment time has already been discussed, not much is gained with a lengthy of the many results found for the various collector chemicals and their different target minerals. If relevant interactions with other factors are found these will be discussed in the relevant sections. However, nearly all of these interactions essentially boil down to either more effective or less effective adsorption of chemicals on the mineral surface, and thus a more or less hydrophobic surface.

*Effect of electrostatic charge, solution pH, and dissolved ions*

The electrical charge carried by the surfaces of both bubble and particle can affect the attachment time. As was mentioned in Section 2.2.1, the stability of the liquid thin film depends on the surface forces acting between the bubble and the particle. As is described by Zawala et al. (2008), electrostatic forces are an important part of this. When the distance between the bubble and the particle becomes smaller, the thin liquid film drains. When the film reaches a thickness that allows the electrostatic surface forces of both bubble and particle to interact, the type of interaction can determine whether attachment takes place. If the particle and bubble have the same charge, they repel one another. This interaction causes the thin liquid film to stabilize. If a particle and a bubble

are oppositely charged however, the liquid film continues to thin until it reaches its critical thickness. Experimental results showed no formation of the TPC for bubbles and fluorite surfaces with similar charge, while opposite charges resulted in attachment (Zawala et al., 2008). Yoon and Yordan (1991) showed that the attachment time between a quartz particle and a bubble was more than 10 times larger when both were charged negatively when compared to an experiment in which the bubble had a positive charge. The value of the charge of bubbles and particles is dependent among other things, on the pH of a solution, the materials' isoelectric point (IEP), and the concentrations of ions present in the liquid. It is well known that when the pH is above the IEP of a material, its surface is charged negatively, while if it is lower it is charged positively. The larger the difference between the pH and the IEP, the larger the magnitude of the charge becomes. An example of this variation of the charge with varying pH is shown in Figure 13 (bottom). Both in the experiments by Yoon and Luttrell (1989) and those by Zawala et al. (2008) the charges were manipulated by varying the pH of the solution.

The effect of electrostatic forces on attachment time was also observed by Ye et al. (1989), although they found it to be of secondary importance to the hydrophobicity. Their results show that that the attachment time for various coal types is shortest at a pH value equal to its IEP, while it becomes larger as the pH becomes more negative or more positive. Their findings are shown in Figure 13. This phenomenon is not unexpected as without the presence of collectors, the IEP is the point at which naturally hydrophobic materials are at their most hydrophobic. At higher and lower pH values the surface becomes more hydrophilic due to the presence of respectively hydrogen and hydroxyl ions. Consequently, in the collectorless flotation of hydrophobic materials, optimal flotation occurs at the IEP of the material (Drzymala, 2007; Ye et al., 1989).

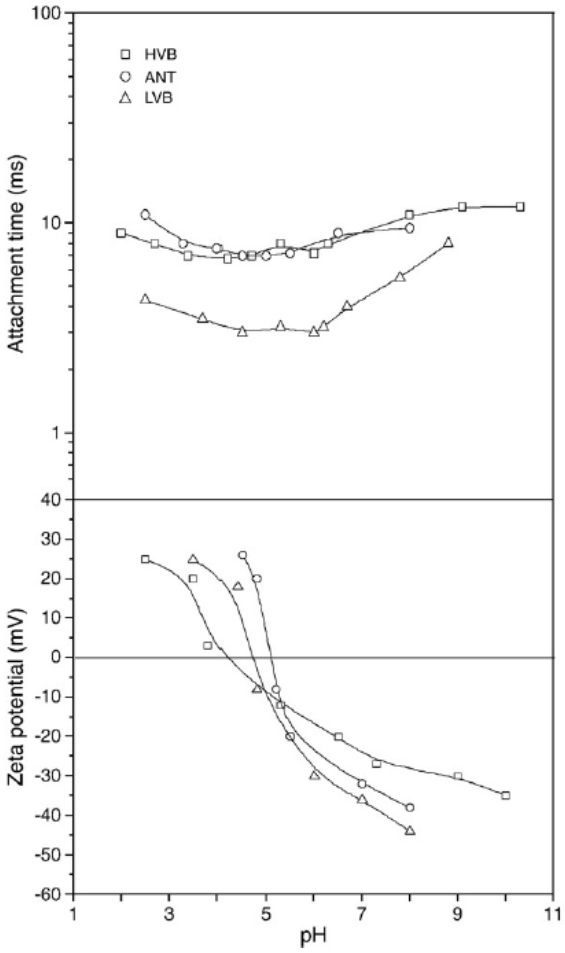


*Figure 13: Top: Attachment time for various types of coal particles plotted against the pH of the solution. Bottom: Zeta potential of the various coal particles plotted against pH. Note the lowest attachment times occurring near the IEP, the point where the charge is zero. HVB: high-volatile bituminous. ANT: Anthracite. LIG: Lignite. Data and original graphs from* (Ye et al., 1989)*, combined and simplified image copied from* (Albijanic et al., 2010).

The fact that the pH of a solution has a large impact on the flotation of various minerals has been known for decades. The pH has in fact been the most used method for control of flotation processes (Fuerstenau et al., 2007). One of the main utilisations of solution pH, aside from the effects on the attachment time that were mentioned above, makes use of the effect of pH on the charge of various materials. By manipulating the pH of the solution, it is possible to have materials with different charges as a result of their differing IEP's. These different charges allow the selective adsorption of anionic or cationic collector chemicals, thereby turning the desired

material more hydrophobic than other minerals. The influences of particle hydrophobicity and the presence of reagents on the attachment time have been discussed in previous sections and will therefore not be discussed further here. The effects of pH on the stability and surface adsorption of the various chemicals that facilitate flotation are considered to be outside the scope of this work.

Although it was not one of the variables they researched in detail, Eigeles and Volova (1960) found that the degree of purification of the water affected the attachment time. They did not go into further details but it is not hard to speculate why this is the case. The effects of various contaminating chemicals and fine solid particles has been well established by now but even the presence of electrolytes can affect the attachment time measurements. Dissolved ions are present at the various phase boundaries and therefore influence the interactions of particles and bubbles (Albijanic et al., 2010). Adsorbed ions can change the electrostatic charge of bubbles or particles, which in turn influences their interactions as has been described above. Additionally, the presence of dissolved ions in high concentrations can compress the electrical double layers (EDL) of both the particle and the bubble (Ralston et al., 1999b; Yoon and Yordan, 1991). When the EDL is thinner, there is less repulsion and so less force is needed to bring the particle and the bubble closer to one another. Experiments by Yoon and Yordan (1991) show a clear decrease of the attachment time for quartz particles in the presence of a low concentration of the collector dodecylamine hydrochloride (DAH) when the concentration of KCl was increased. With higher concentrations of DAH, increasing the ion concentration initially had less of an effect on the attachment time. When the KCl concentration was increased past $10^{-3}$ M it resulted in a sharp increase in the attachment time due to the ions interfering with the effectiveness of adsorption of the collector molecules, but such interactions are outside the scope of this work. Experiments with methylated quartz particles performed by Hewitt et al. (1995) showed the same trend of drastically decreased induction time with increasing concentrations of KCl but they noted that this only occurred for moderately hydrophobic particles, with the effect being much less pronounced for strongly hydrophobic particles. These findings suggest that the importance of the electrostatic interactions in the attachment process becomes more pronounced as the strength of the hydrophobic interactions decreases. As the TPCL expansion time was found by Newcombe and Ralston (1994) to be constant with changing ionic strengths, the reduced attachment time with increasing ionic strength must result from a reduction of the film thinning time.

Ozdemir et al. (2009) found that flotation of coal particles in hypersaline water containing 0.7 M NaCl was possible but that the attachment times were higher than in deionised water where attachment was instant for all size classes. The attachment time was found to depend on particle size. Attachment took around 10 ms for fine particles, while coarser samples could take up to 100 ms. Their AFM experiments did show reduced repulsive forces between particles and bubbles in the hypersaline water, which might be attributed to the compression of the EDL. Gu et al. (2003) found that the attachment time for bitumen droplets was always the shortest when the experiment was performed in de-ionized water and that addition of $Ca^{2+}$ did not influence the attachment time. When experiments were performed in process water, the attachment time was higher than compared with the de-ionized water experiments. But in process waters the addition of $Ca^{2+}$ did produce some decrease of the attachment time. When fine solids were present in the process water however, addition of $Ca^{2+}$ caused interactions between the solids fines and the negatively charged bitumen. Adsorption of fines on the bitumen changed the surface hydrophobicity which resulted in a significant increase of the attachment time.

As described by Albijanic et al. (2010) there is conflicting information on the exact effect of dissolved ions in coal flotation, but as this is mostly related to effectiveness of collector chemicals, bubble coalescence, solid aggregates, and ion adsorption to coal surfaces rather than to direct effects on the attachment time this subject will not be discussed further in this work.

*Effect of temperature*

The influence of solution temperature is one of the main factors that was researched by Eigeles and Volova (1960). They found that attachment time for various minerals varied exponentially with changing temperature. In their measurements, the attachment time could drop by as much as 3 orders of magnitude when the solution temperature was increased from 15 to 60 °C. This exponential relationship was later also found by Yoon and Yordan (1991) for quartz particles and by Gu et al. (2003) and Gu et al. (2004b) for bitumen droplets. Increasing the temperature also increased the critical bubble diameter above which no attachment can take place and lowered the attachment time at the critical bubble size (Gu et al., 2004a).

Eigeles and Volova (1960) found that the rate of change of the attachment time with increasing temperature was independent of particle size, although bigger particles always had longer induction times as has been established in Section 2.4.2. For some minerals such as calcite and apatite the effect was found to be reversible, i.e. the attachment time after heating and subsequent cooling down was the same as before. For other minerals like quartz however, the effect was not reversible and the attachment time after heating was shorter than before. This irreversibility was attributed to the fact that the attachment time of quartz was more dependent on the mineral surface state compared to the other minerals. It was proposed that iron from the steel mill in which the materials were ground, present on the quartz surface had oxidized during heating and prevented the return of quartz to its normal state.

Eigeles and Volova (1960) ascribe the decrease of attachment time as a result of temperature increase to increasing instability of the hydrate boundary layers. An increase in temperature can cause changes in the state of the EDL, the chemical composition of the mineral surface, and the liquid viscosity. All of these affect the stability of the thin liquid film. The most important factor however is the increase in thermal movement of the liquid molecules. These effects decrease the thin film stability and therefore increase the film draining rate. Both Gu et al. (2004b) and Lazarov et al. (1994) mention that the temperature of the solution, through its effect on solution viscosity, also inherently affects the movement velocity of bubbles, which itself has a significant effect on the attachment time as will be described in Section 2.4.4. Both publications report increased bubble velocity with increased temperature. This additional effect should not have been an issue in the measurements where the bubble is captive and the approach velocity is controlled (Eigeles and Volova, 1960; Yoon and Yordan, 1991).

As is shown in Figure 14, increasing the concentration of collector while also increasing the temperature was found to reduce the attachment time even more, but simultaneously diminished the individual effect of increasing temperature as can be seen from the decrease of the slopes of the lines (Eigeles and Volova, 1960). It was assumed that both additional collector and increase of temperature worked in the same way to lower the attachment time. Yoon and Yordan (1991) later obtained similar results. This plot of attachment time versus temperature for various collector

concentrations can be used to calculate the activation energies by using the Arrhenius equation (Eigeles and Volova, 1960; Gu et al., 2004a; Yoon and Yordan, 1991). These activation energies indicate the amount of work that has to be done by a collector to turn the surface of the mineral hydrophobic and therefore they also give an indication of the hydrophilicity of the mineral (Eigeles and Volova, 1960). In both publications, the activation energy was found to decrease as collector concentrations increased. Eigeles and Volova (1960) make note of the fact that the activation energy is not a sole parameter for indicating flotation performance and particle-bubble attachment, but rather that it has to be reviewed together with the measured attachment times.

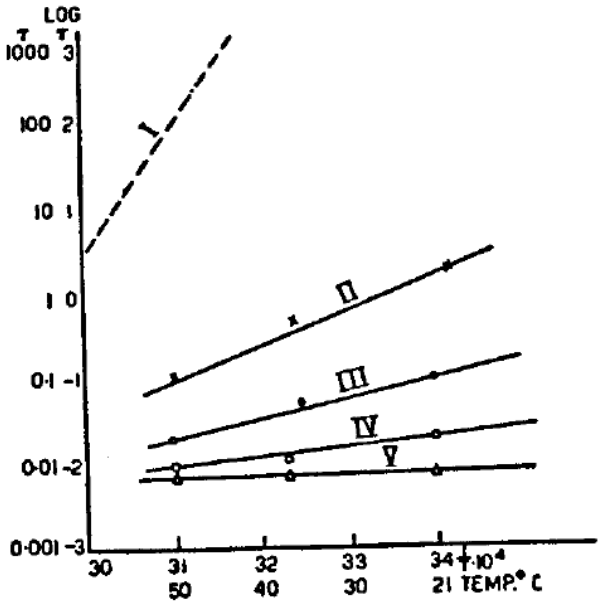


*Figure 14: Attachment time (y axis) for quartz particles plotted against solution temperature (decreasing from left to right on the x axis) for various concentrations of collector chemicals (Concentration increases from I-V). The slopes of the respective lines can be used to calculate activation energies.* (Eigeles and Volova, 1960)

Lazarov et al. (1994) directly observed the kinetics of film thinning and TPC expansion for ballotini and quartz particles using a metallographic microscope and a high speed camera. With increasing temperature, they measured a substantial decrease in the induction time. The rate of TPC expansion however, decreased with increasing temperature. They state that the decrease in the kinetics of TPC expansion is most likely related to the mechanism of physical adsorption, as the adsorption density is known to decrease when temperature increases (Ball and Fuerstenau, 1971). As the results by Eigeles and Volova (1960) and Yoon and Yordan (1991) show an exponential decrease of attachment time for increasing temperatures, Lazarov et al. (1994) reason that $t_i$ rather than $t_{TPCL}$ must be the dominant factor in the total attachment time. In contrast to the results of Eigeles and Volova (1960) a size dependence for this phenomenon was found in flotation tests. Ballotini particles larger than 100 µm did not exhibit increased flotation kinetics for rising temperatures, while for particles over 300 µm a decrease was measured. This was attributed to the fact that it was more difficult for a stable TPCL to form due to increased bubble-particle collision velocities.

### 2.4.4 Effect of measurement parameters

*Effect of approach distance & velocity*

As has been described in Section 2.1.2 the angle of impact and energy with which the bubble and particle collide influence the efficiency of attachment. For attachment time measurements the way this factor is controlled depends on the system in question. In many cases it is the velocity of the bubble, which can be either free rising or controlled by the system in case of captive bubbles. In some devices it is the particles that move. In case of free rising bubbles the viscosity of the liquid and the bubble size are of importance, while for systems with a captive bubble the velocity is set by the user. As was described in Section 2.4.3, the viscosity can depend on solution temperature. To keep the summary simple, the discussion here will be about the actual factor of importance, which is the relative velocity of collision between a particle and a bubble.

Whether or not the bubble surface is mobile or not has an influence on the film drainage (Ralston et al., 1999b) and on its surface contaminations, as has been mentioned in Section 2.4.1. An increasing velocity of collision has been found to result in lower attachment times in experiments with various types of measurement devices (Gu et al., 2004a, 2003; Verrelli et al., 2014). This shorter attachment time is caused by an increase in the rate of liquid thin film draining. A faster collision velocity results in a higher applied pressure, which in turn causes faster expelling of water from the liquid film (Evans, 1954; Gu et al., 2004a, 2003; Jowett, 1980). This result can be slightly misleading. If one were to just take into account the attachment time, one might conclude that faster collision speeds result in better flotation performance as a result of shorter attachment times. However, a higher relative speed of collision increases the chance of particles rebounding from bubbles, causes larger bubble deformation, and shorter particle-bubble contact times (Lazarov et al., 1994; Nguyen Van, 1993; Schulze, 1992; Schulze et al., 1989) as has been described in Section 2.2.2. For all of these reasons, higher collision velocities are generally found to negatively affect the overall efficiency of attachment. This serves as a good reminder that one has to keep in mind there are other parameters of influence in the flotation process besides the attachment time.

In systems such as the Induction Timer, a bubble is brought into contact with a bed of particles for a set amount of time before being removed again. In these cases, the speed of retraction is of influence on the attachment time. Which of the two components is being moved depends on the specific system, but is in essence irrelevant for this discussion. Both Eigeles and Volova (1960) and Gu et al. (2003) have found longer attachment times for increasing speed of retraction. A faster speed of retraction means that the bubble and particle move away from one another with a bigger kinetic energy. As was mentioned in Section 2.1.1, for a particle to stay attached to a bubble the attractive forces between them have to be big enough to balance out forces that pull them apart such as kinetic energy due to impacts from other objects or the gravity acting on the particle. These attractive forces become bigger as the area of TPC increases. Therefore, to overcome larger kinetic retraction forces, a longer time is needed to allow spreading of the TPCL. This results in a longer total attachment time. In these systems the measured attachment time will therefore depend on the speed of retraction.

*Effect of surface deformation*

Another factor is the bubble surface deformation. Bubbles with a more deformed surface have less effective particle attachment (Nguyen Van, 1993; Schulze et al., 1989). Although there seems to be no direct influence on the actual physical attachment time, it does have an influence on the measured attachment time. Deformed or oscillating bubble surfaces can make it hard to determine the actual thickness of the thin liquid film (Verrelli and Albijanic, 2015). In addition, the deformed surface can cause the bubble or particle to initially bounce away, resulting in a lower contact time than was estimated. All this can affect the measured attachment time. The effects of bubble deformation are difficult to estimate and in fact many models and measurements systems simplify the situation by assuming a perfectly spherical, non-deformable bubble in a system with a zero-resistance liquid (Wang et al., 2005; Ye et al., 1989), although some methods make an effort to take the deformation into account (Gu et al., 2003). In attachment time measurements it's therefore best to keep the distance of approach as short as possible and the bubble sizes small, as this causes less bubble deformation (Ralston et al., 1999b; Ye et al., 1989). Bubble surfaces can also become deformed as a result of the electrostatic interactions, as they get flattened due to electrical

repulsion forces on approach to a solid surface (Miklavcic et al., 1995). This means the ionic strength of the solution can have an influence on the extent of bubble deformation.

*Effect of applied load or bubble compression*

For attachment time measurements, the amount of compression the bubble experiences as it is pushed into the particle bed is a very influential factor, as with a change in the amount of compression several other factors of importance change. A schematic representation of bubble compression during an attachment time measurement with an Induction Timer is shown in Figure 15. This bubble compression is usually described by the 'applied load' or 'bubble compression'. Gu et al. (2003) measured a shorter attachment time with increasing bubble compression. The attachment time decreases because the pressure the bubble exerts on the particle surface with increasing compression will be higher, which causes a faster rate of film draining (Evans, 1954; Jowett, 1980). There are several other effects when a captive bubble is driven deeper into the particle bed. It is possible the area of contact between the bubble and an individual particle becomes bigger which results in longer film drainage times (Wang et al., 2005). There will be more pronounced surface deformation, which causes less chance of successful attachment (Nguyen Van, 1993; Schulze et al., 1989). Furthermore, there will be a larger area of contact between the bubble and the particle bed surface. This means more particles are in contact with the bubble, so there are more possibilities for attachment to occur. This can significantly influence the results of attachment time measurements that are based on a certain percentage of bubbles obtaining particle attachment. Another possible consequence results from the fact that if the bubble is pressed into the bed deeper, the time of contact between particles and bubble becomes longer than if it just touches the bed surface slightly. In principle, this effect can be calculated and compensated for beforehand but when a bubble is unexpectedly larger or bigger than the estimated size, this has to be taken into account. In such a case, the actual contact time will be different than the one set by the user and, if not compensated for properly, will cause a discrepancy between the set value and actual contact times which can lead to false interpretation of results.

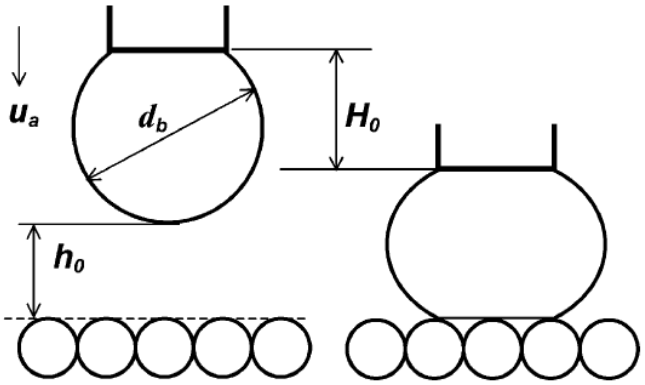


*Figure 15: Schematic depiction of bubble compression in an Induction Timer as the bubble gets pushed into the particle bed. The compression here is equal to $H_0$-$h_0$. Original image from* (Gu et al., 2003)*, edited for this publication.*

# 3. Instrument design and development

## 3.1 ACTA introduction

Most recently, a new attachment time measurement device has been developed in the Research Group for Mineral Processing and Recycling of the Department of Chemical and Metallurgical Engineering at Aalto University School of Chemical Engineering. This device was first described in a conference poster presentation (Javor et al., 2016).

### 3.1.1 Device features

ACTA, shown in Figure 16, is based on the principle of the Induction Timer as it has been described in Section 2.3.3. It has however, a number of significant differences and benefits. Standard induction timers create a single bubble, which is then brought into contact with the particle bed. This process is usually repeated around 10 or 20 times before another contact time is measured. In comparison, ACTA has an array of six needles, which makes it possible to create six bubbles at once. In its current mode of operation at time of writing, the 9$^{th}$ of May 2017, this allows for the creation of 396 bubbles per measurement run of 40 minutes. It can therefore generate significantly more data than the standard Induction Timer in only a short amount of time. The statistical benefits of this approach should be clearly apparent.

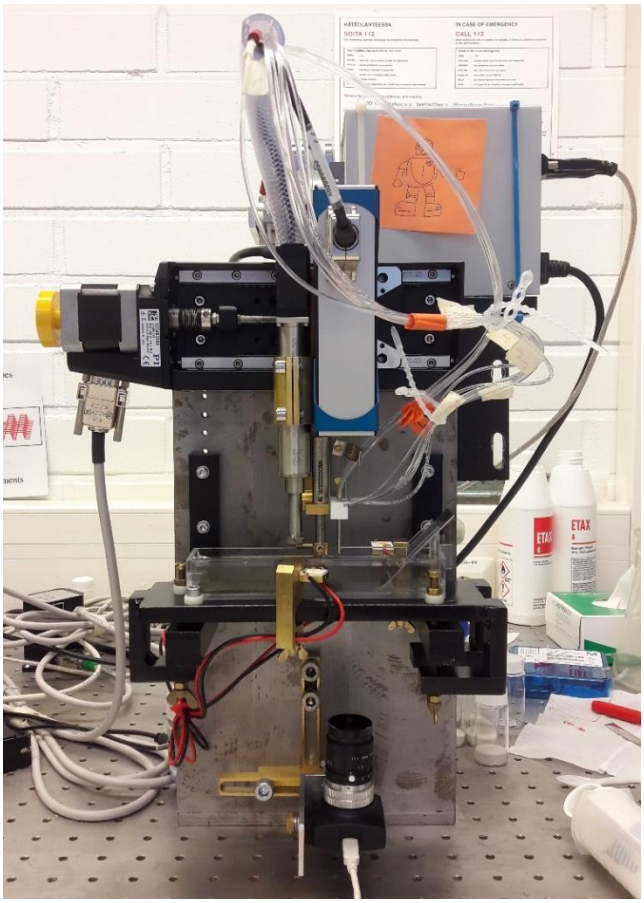

*Figure 16: Photograph of ACTA in its most recent state (1-7-2017).*

The device is operated with National Instruments™ LabVIEW code. With the exception of the particle bed preparation and the processing of data to calculate the attachment probability, ACTA measurements are performed fully automatic. Furthermore, the operating code and device components allow all parameters of interest to be set by the user. This includes the particle bed height, approach velocity, approach distance, bubble age, bubble compression, contact time and desired approximate bubble size. The wave function used to define the vertical bubble motion is completely configurable, allowing for both linear approach velocities and varying approach velocities simulating true bubble-particle collision. The actual vertical movement data of the needle array is accurately recorded and saved for each cycle which allows calculation of true movement distance and velocity.

Photographs are made of all created bubbles after their contact with the particle bed. These can be analysed to determine the size of each bubble and the attachment of particles. This data is used to determine attachment efficiency. The option to vary all parameters and the fact that all data is collected allows each factor to be examined for its respective influence on attachment efficiency.

Aside from the influence of these physical factors, the setup allows for study of other variables and interactions. Changing the liquid in which the experiments are performed allows for the examination of the influences of bulk fluid chemistry, water quality, reagent concentrations, pH, Eh and dissolved organics. The type of gas used for bubble creation can also be varied and the transport of the bubbles to the collection bin mimics the effect of water flow in flotation cells on particles attached to the bubbles. The collection of attached particles allows for further ex-situ processing and analysis, revealing information about the mass, shape, and mineralogy of the collected particles. The development of ACTA was started out of a desire to be able to quickly and systematically analyse the floatability of samples both in lab and in actual flotation plant situations. To achieve this, the device has been developed to be easily transportable, easy to assemble and easy to operate. This allows it to be brought to an actual flotation plant and examine samples that were taken from the process as rapidly as possible. In these situations, the time between sampling and analysis is crucial to obtaining qualitative and useful data, therefore the ACTA provides an invaluable benefit over those methods that have to rely on dated samples that have been treated with chemicals or frozen to partially prevent degradation.

### 3.1.2 ACTA measurement cycle steps

A schematic depicting one ACTA measurement cycle is shown in Figure 17. (1) Bubbles are created at the array of needles. They are then brought into contact with a particle bed for a predetermined amount of time. (2) The bubbles and any attached solids are transported to a viewing window where a camera is used to photograph the bubbles from below. LED lights positioned at both sides of the pool are used to temporarily illuminate the surroundings, allowing for a clear photograph. (3) The bubbles are moved to a separate collection bin. Once they are inside, more air is pumped through the needles, increasing the bubbles' size until they detach, effectively trapping them and any attached particles inside the container. (4) The needles are taken above the surface of the liquid and moved back to an untouched area of the particle bed. While moving they are flushed with air to remove any contaminating liquid. (5) The needles are submerged and new bubbles are made. This cycle is repeated until there is no clean particle bed surface left.

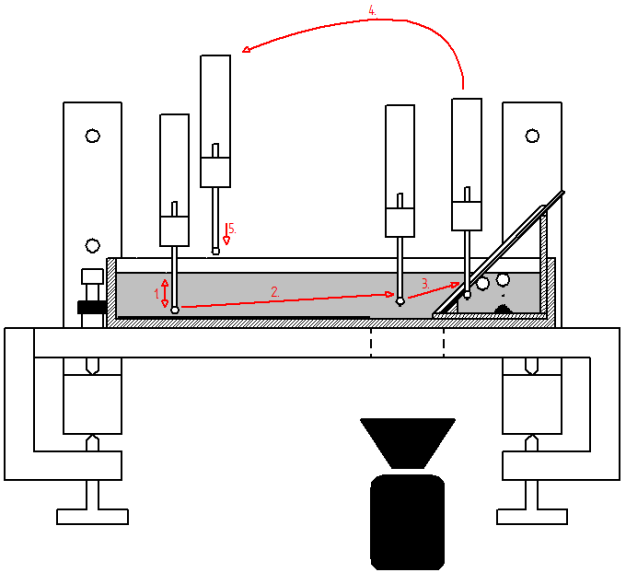


*Figure 17: Schematic representation of an ACTA measurement cycle. 1: Formation of bubble and contact with particle bed. 2: Movement to viewing window for image capture. 3: Movement to collection bin for particle collection. 4: Flushing and movement back to untouched particle bed. 5: Submergence of needles and new bubble formation.* (Javor et al., 2016)

### 3.1.3 Moving components

The movements of the various components are accomplished with three actuators, as is depicted in Figure 18. These actuators and their controllers are listed in Table 1. In blue are shown the respective parts of the actuator names that will be used in this work to refer to them. All three original actuators as well as the replacement actuator and all their controllers were manufactured by Physik Instrumente (PI) GmbH & Co. KG. The particle bed is prepared by depositing particles in front of a shovel, which then moves along the length of the pool to spread the particles and create the bed. The height of this shovel is controlled by the MP-15 actuator. The V-273 actuator moves the needle array vertically. Based on the user-defined measurement parameters, a trapezoidal wave function is generated and preloaded onto the C-413 controller. This wave function is then used to define the vertical motion for the contact between the bubble and the particle bed during each cycle. This method allows for high-precision movement during these vital moments. All other movement commands are sent from the PC to the C-413 and the SMC pollux in real time. The vertical movement data of the needle array is accurately recorded and saved for each cycle. This data can be used later for calculating the true movement distance and velocity. The shovel, the needle array and their actuators are all assembled on a stage, which can be moved horizontally by the PLS-85 actuator.

*Table 1: The various actuators that move the ACTA components and their controllers. In blue is shown the names that will be used in this work to refer to the various parts.*

| **Movement** | **Actuator** | **Controller** |
|---|---|---|
| Needle Array Vertical | V-273 PIMag® Voice-Coil-Linearaktor | C-413 PIMag® Motion Controller |
| Shovel Vertical | MP-15 Micro Pusher | SMC pollux SMC-series |
| Shovel Vertical Replacement | MP-20 Micro Pusher | SMC pollux SMC-series |
| Horizontal | PLS-85 Precision Linear Stage | SMC pollux SMC-series |

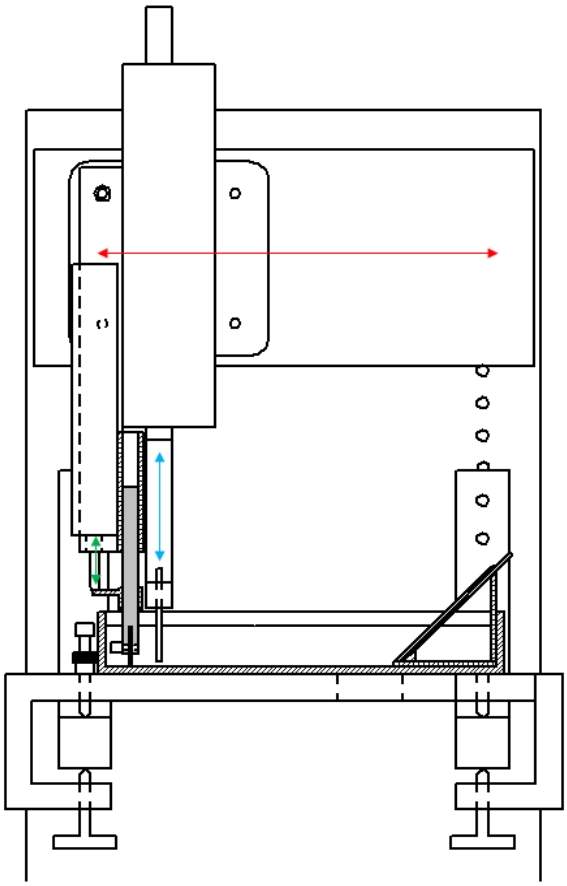

*Figure 18: Schematic depiction of the ACTA. The arrows depict the axes of movement. Blue: Vertical movement of the needle array. Green: When the shovel is calibrated according to procedure this actuator presses against a locking piece attached to the shovel shaft, thus vertically moving the shovel. Red: Horizontal movement of the shovel shaft, the needle array and their actuators. Original schematic by D.Sc. M. Aspiala. Edited for this publication.*

### 3.1.4 Collecting the particles

For the collection of the particles, a metal cover plate is slid onto the collection bin, which is then hooked in place in the ACTA pool. During measurements, the needles and the attached bubbles enter the bin through the six holes in the cover plate. Once inside, additional air is pumped to increase the size of the bubbles until they detach from the needles. The bubbles, now too big to exit through the holes in the metal cover plate, float to the surface of the water inside the bin where they burst. The particles then settle onto the bottom of the collection bin while the needles are moved back to the particle bed for another cycle. The bin and the particle collection mechanic can be seen in Figure 19.

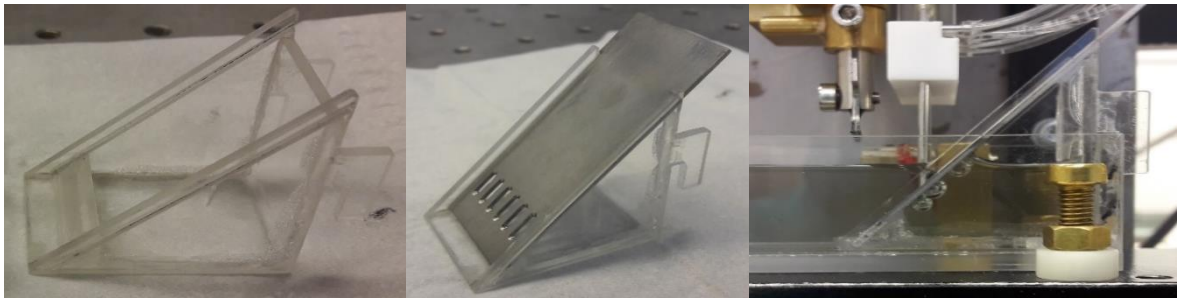

*Figure 19: Three photographs of the plastic collection bin and its cover plate.*

### 3.1.5 Calibrating the shovel

The particle bed is created with the use of a shovel. This shovel is shown together with the tips of the needle array in Figure 20 and in Figure 21, respectively in a side view and a front view of ACTA. To ensure the particle bed is created at the correct height, the shovel is calibrated by attaching a calibration piece to it. This piece aligns both the tilt of the shovel and its overall vertical position with the needle array. During calibration, the V-273 actuator is set to a standard position of -10 mm. A screw is then tightened in the vertical locking piece, which aligns the calibrated position of the shovel with the zero position of the MP-15 actuator. This alignment is depicted schematically in Figure 22. Afterwards the calibration piece can be removed. With this procedure completed, the MP-15 moves the shovel to the correct height when a certain particle bed thickness is set. It is important that the shovel is moved to the exact position where a bed of that height should be according to the ExperimentalController VI that sets the movement of the needle array. If this initial calibration is performed incorrectly the expected position of the bed surface will not be the same for the shovel as it is for the movement of the needles, in which case there will be a systematic error in the results as the needles will consequently be either too close or too far from the particle bed, resulting in a different amount of bubble compression than was intended, which in turn influences the attachment probability. Aligning the tilt of the shovel with that of the array ensures that all six needles have the same distance to the created particle bed.

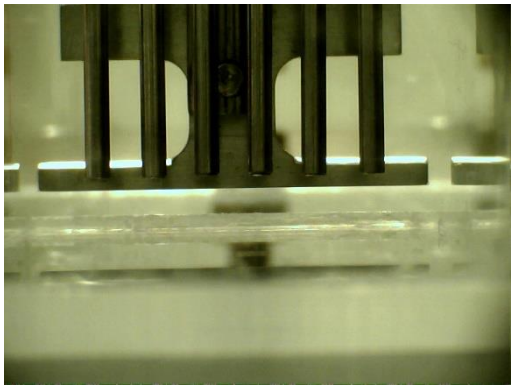

*Figure 20: The shovel and array of needles as seen in a side view of ACTA from the side of the collection bin. The shovel is aligned to the tilt that the array has with respect to the bottom of the pool*

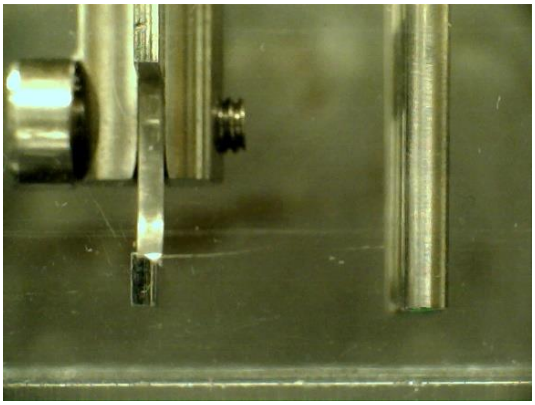

*Figure 21: The shovel and array of needles as seen in a front view of ACTA.*

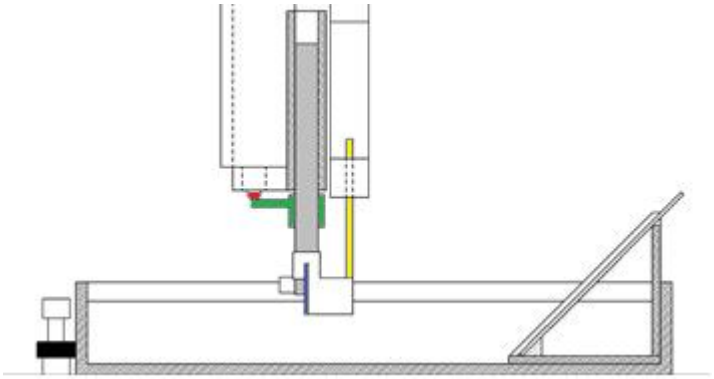

*Figure 22: Schematic of the original ACTA design showing the calibration of the shovel. Front view showing shovel (blue), needles (yellow), calibration piece (white), vertical locking piece (green) and PM-15 actuator (red). Original schematic by D.Sc. M. Aspiala, edited for this publication.*

## 3.2 ACTA preparation work

### 3.2.1 A note on LabVIEW

Regarding the coding part of this thesis, a preliminary note is in order. LabVIEW is a graphical coding environment in which the user creates so-called Virtual Instruments (VIs). Each VI consists of two screens, the front panel which allows for user interaction with the Virtual Instrument when it is running and the block diagram which is in essence the code making up the program. By linking VIs together with operating lines, bigger, more complex VIs are created. Figure 23 shows the current front panel of the ACTA operating VI. Example parts of the code can be seen in Figure 24 and Figure 25. As LabVIEW is a visual based coding environment, the code can appear exceedingly complex and quite messy due to the various lines connecting the VIs. Due to the lack of a zooming feature, several large PC screens would be needed for showing only the top level of the ACTA operating block diagram in its entirety and showing the code in image form in this work would take up immense amounts of space. Even then, every single sub-VI would have to be explained separately as their purposes cannot always be deduced from the pictogram. In addition, each of the pictograms itself often contains multiple other layers of sub-VIs. In any case, the LabVIEW coding is not the focus of this work. It is considered as just a tool with which to operate ACTA and change its features. For these reasons, an explanation of the code is beyond the scope of this work. The following sections will mention which additional functions have been added, but will refrain from explaining exactly how.

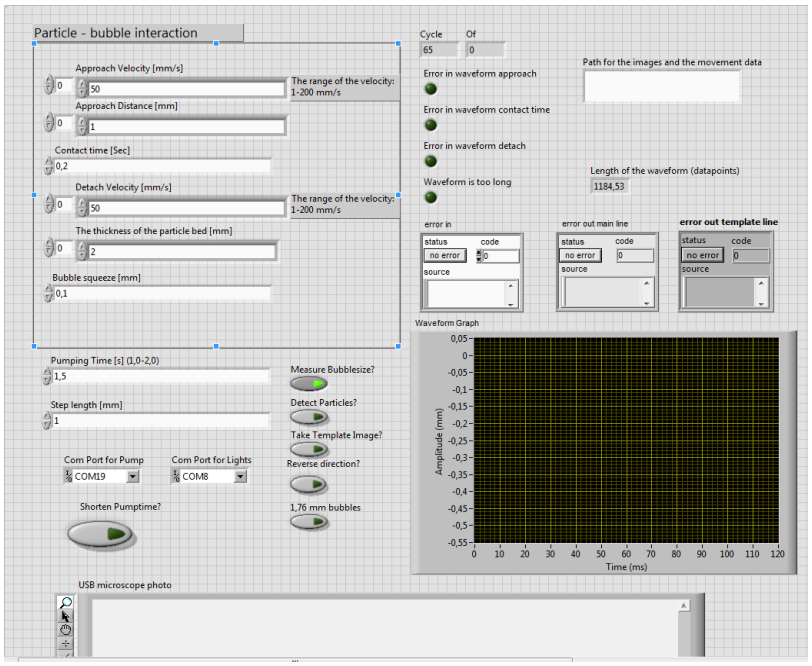


*Figure 23: The Front Panel of the main ACTA operating VI. This panel allows for setting the various operating parameters and options as well as such things as the data saving location and device connection ports. It also shows the movement graphs and the photographs taken while the device is in operation as well as any potential error messages.*

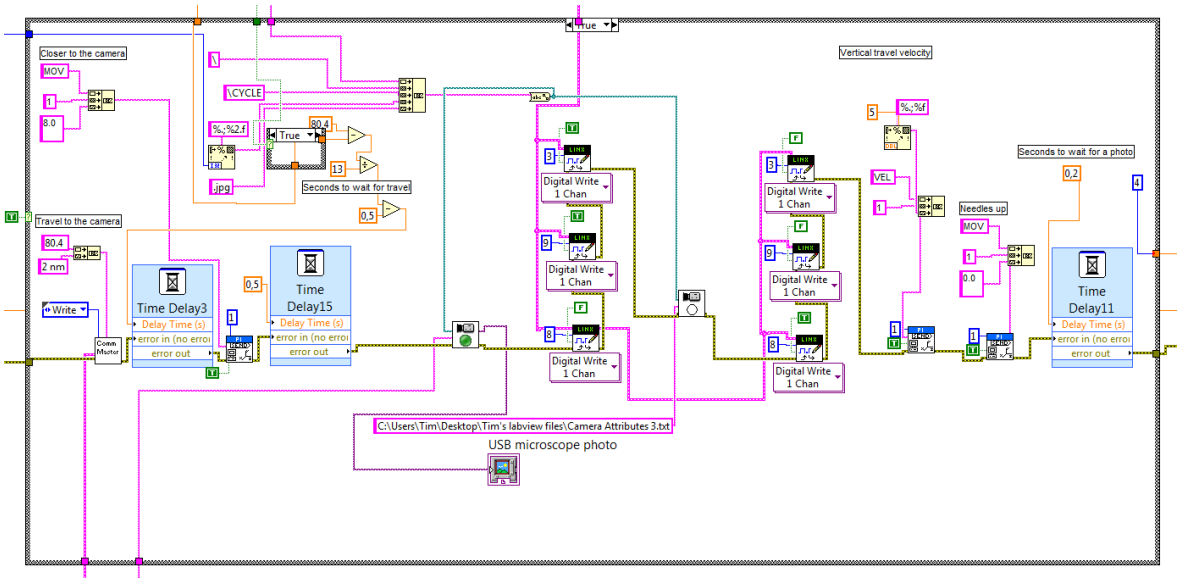


*Figure 24: Example part of the topmost layer of the main ACTA operating code block diagram. All square pictograms are sub-VIs that can contain multiple layers their own block diagrams. The displayed part of the code is responsible for making the photographs and providing the correct camera settings and lighting options for each of the two photographs.*

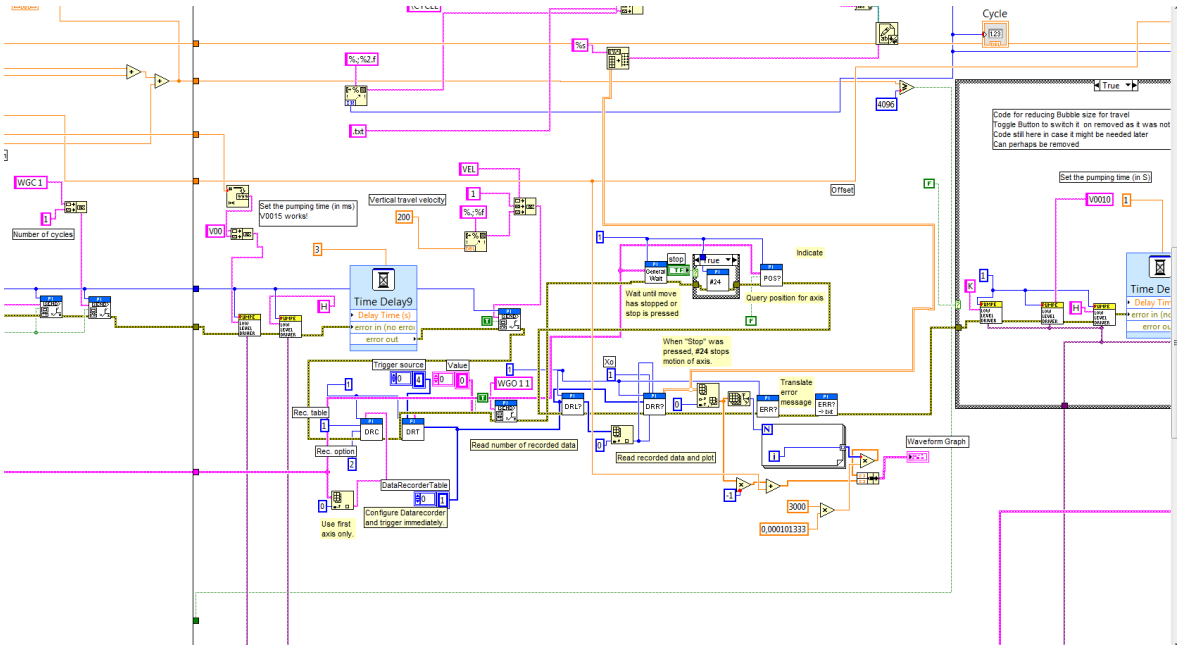


*Figure 25: Example part of the topmost layer of the main ACTA operating code block diagram. All square pictograms are sub-VI's that can contain multiple layers their own block diagrams. The displayed part of the code is responsible for saving the movement data of the V-273 actuator controlling the vertical movement of the needle array.*

### 3.2.2 The new camera & bubble size measurements

Immediately at the start of this thesis, the first important changes were made to the hardware and software of ACTA. The original camera that was used to take pictures of the bubbles was a VEHO VMS-004D - 400x USB Microscope with a resolution of 2 MP. This camera was replaced by an IDS UI-1580LE camera with a 4.92 MP resolution fitted with a Tamron 23FM25SP lens. The increase in image resolution allows for better bubble size measurements and easier determination of whether or not particles have attached to the bubble. The mount for placing the new camera was already prepared but due to an error in its design, the camera was rotated 90 degrees with respect to the ideal position. This resulted in inefficient use of the camera resolution. It was replaced with a make-shift version that had the camera rotated correctly. The height of the mount and the focus of the camera were then adjusted so the widest parts of the bubbles were in focus. This would allow for a more accurate measurement of their radii. A comparison of image quality between the two cameras can be seen in Figure 26. The original VEHO camera was operated by a MATLAB script that had been integrated in the main LabVIEW code. The new IDS camera could be operated with LabVIEW code. New code was written to replace the MATLAB code. With the replacement of this code MATLAB was no longer necessary and ACTA could run solely on LabVIEW code.

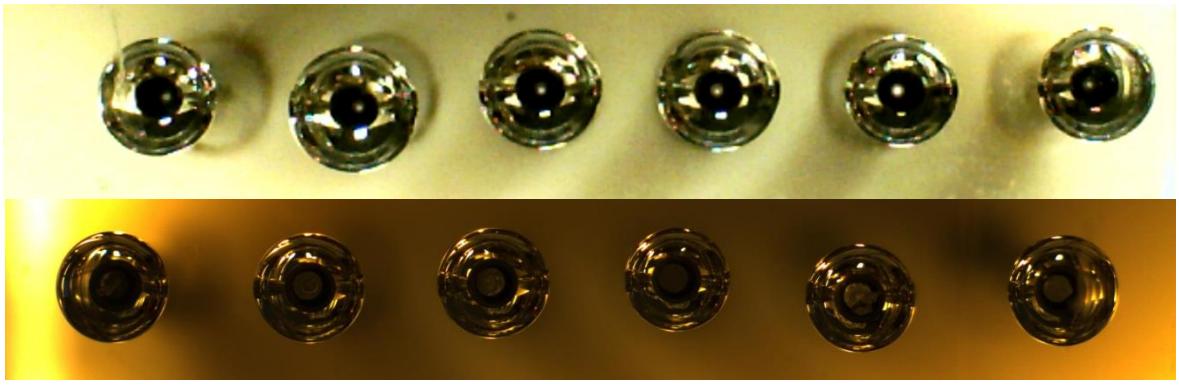

*Figure 26: Image quality comparison between the original VEHO camera (top) and the new IDS camera (bottom). The change in lighting is a result of different recording settings.*

Aside from taking photographs and saving them, this new code was made to load various predetermined camera settings from a .txt file, measure the radius of the bubbles and export this measurement data into Microsoft® Excel™ files. Figure 27 displays how the bubble size is measured using the LabVIEW Vision Assistant image analysis toolbox. The bubble size measurement code works by transforming the taken images into greyscale and then analysing a certain pre-set area of the image (in between both green circles) for contrasting edges between light and dark pixels. Using several predetermined criteria the area is then analysed along each radial blue line and the point best fitting the criteria is selected (yellow dots). A circle (red line) is then drawn that best fits all the selected points. The size of this circle is calculated based on calibration images.

Choosing the settings for the camera and the circle search criteria was a challenge. The created bubbles can vary in size between cycles and a different bubble size results in different light reflections on the edges of the bubble. These changes in lighting make the consistent determination of the location of the bubble edges difficult. As a result of the placement of the LEDs, the bubbles on the side needles are often more illuminated than those that are in the middle of the image as can be seen Figure 26. Due to this there were many attempted settings in which either the side bubbles were too light or the middles ones were too dark. In theory it is possible to take multiple images with various settings, to allow for the best possible lighting for each separate bubble. This would however result in lengthy experimental and data analysis times in addition to a large increase in the combined size of all collected images. Therefore, camera settings had to be found that allowed for acceptable image analysis for all bubbles at once. Various light and camera parameters such as exposure time, brightness, and contrast levels were examined to find those that would allow for the best quality image for analysis. Relatively dark images with short exposure times could be analysed the best, as there was less reflection of light off the bubble edges, which made them easier to detect. The difference in lighting of the various bubbles could be compensated for a bit by setting slightly different bubble size measurement parameters for each bubble. The final parameters were chosen by visually examining multiple images and finding those settings that consistently resulted in a good fit for various sizes of bubbles. The image shown in Figure 26 (bottom) is made using the parameters that were deemed the most effective. The consequences of using this approach regarding the measurement errors are discussed in Section 5.2.

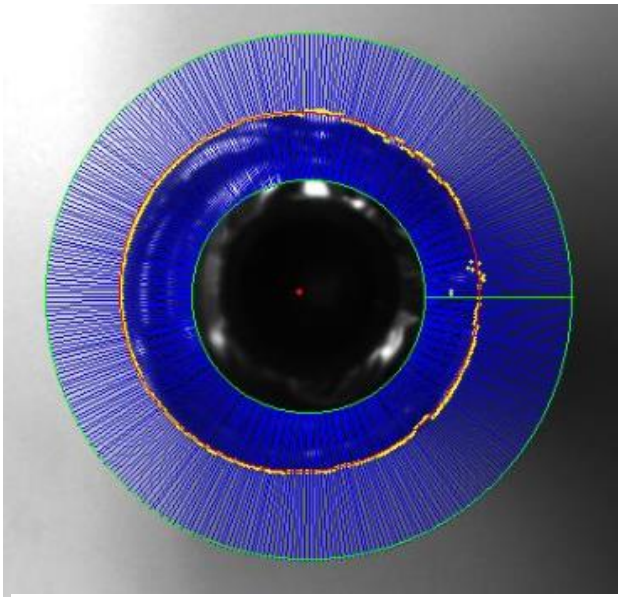

*Figure 27: Image depicting how the size of a bubble is measured. Green lines define the boundaries of the search area. Blue radial lines are the search grid. Yellow dots are those points that best fit the search criteria. The red circle is the circle that best fits the yellow dots, whose size is subsequently determined by comparison with a calibration grid image.*

### 3.2.3 The calibration grid

For the measurement of the bubble sizes a calibration photograph was needed. A 1x1 mm dot grid was created with Adobe Photoshop and subsequently printed on photo paper. Due to the use of photo paper, the grid could be printed with a high resolution, which is important for the accuracy of the calibration. Photo paper is quite thick and water resistant. This meant the grid could be submerged without it sagging or breaking, which would have invalidated the calibration. For an optimal calibration, the grid should be at the same height as the widest part of the bubble because this is the circumference that is being measured. The dot grid was attached with double-sided tape to the bottom of the calibration piece as shown in Figure 28. This piece can be attached to the shovel and is used in calibrating its vertical position. It also ensures it is tilted at the same angle as the needle array which is useful for making an accurate calibration image. From the extension of the V-273 actuator at the moment the photographs are taken and the expected bubble size, the approximate location of the middle of the bubbles was determined. The double-sided tape and grid

paper add 0.4 mm to the thickness of the calibration piece. With this value known the calibration dot grid could then be placed at the correct height by moving the shovel with the MP-15. The PLS-85 was used to position the grid so that it overlapped with the horizontal location of the bubbles during a photograph. The pool was filled with water and several photographs were made of the grid, similar to the one shown in Figure 29. Different camera parameters and lighting settings were used for the various photographs. The sharpest photo with the best lighting was chosen and loaded to the LabVIEW Vision Assistant image analysis toolbox. A calibration image was made according to the 'Distortion Model: Polynomial (K1, K2, K3)' model. The program detects the location of all the black dots. The user then indicates that each of these dots is 1 mm from the other and the program calculates the distortion of the image and how to correct it. This data is saved and used to calculate the real size of the bubbles on any subsequently acquired photographs. The model corrects the pictures for lens distortion and the differences in height due to the tilt of the needle array. The mean error of the calibration image was 0.0050 mm and the standard deviation of the model is 0.0014 mm.

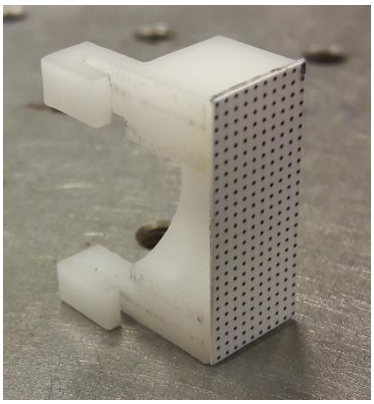

*Figure 28: Photograph showing the Teflon calibration piece used to calibrate the height and tilt of the shovel. The piece is tilted on its side to show the calibration dot grid that is taped to the bottom of it.*

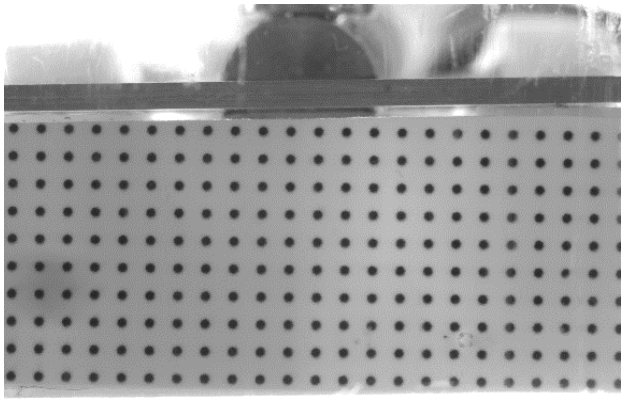

*Figure 29: Calibration photograph showing the shovel as seen from below and the calibration dot grid.*

### 3.2.4 New needles and optical fibres

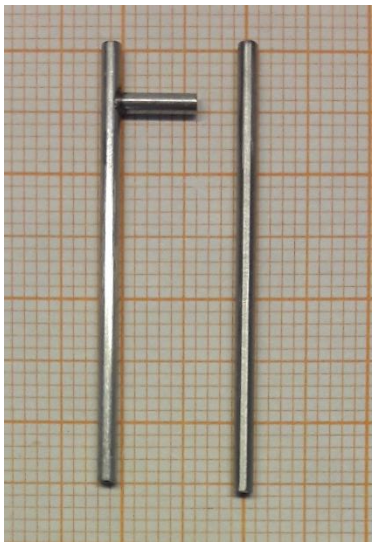

*Figure 31: Left: New needle with additional input for optical fibre. Right: Old Needle.*

After the addition of the new camera, the second large upgrade made to the ACTA device was the installation of new needles that accommodated the placement of optical fibres inside of them. The difference between the new needles and the initial needles can be seen in Figure 31. In the new needles, the optical fibres enter from the top and the air hoses are attached to the perpendicular part. In the initial build of the device, it had been difficult to discern any attached particles, partly due to the low image quality and partly due to low contrast between the particles and the bubble. By having an optical fibre inside each needle, with the other ends bound together and attached near a green LED light, it was possible to have the needles and the created bubbles lit from the inside. This allows for much greater contrast between attached particles and the background. With the addition of the optical fibres, the ACTA operating code was altered so a second photograph was taken with the optical fibre LED turned on, no side-LED lighting and specific camera settings. This second photograph would be used for detecting whether or not particles had attached to the bubble while the original photograph would be used for bubble size measurements as described above. Both types of images made using their respectively chosen settings and parameters can be seen in Figure 30. Next follows a summary of the process of installing and fine-tuning the optical fibres and the various parameters related to them. In this and any future descriptions, the needles will be named Needle 1 to Needle 6. In images such as Figure 30, Needle 1 is the one located at the far left. This corresponds to the only needle that can be seen in the front view and the leftmost needle that can be seen in the side view of the needle array shown in Figure 32.

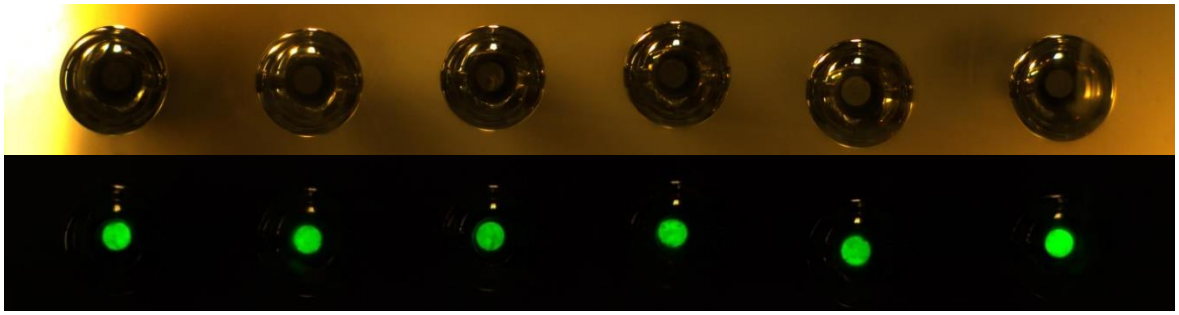

*Figure 30: Example of the two photographs taken of each set of bubbles. The top image is used for measuring bubble size while the bottom image is used for particle detection (no particles are present in this particular image). The needles are numbered 1-6 from left to right.*

The optical fibres had to be attached in such a way that they were unmovable to prevent any variation between images. Furthermore, the seal had to be airtight to prevent any leakage of air during bubble formation. After several unsuccessful attempts with silicon paste and Teflon tape the optical fibres were attached using CASCO LiquiSole glue. The use of this glue resulted in a seal that was airtight, but still flexible enough for the fibres to bend a little during assembly and ACTA operation. The array of needles with the attached optic fibres and air hoses are shown in Figure 32. The glue seal is relatively easy to detach when enough force is applied. This was a major benefit as the final height of the optical fibres in the needles was determined by a lengthy process of trial-

and-error. The downside of using glue was that it had to harden overnight and therefore only one position of the fibres could be tested per day. Any leaks in the glue seal would take yet another day to repair. If the configuration was then determined to be unsatisfactory all glue had to be removed before the entire process was repeated. After removal of the glue it was necessary to meticulously clean the needles with ethanol and water both inside and outside as pieces of glue getting into the needles would have been disastrous for bubble formation and the overall cleanliness of the experimental setup. Although it is perhaps not an ideal permanent solution, the glue method suffices very well as a makeshift option in these initial trial stages of the device. Other options have been tested but none so far have been both practical and airtight.

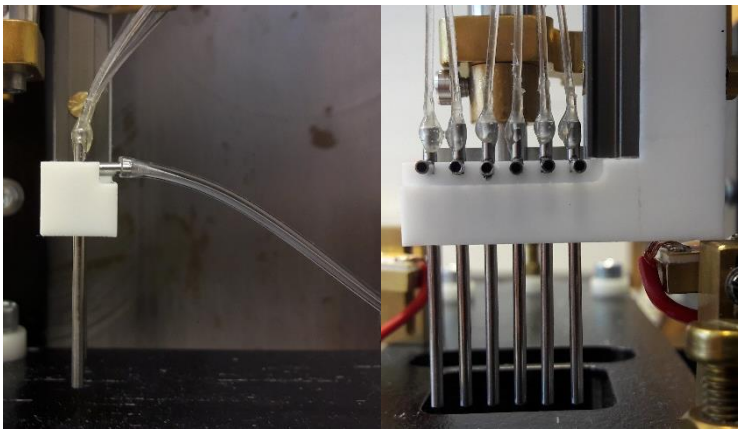

*Figure 32: The array of needles as seen in a front (left) and side (right) view of ACTA. The optical fibres enter from the top while the air hoses are attached from the side input. Air hoses have been removed in the right image to allow for a better view. In the side view, the needles are numbered 1-6 from left to right.*

The tips of the fibres were polished using sandpaper to remove any cracks and impurities from the surface that would show up in the images. This process was only partly successful as impurities can still be seen on the fibre surfaces in the images, as exemplified by Figure 30 (bottom). To have each fibre receive an equal amount of light from the green LED, they were bound together around a dummy fibre that was not placed in any of the needles. This was done because it was found that when bound together and placed near the LED, the middle fibre received a disproportionately large amount of light, which resulted in one needle appearing brighter than the rest.

*Figure 33: Effect of the optic fibre location in needle. All three images are of the same needle, taken with the same camera parameters and optical fibre LED power. The distances between the tip of the needle and the tip of the fibre are (l-r): 5 mm, 0.5 mm and 0 mm.*

In an ideal particle detection photograph the particles would stick out as highly contrasted black objects against a bright, evenly coloured green background. This would make them easily detectable by eye or with an automated program. The placement of the optical fibres within the needle is an important factor in the quality of the images as is shown in Figure 33. Initially the tips of the optical fibres were placed 10 mm above the bottom of the needles. In this configuration, the light was not bright enough to sufficiently and evenly illuminate the bottom of the needles and thus the particles were not adequately detectable. In the hopes of improving the quality of the lighting the optical fibres

were moved to a position 5 mm from the bottom of the needles. Trial experiments showed that this change in position did not result in a sufficient improvement of the lighting quality. Another issue was that there was ample space between the bottom of the needles and the tip of the optical fibres for so-called 'artefacts' to form. These artefacts are caused by water droplets that have gotten into the needles and consequently block the light coming from the optical fibres, resulting in images in which particles are difficult to detect. These artefacts often persevere for multiple cycles and tend to get bigger and more problematic over time. Their presence severely lowers the ease with which the images can be analysed for detecting attached particles. Although artefacts have been a problem with any configuration of the optical fibres, they were a worse problem with the fibres at heights of 10 mm and 5 mm than they are in the current setup. Examples of the problematic types of artefacts can be found in Figure 34.

*Figure 34: Six examples of the various artefacts that frequently occurred with the 10 mm and 5 mm optical fibre configurations.*

In an attempt to remove any space for artefacts to form the fibres were lowered to be as close as possible to the tips of the needles without sticking out. This configuration had as an additional benefit that the light from the optical fibres would be brighter and less diffused because the surface of the fibres was closer to the camera. Although this configuration did in fact prevent the presence of the artefacts that hindered particle detection and gave a backdrop for the images in which particles were visible with good contrast, it compromised the formation of the bubbles. The optical fibres are never perfectly in the middle of the needle but instead are usually touching one side, blocking the flow of air in that location. This blocking of one side, combined with the fact there was no space left in the tip of the needle, resulted in formation of bubbles at the sides of the needles rather than in the middle. Due to these issues, it was decided to place the optical fibres at a distance of 0.5 mm so they would be as close as possible to the needle tip while still leaving room for normal bubble formation. This setup is the one that was found to be the most successful overall in terms of the amount and invasiveness of artefacts, the amount of light coming from the fibres and the background contrast for particle detection. Artefacts are still present in this setup, but in this configuration, they less frequently impact the process of particle detection. This is due to the fact that there is no space for large droplets to form in the tip of the needle and any artefacts that do form are closer to the fibre, which means they often appear relatively transparent. Only two major types of artefacts form in the current setup. Both types can be seen in Figure 35. The first are droplets that are attached to the tip of the fibre itself, which do not pose a huge problem as they are largely transparent. The second is the crescent type which is a result of the optical fibre being positioned against the side of the needle. Some fibres block the airflow on one side. During the flushing stage, any liquid in the needles is then only removed from the

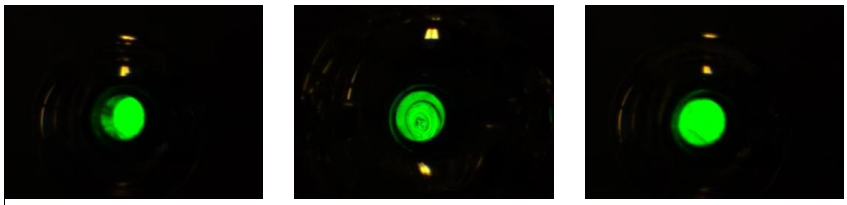

*Figure 35: The two artefact types occurring in the current setup and a clear image for comparison. Left: Crescent type artefact caused by blocked airflow. Middle: Droplet attached to the tip of the optical fibre. Right: Artefact-free image for comparison*

opposite side of the needle. Other attempts at preventing the formation of artefacts aside from lowering the optical fibres are detailed in Section 3.2.5.

When the height of the optical fibres had been selected an external power source was hooked up to the LED light and several experimental runs were performed. Different levels of current were used to determine which gave the best contrast settings for the detection of particles. The effect of LED brightness on the detectability of particles can be seen in Figure 36. When the current is too high the particles appear to be enveloped by the green background and when chosen too low both the contrast and the illuminated area are insufficient to easily detect particles. The selection of the ideal current was inconvenienced by the fact that from the camera point of view, each of the six needles is seen at a slightly different angle. Therefore the amount of light coming from each needle differs, making the selection of an ideal LED brightness relatively difficult. It is a trade-off between receiving too much light from the middle needles that point straight at the camera and not having enough lighting of the side most needles. In an attempt to compensate for this effect, the light-fibres were placed in such a way that the two least bright ones were placed in the middle two needles. This difference in the brightness of fibres is a result of the impurities on the fibre surfaces and their placement near the green LED. As this is different for each fibre there are slight variations in the amount of light that is emitted by each individual fibre. For each brightness setting of the LED, several different camera settings were tested to determine which combination resulted in the best quality images. A current of 0.42 mA was eventually chosen as the ideal amperage, after which resistors were soldered into the LED system so the LED would always operate at this approximate current and the rather bulky external power source could be discarded.

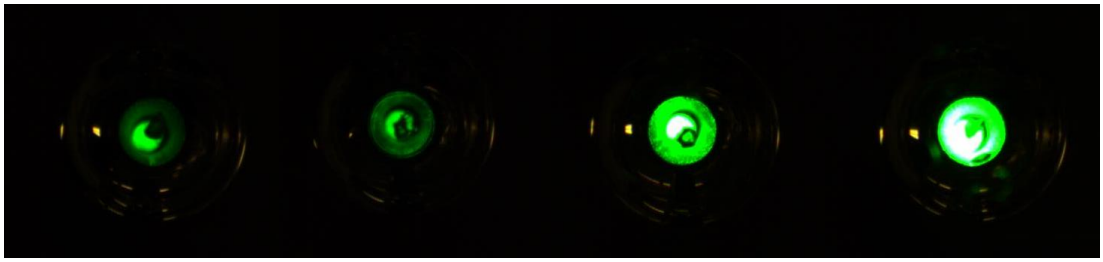

*Figure 36: Influence of LED operating current on the quality of the images. From left to right the LED is running respectively at 0.3, 0.42, 2.0, and 5.0 mA. A quartz particle is attached to the bubble in each of the images. In these images the optical fibre tip is 5 mm from the bottom of the needle.*

After the optical fibres had been placed at their final height and the optimal LED current and camera settings had been determined, it was found that in the cases of Needle 1 and 6 there were still problems with particle visibility. Due to gravity forces, the attached particles will always be present at the lowest point of the bubble. This means that for each needle, attached particles always appear in approximately the same position on the image which is convenient for quickly determining if attachment has taken place. How well this particle position overlaps with the green background of the optical fibre depends on the position of the needle with respect to the camera lens and how the fibre is positioned in the needle and therefore differs for each respective needle. This can be seen in Figure 37 where the locations of the attached particles are marked on an example image. In case they overlap well, the contrast is good and detection will generally be easy. When they do not overlap well, the particle will not appear in contrast to the green background and detection can be difficult, especially for smaller particles. In the case of Needle 1, crescent artefacts such as the one in Figure 35 consistently appeared, shading the location where the particles would be. In the case of Needle 6, the location of the particles on the image did not sufficiently overlap with the

position of the optical fibre. In both cases, a thin plastic strip with a thickness of 0.1 mm was cut and shoved inside the needle, forcing the fibre to a different position without affecting bubble formation. For needle 1 this opened up the left side of the needle, effectively shifting the artefacts to a position where they overlapped less with the particle location. For Needle 6 this resulted in better overlap between the particle location and the optical fibre.

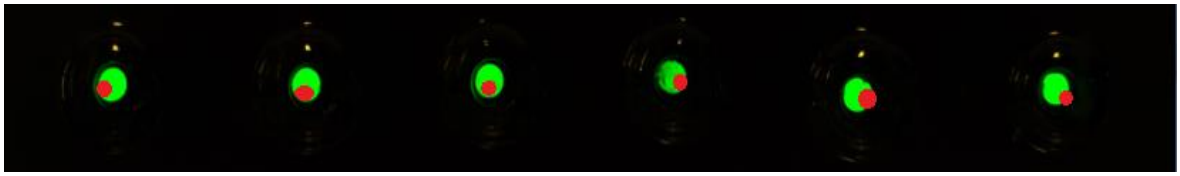

*Figure 37: Example particle detection image. The red spots indicate the location of attached particles on the image for each respective needle before adjustments were made to needles 1 and 6. The variations between needles are a consequence of a different viewing angle and variations in the exact positioning of the optical fibre within the needle.*

### 3.2.5 Artefact removal

It is believed that the artefacts can form either when the needles drop down into the liquid or during the flushing of the needles in the particle collection bin when the bubbles detach from the needles. At both these times, it is possible for small water droplets to shoot up into the needles and adhere to the inside of the needle or to the surface of the optical fibre. Once there, these droplets seem to facilitate the formation of further artefacts as they tend to grow or multiply for multiple cycles. The artefacts tend to disappear after several cycles when they have become so big they finally get removed during the flushing stage but by then they have often been present in multiple images. The artefacts were a severe problem in the 10 mm and 5 mm configurations. Although the artefacts are less invasive in the current ACTA build, they are still undesirable and have interfered with both manual and automatic image detection attempts. Several changes to the way the device operates were considered to prevent them from forming. The first of these was an increase in time of flushing that takes place between the collecting of the particles and the start of the next cycle. However, the needles were already being flushed with air before the start of each new cycle. Therefore, the artefacts had to be droplets that either form when the needles drop in the water or that are hard to flush out with the provided airflow. It was therefore assumed that a few extra seconds of flushing air through the needles would not result in a significant improvement in the artefact removal. In addition to that, each second added to the flushing step would be multiplied by 66 cycles. Therefore, any significant addition of time to the flushing step would add multiple minutes to the full measurement time. It was decided that any potential benefits did not compensate for the time that would be lost. Another measure that was considered was flushing the needles very close to the water level. During experiments, it could sometimes be seen that a film of water was present in the tips of the needles that could not be removed completely. The idea was that if flushing took place very close to the liquid surface, the water film near the tips would be attracted to the liquid phase instead of adhering to the needles. This method failed as the needle array is not aligned parallel to the water level as can be seen in Figure 38. This meant Needle 1 would be very close to the liquid surface while Needle 6 was not. The close proximity of the needles to the liquid

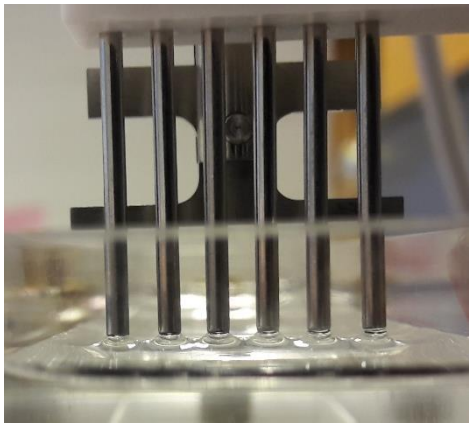

*Figure 38: Photograph of the array of needles close to the level of the water. The water can clearly be seen to adhere to the tips of the needles.*

surface also caused the water to adhere to the needles as can be seen in Figure 38. This effect was counterproductive as it only caused more water to be introduced to the needles. Coating the needles with a hydrophobic material to prevent the water from adhering to them was discussed as a possible option. This was eventually not done as the effects this would have on the formation of bubbles and the attachment of particles were unknown. In addition, it could not be guaranteed that this coating would not eventually end up in the investigated systems, thereby influencing measurements. Other ideas such as a physical cleaning stage using sponges or brushes were deemed impractical. Experiments with various velocities ranging from 1 mm/s to 200 mm/s were performed to examine the influence of the needles' speed when entering or leaving the liquid with respect to the formation of the artefacts. None of the attempted methods were however particularly practical or effective. As the artefacts were at that time not a severe problem it was decided to leave the system as it was and continue with preparing ACTA for real experiments.

### 3.2.6 The switch to PC

The initial plan was to operate ACTA from a laptop, which had the benefit of being easily transportable. When operated from a laptop the ACTA device could easily be taken to do in-situ experiments in actual flotation plants as per its concept design. Initially all LabVIEW VIs were coded on the laptop which ran LabVIEW 2016. Unfortunately, there turned out to be unsolvable issues with the amount of data coming from the new camera. The large amount of data produced during the experiment could not be processed by the laptop hardware. This caused the situation that taking photographs with the camera while there was any other open connection to a USB-based device, resulted in drastically lowered image qualities and eventually in software crashes. Operating ACTA requires six USB-connected devices, respectively the camera, the PLS-85 actuator, the V-273 actuator, the MP-15 actuator, the air pump and the LED light control. Abandoning any of these devices was impossible and the issue itself was seemingly unsolvable by merely updating the laptop's software. Therefore, the laptop had to be abandoned and a desktop PC was used instead. This PC was running LabVIEW 2015 while the VIs made on the laptop were from the 2016 version. This version was not backwards compatible, so all code written up until that point had to be remade.

### 3.2.7 Automating the bubble size measurement

For automatic measurement of the bubble size, a search area had to be defined in which the program analyses the image. To measure all of the bubbles there needed to be six different search areas, which can be seen as the green lines in Figure 27 and Figure 39. During testing, it was found that the way in which the ACTA is assembled has an influence on the precise location of the needles. Therefore, each time ACTA was reassembled, small variations occurred in the exact locations of the needles in the image. This occasionally caused the search grids to be in the wrong location, which

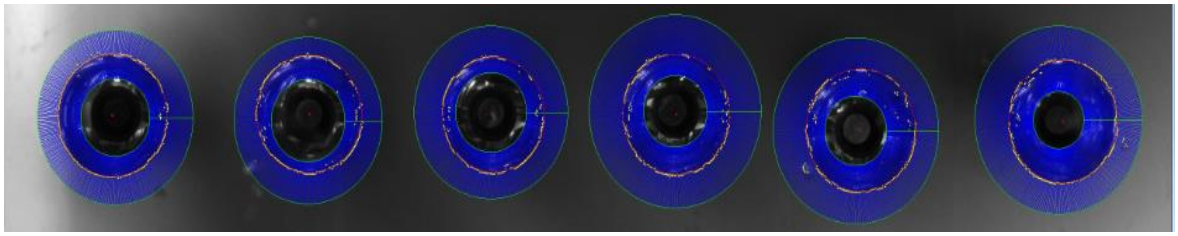

*Figure 39: Example of a bubble size measurement image after processing. Green lines define the boundaries of the search area. Blue radial lines are the search grid. Yellow dots are those points that best fit the search criteria. The red circle is the circle that best fits the yellow dots, whose size is subsequently determined by comparison with a calibration grid image.*

interfered with the consistent measurement of the bubble sizes. These variations in the location are most likely caused by the Teflon piece that holds the needle array. The white Teflon array holder can be seen attached to the grey V-273 actuator in Figure 32. This piece is attached to the actuator with two screws. Teflon is a relatively soft material and, combined with how well the screws are tightened, this leaves room for discrepancies in the exact horizontal location. Due to the large amount of zoom being used in these images, a small variation in needle location can result in them being in a significantly different location on the image. Potentially they could be too far from the search area for efficient measurements to be possible. To counter this issue the operating code was changed so that at the beginning of each ACTA measurement a template image is made of one set of bubbles. This template image exactly similar to the particle detection images. The template is analysed for the exact location of the six green spots of the optical fibres to determine the position of the needles on the image. The bubble size search areas are then automatically placed in such a way that they will overlap with the location of the bubbles. As the location of the needles only changes as a result of dismantling and subsequent rebuilding of the device, one template image at the start of each experimental run suffices for this purpose.

### 3.2.8 An attempt at automation of particle detection

In a measurement with ACTA, the most important thing to determine is whether attachment of particles has taken place. For this, all the obtained photographs have to be examined. In this work, attachment is defined as the attachment of one or more particles to a bubble as is described in Section 5.1. An attempt was made at automating the detection of particles. The addition of a particle detection VI would drastically increase the user-friendliness of the device as well as save significant time now spent on checking each image and counting the particles manually. In fact, such a program is essential for the ACTA device to be eventually usable as a truly effective measurement tool. One of the main reasons for the decision to revert back to manual counting was the fact that the created code was too unreliable, which meant that all results had to be counted regardless to check the effectiveness of the code. At one point, an accuracy of 99.5% was achieved for pre-made sets of images containing 1560 different bubbles. When this code was tested with new sets of images however, the results were suddenly much less promising. This was the main problem with this sub-project. For any set of images the parameters of the detection program could be altered and sculpted to reach near-perfect accuracy of detection, but once new images were measured these parameters were no longer reliable. Even though the automated particle detection project was eventually abandoned due to time restraints, a short summary of attempted techniques will be given below.

Most of the attempts were based around writing a particle detection VI that would automatically detect any attached particles by comparison of the optical fibre images with the template image taken before the start of the experimental run. As this template image is made before the experiment starts there is no liquid in the needles and any impurities of the optical fibre surfaces present in that image would not be mistaken as particles in the subsequent images. The program compares greyscale images against a template image and finds areas that are darker than in the template. These darker areas are then shown separately in a red-black binary image. This process can be seen in Figure 40. As the particles block part of the background light when they attach, in theory all particles show up in this this comparison image. But making the distinction between particles and artefacts, that also block the background light proved to be a challenge. It often was the case that when the limits were set too strict, small or semi-transparent quartz particles were

not detected. When the parameters were changed, artefacts were identified as particles. The particles always appear in the same approximate location which was helpful in this process.

Several different methods of filtering out artefacts were tried, including filtering the binary image based on particle size, sphericity and elongation factor. The best results obtained were when the images were analysed in two separate steps. A comparison step as shown in Figure 40 was used to show whether there was an object that had not been present in the template. A separate analysis step would analyse whether there were any angular objects present in the unprocessed image shown in Figure 40 (middle). The reason this worked so well is that the artefacts are generally circular in shape since they are water droplets, while clearly the particles are more angular in shape. Angles were sometimes found in reflections of light and the points of the crescent artefacts as well however, causing false positive measurements. Another problem was that in some cases when the program was executed to analyse multiple images, it did not detect particles without there being any clear reason for it. In these cases, particles were detected when the images were opened and examined one by one within the Vision Assistant toolbox but not when the code was executed automatically even though the same parameters were in use. This was a problematic and frustrating issue for which no solution was ever found.

*Figure 40: Example of one of the attempted methods for creating an automated particle detection system. Top: Template image. Middle: Image with attached particles. Bottom: Comparison between particle image and template image. Areas that are darker in the middle image with respect to the top image and that fit that fit the pre-set parameters are depicted as red. The top and middle images are transposed into greyscale from their original colours as the comparison program only works with the greyscale format.*

Another series of attempts was based around the Particle Detection VI that is part of the LabVIEW Vision Assistant toolbox. This VI can analyse images, recognize particles or items from them and categorize these as a certain class of objects. The recognition of these objects is based on template images that have been 'taught' to the program by the user to show which shapes belong in which category. Attempts were made to teach the program the difference between how the green optical fibre background of the bubble detection images looked with and without attached particle based on dozens of bubble images. Furthermore, categories were made to distinguish between particles and artefacts. However, the varied nature of the particle shapes, the impurities and cracks on the fibre surfaces and the presence of various randomly shaped artefacts that may or may not have overlapped with a particle prevented this from being effective. The key to the success of these kinds of programs is often a database containing thousands of comparison images so an attempt with a larger set of templates is recommended as future work.

In the end, the attempts to create a VI that produces a reliable automatic account of attached particles proved unsuccessful. The varied and small nature of the particles and the presence of

artefacts and cloudy liquids which lower the quality of the images, made it so that designing a program that can reliably and unconditionally detect particles while ignoring artefacts for all sets of images is seemingly outside the scope of both LabVIEW's Vision Assistant toolbox and the author's coding skills. After sinking several weeks into achieving a detection system without obtaining definitive results it was determined that with the thesis schedule in mind, it would be a more effective use of time to abandon the development of this automatic particle detection code. For the time being, researchers working with ACTA will have to rely on manually counting the number of bubbles with attached particles.

### 3.2.9 Reversing the direction of movement

The ACTA movement direction during measurements was reversed from starting at the far end of the bed, to starting at the side of the collection bin. Although not a particularly large or difficult adjustment it means that the device doesn't move over any untouched particle bed after contact between the bubbles and the bed. Consequently, no particles can accidentally be dropped on untouched particle bed. This prevents any influence on the results of future cycles. This change is schematically depicted in Figure 41.

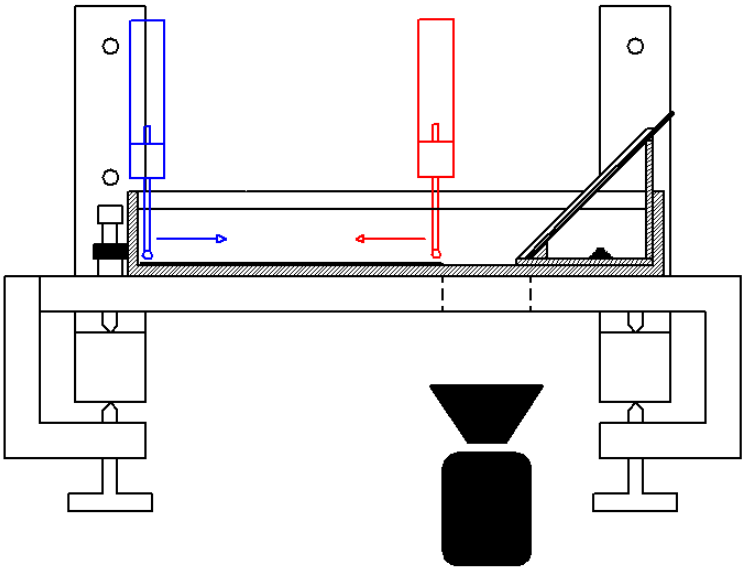

*Figure 41: Schematic depicting the starting point and the direction in which the array of needles progresses stepwise along the particle bed during an experimental run for both the new (red) and original (blue) situations. Original schematic by D.Sc. M. Aspiala. Edited for this publication.*

### 3.2.10 Bubble height calibration

The radius of each bubble is measured automatically. The measured radius is that of the bubble as seen from below. However, in measurements with ACTA the more important parameter is the bubble height, defined as the vertical distance between the bottom of the bubble and the tip of the needle. In measurements with ACTA, a single bubble height is assumed for all created bubbles. The movement parameters for the V-273 actuator are calculated based on the users' choices for this assumed bubble height, the particle bed height, bubble compression, and movement speed. When the true bubble height varies from the expected height (which it inevitably does, due to the fact that created bubbles show a size distribution, as can be seen in Chapter 6) the actual compression of the bubble into the bed differs from the set value. A different bubble compression in turn results

in a different bubble contact area, applied load and contact time, which affects the probability of attachment. As long as the bubble height is known however, all these values can be calculated.

It cannot be assumed that the bubbles are perfectly spherical. There was no practical way to place an additional camera that allowed for a front view photograph of all six bubbles, so the height had to be calculated from the measured radius. To find the relationship between the two parameters, a calibration experiment was performed. As has been mentioned above, the created bubbles are not all the same size. Even though all bubbles are created by pumping air for 1.5 seconds, the resulting bubbles show a size distribution.

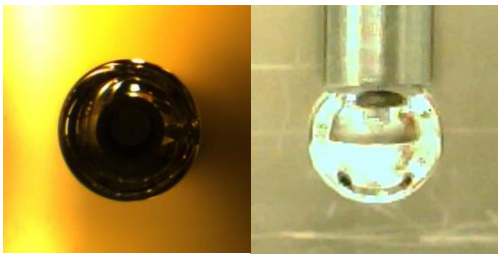

*Figure 42: The same bubble seen from below (left) and from the front (right).*

For this calibration therefore, 40 bubbles of various sizes were created and photographed both from below as in normal ACTA operation and from the front with the old VEHO VMS-004D - 400x USB Microscope. Although the quality of these photographs was less than ideal, the camera could be placed on a stand and be controlled from the PC so it could remain in exactly the same location for all photographs. One example of such a set of photographs is shown in Figure 42. A separate calibration image had been made for the measurement of the vertical height. Most of the bubbles were made by running the pump for either 1.4, 1.5 or 1.6 seconds as these pump times would result in bubbles that were the closest in size to the actual operating time of 1.5 seconds. Some 'extreme' bubbles were also created to account for the fact that during experiments on occasion very large and very small bubbles are formed. As they appear less frequently, and are generally filtered out during data processing, less of these extreme sized bubbles were made in this experiment than of the 'normal' bubbles. The photos taken from below were then analysed using the radius measurement code as it has been described above. No automated code existed for the front view photos so these were analysed one by one, during which the distance between the bubble tip and the needle tip was manually determined. An automated measurement program was written but proved ineffective due to the low resolution of the images. The measured radii and heights were plotted and a trend line was fitted to the data. A logarithmic trend resulted in the best fit, with an $R^2$ value of 0.9942. The results of this experiment can be seen in Figure 43. The obtained trend line would from this point on be used to calculate the approximate height of each bubble. The consequences of using an approximated relationship for calculating the bubble height is discussed in Section 5.2. The code was altered so that after each experiment both the height and the radius of each bubble would now be exported to the size data Excel file.

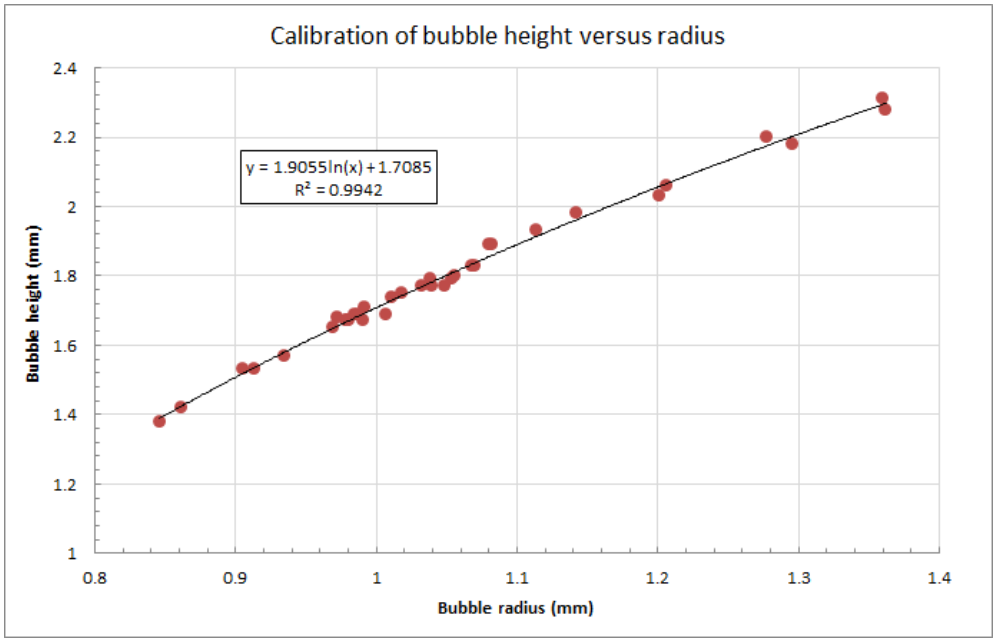


*Figure 43: Bubble height calibration graph plotting the measured radius against the measured vertical height. A logarithmic trend line has been fitted to the data.*

### 3.2.11 The measurement cycle limit

The bubbles created by ACTA show a size distribution. To examine if the measurement length had a clear effect on the size of the created bubbles, a measurement was started with a step size of 0.15 mm which should have resulted in the device running 434 cycles, a process that was expected to take around 5 h. A software crash occurred after approximately 2 h and 20 min, or 259 cycles, due to the PC memory running out. Changes were made to the part of the code regarding the storage of the acquired photographs. The code was altered in such a way that all photographs should have been removed from the program memory after they had been saved on the PC. To test the new additions to the code a program was written that took several photographs per second. This removed the need to run another extended ACTA measurement. For unspecified reasons, the program crashed at the exact same number of images. It seems that even though the program was written to discard any images from memory, LabVIEW would not free the available memory regardless. As the program was running, the memory in use could be seen to increase steadily until the inevitable crash. This problem only occurred in continuous operation of the program. Once a measurement was done and the program had ended, the memory would be freed. As 259 cycles is far past the currently used 66 cycles, the issue is not a severe problem. For a measurement with 259 cycles, a step size of approximately 0.25 mm would have to be used, in which case the area of contact between the particle bed and the bubble for any cycle would consistently be overlapping with that of the previous cycle. The attachment probability would therefore be influenced by previous cycles and the measurements would be pointless. For the moment, this problem is therefore irrelevant. It is however good to keep this limitation in mind. If ACTA is ever operated from another device a cycle limit check is in order to determine any possible changes in the maximum amount of possible cycles.

### 3.2.12 The length of the needles

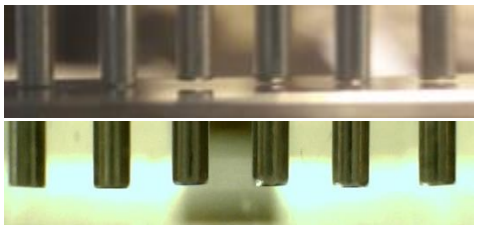

*Figure 44: Photographs of the tips of the needle array. Top: Metal plate pressed against needle tips before adjustment. Bottom: Needles after adjustment.*

During the installation of the new needles and their optical fibres it was found that Needle 3 was leaking at the weld where the horizontal hose input connects to the main part. This needle was therefore replaced with a new one that was airtight. During initial trial experiments it was observed that Needle 3 consistently had a significantly lower attachment probability than the other needles. On closer inspection, it was found that the replacement needle in question was slightly shorter than the other five. Bubbles made at Needle 3 therefore barely reached the particle bed and only the larger size bubbles had a chance to have particles attaching, which caused a lower overall probability. Using a scalpel, the Teflon array holder was altered to allow the needle to move slightly further downwards. It was impossible to entirely fix the problem as that would have caused too much damage to the holder. Figure 44 (top) shows a photograph of a metal plate pressed against the needle tips. From this image, the difference in length of Needle 3 is easily visible. Needles 1, 2 4 and 5 can be seen to touch the metal plate while Needle 3 clearly comes up short. Needle 6 is also slightly too short to touch the plate. The current position of the needles can be seen in Figure 44 (bottom). The situation after adjustment is slightly better but still not ideal. As can be seen from Figure 44 (bottom) there are still differences in length between the various needles and some appear to be slightly tilted. There is no way to change this without ordering an entire set of new needles that are all manufactured at the same time and then all simultaneously cut at the exact same length and tilt with the use of high-precision equipment. Plans to order such an array of needles are currently under consideration. The possible effects of the differences in needle height on the measurement results are discussed in Section 5.2.

### 3.2.13 The V-273 actuator movement graph

In the early stages of testing the ACTA device, a contact time of 200 ms was often used, as well as a large approach distance of 1 mm. As a consequence of this, the graph displaying the V-273 actuator movement data was compressed in such a manner that it seemed to relatively well resemble the ideal trapezoidal movement graph that is loaded to the C-413 controller. However, when a shorter contact time and approach distance were chosen it became clear that the movement of the actuator was in fact not at all linear. After increasing the size of graphs from previous experiments, it was found that these too, were not as linear as they had appeared when they were displayed on a small scale. An example of the non-linear movement of the actuator is displayed in Figure 45.

At several moments during the descent of the bubble towards the particle bed the actuator movement speed slows down and in some cases even comes to a halt for several milliseconds. This same phenomenon occurred during the retraction of the bubble. If this slowdown occurs when the bubble is already in contact with the particle bed this means the bubble contacts the particle bed for several milliseconds and is then pushed even further into the bed. This type of movement was deemed undesirable as there was no telling what the effects would be on the bubble-particle interaction. The variations in bubble velocity during the approach might cause additional deformation of the bubble surface. All this greatly complicates the characterisation of the interactions taking place and would if possible be best avoided. A constant approach velocity was

required to allow for a more easy approximation of the forces acting on the bubble and particles. It was believed that this nonlinear behaviour was the result of the PID controller governing the actuator velocity being badly tuned. This assumption is substantiated by the fact that most irregularities seemed to occur when the actuator was supposed to increase its speed or start slowing down. Using a Photron FASTCAM SA1.1 high-speed camera it was confirmed that the movement data recorded by the actuator was correct. In 15000 fps videos the actuator could clearly be seen to slow down mid-movement. The Photron FASTCAM Analysis motion tracking software showed a similar graph to that obtained from the actuator itself.

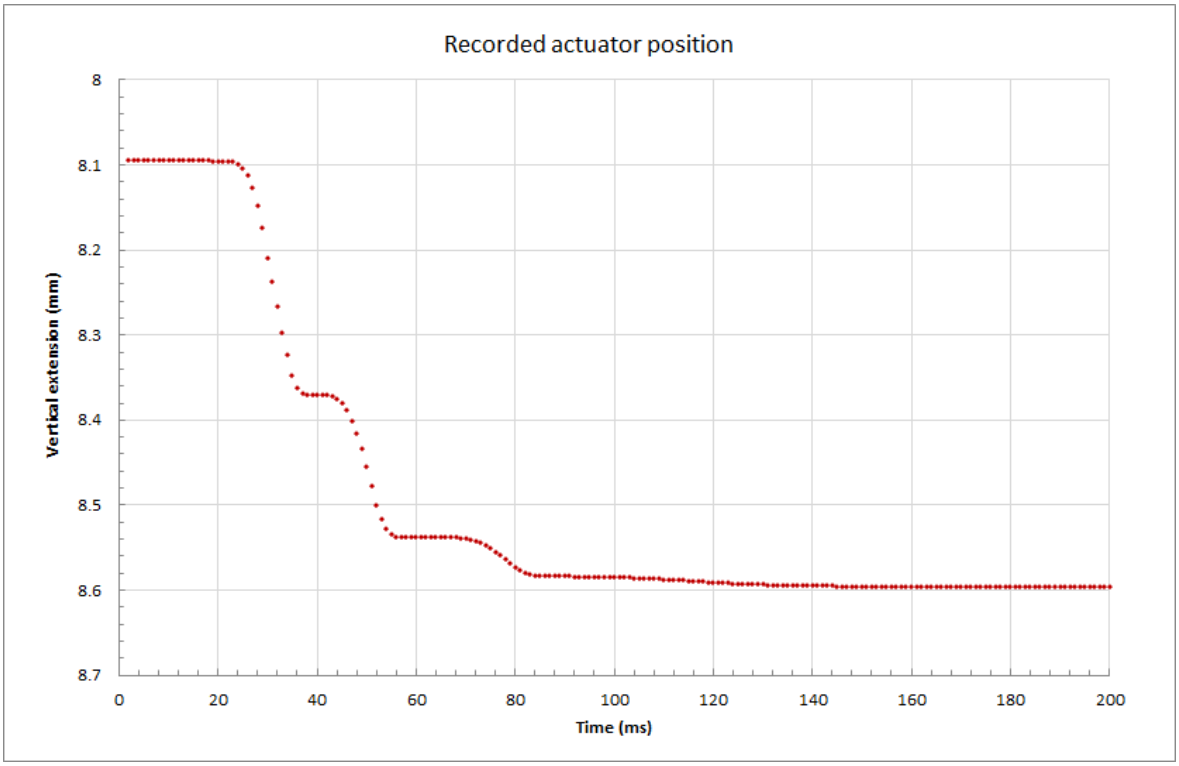


*Figure 45: Recorded vertical position of the needle array actuator plotted against time showing the non-linear approach. Only the approach part of the graph is shown.*

Several changes were made to both the device and the controller settings in attempts to smooth out the actuator movement. Tests showed that the addition of extra weights to the actuator resulted in a slightly smoother movement, especially near the final part of the descent as can be seen in Figure 46 and Figure 47 respectively. Overall however, the movement was still not completely linear. Three weights of 10 g each were manufactured that could be attached to the needle array actuator without blocking any of the device movement. This meant additional weight could be used in the actual measurements if no better solution was found. As the expected cause of the non-linear movement was the velocity PID controller, changes were made to the parameters but none had any clear effect. In hindsight, this turned out to be caused by the C-413 controller reporting the new values as being loaded while in fact a restart procedure was necessary for their true implementation. The engineers from PI then sent over a new parameter file. After loading this file however, the V-273 actuator started making a high-pitched sound and the movement was much faster than it should be. The power supply was quickly unplugged to prevent further damage and after extensive contact with the engineers from PI, it was decided the actuator would be sent back to their labs so it could be better configured. The request was made for the actuator to be tuned for rapid movements in the 0.5 mm movement range with an attached stage of 25 g. This 25 g stage

represents the needle array without any additional weight. ACTA was dismantled and the actuator and its controller were sent to the PI manufacturer in Germany. The five week period during which it was unavailable, no experiments could be performed. This hiatus is referred to as the maintenance break.

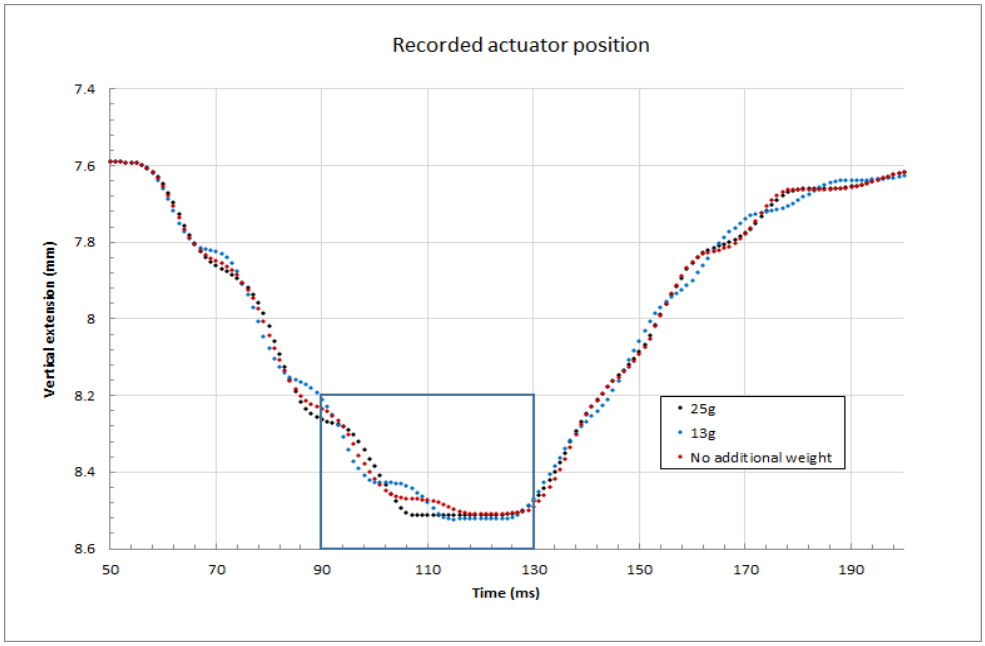


*Figure 46: Comparison of the recorded vertical actuator position plotted against time with and without the addition of extra weight to the needle array. The amount of weight added was respectively 25 g and 13 g. The same settings were used for all three movements. The blue rectangle indicates the area shown in close up in Figure 47.*

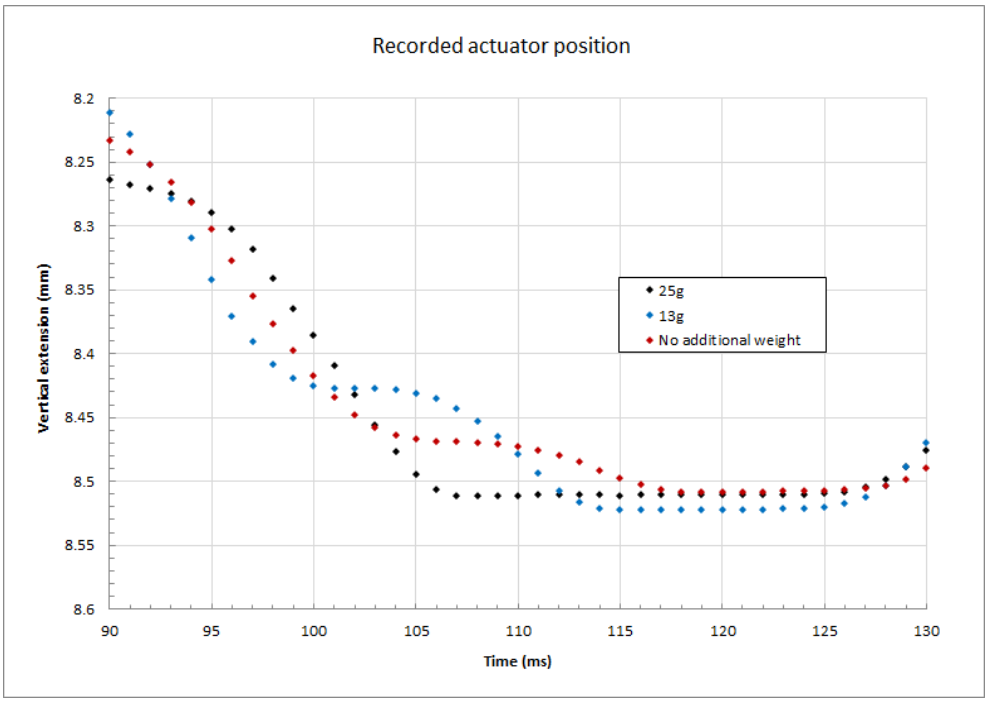


*Figure 47: Partial close-up of the graph shown in Figure 46. Comparison of the recorded vertical actuator position plotted against time with and without the addition of extra weight to the needle array. The amount of weight added was respectively 25 g and 13 g. The same settings were used for all three movements.*

## 3.3 After the maintenance break

During the break, some important changes were made regarding the replacement of the MP-15 actuator. Unfortunately, not much more could be done as the absence of the V-273 actuator meant none of the changes to the device or its code could be tested in practice. Only when it was back, could all the new parts be installed and the changes to the code and calibration procedures be implemented. Due to this it took another two weeks before experiments could be performed again.

### 3.3.1 Less abrupt movement

During the first few rounds of experimenting, it was noted that particles were lost between the moment the photograph was taken and the collection moment of the particles in the ACTA collection bin. The movement was relatively abrupt. The approximate directions of movement are depicted schematically in Figure 48. The diagonal movement was achieved by moving the needle array upwards with a velocity of 10 mm/s while the horizontal movement was set to 13 mm/s. To reduce the loss of particles the speeds were lowered to respectively 5 mm/s upwards and 8 mm/s horizontally. Reduced loss of particles would improve both the accuracy of the collected solids analysis and prevent the problem of fallen particles settling onto the camera area and subsequently interfering with the particle detection.

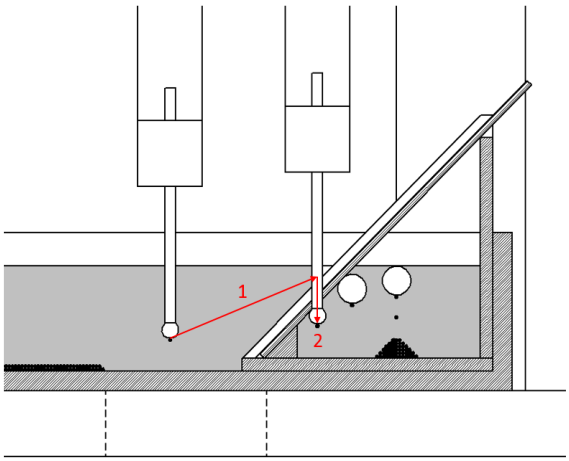


*Figure 48: Schematic depiction of part of the ACTA pool depicting the direction of the needle array movement after the photographs have been taken. Original schematic by D.Sc. M. Aspiala. Edited for this publication.*

### 3.3.2 Updated V-273 actuator

The first tests with the updated actuator showed that the movement had become significantly slower than it had been before the maintenance. Fortunately, it was realized quickly that the PI engineers had updated several key parameters without giving clear indication of this. One of these parameters was the servo cycle time which had been changed from its original value of 2.02666e-4 to 1.01333e-4. This key value indicates with which time interval the C-413 controller contacts the actuator and is used in the creation of the ideal trapezoidal wave function as well as in the calculation of the actual contact time. Once the code had been updated the movement of the updated actuator could be compared to the movement before the update. As can be seen in Figure 49 both the descent and the retraction movements had become more linear. With the new settings, the actuator no longer temporarily stopped moving halfway through the motion. Due to the increased servo cycle time, twice as many data points are collected which increases the accuracy of the true contact time estimations.

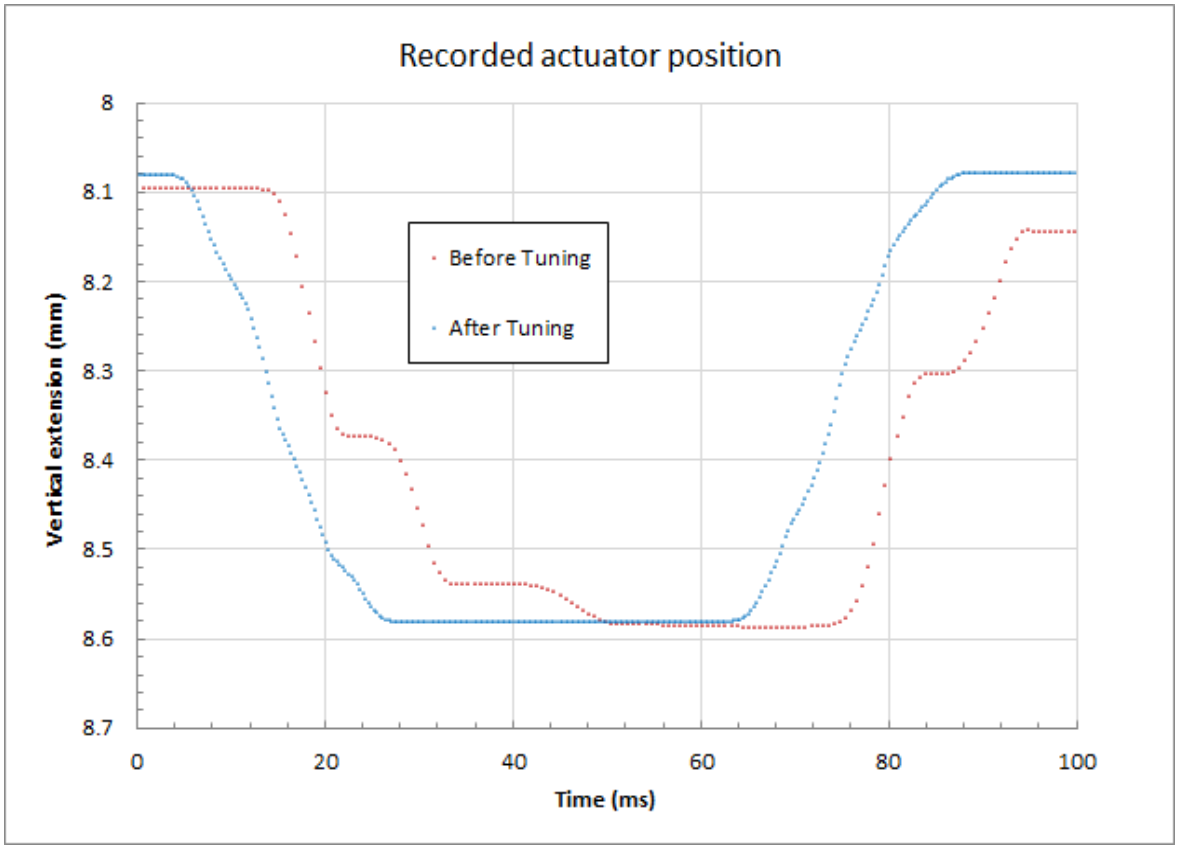


*Figure 49: Comparison of the recorded vertical actuator position plotted against time before and after the PID tuning. The same settings were used for both movements.*

### 3.3.3 Replacement of the MP-15 actuator

During the maintenance break several changes were made to the ACTA design, VIs and procedure. The most significant of these was the change of actuator controlling the vertical movement of the shovel. The original PI MP-15 Micro Pusher was replaced by a PI MP-20 Micro Pusher, which has the benefit of increased repeatability, movement speed and movement range. The frame that holds the actuator in place was adjusted to accommodate for the new actuator and its increased movement range. The increased repeatability should result in a more equal bed-height for various experiments, which is vital to the reproducibility of the results. The maximum movement speed of the MP-20 is 12 mm/s compared to the 0.1 mm/s of the MP-15.

Just after installation, the initial MP-20 actuator settings had to be adjusted as the position values it reported were seemingly random, it did not move at maximum speed, and the actuator could move beyond its intended movement range, resulting in damage to the actuator and potentially the setup. The settings were changed so the MP-20 performs an automatic calibration for the 0 mm point every time it starts up. In addition, the default velocity was set to the maximum of 12 mm/s and the maximum extension was limited to 26.44 mm.

### 3.3.4 The new shovel calibration

After each measurement, the pool is removed for cleaning. This is done by sliding it out of the ACTA. When facing the device from the front as in the view of Figure 22 the direction of movement is to the right. When the shovel was calibrated in this original design of the ACTA, its upwards movement is blocked by the vertical locking piece as illustrated in Figure 22. This meant it could not be moved

upwards far enough for the pool to be removed without spillage of liquid and the particle bed remainders. The locking piece had to be at that exact position due to the short movement range of the MP-15. Changing its location was not an option. To remove the pool, the locking piece had to be loosened. This meant that in between each experiment the shovel had to be recalibrated, leaving room for experimental variation.

The main benefit of the MP-20 was the fact that due to the extended movement range it was now possible to tighten the locking piece closer to the shovel itself. As a result, the shovel could be moved upwards far enough for the pool to be removed without having to recalibrate the shovel afterwards. This, in combination with the higher repeatability of the actuator should prevent any variations in bed height between the experiments. However, due to the new actuator and the different location of the vertical screw piece a new calibration procedure had to be invented. In addition, a new ShovelController VI had to be made. The first step was finding a position for the locking piece that allowed sufficient vertical shovel movement while not being so low that the piece or actuator were submerged in any liquid. It also turned out that when attached too low, the protruding part of the vertical piece would touch the pool wall if the shovel was lowered. If the setup was moved all the way to the left, this meant the locking piece would crash into the wall of the pool, blocking movement of the horizontal actuator and doing significant damage to the entire setup. This meant the vertical piece had to be adjusted. Parts of both the top and bottom were removed to allow more vertical movement of the shovel while also lessening the amount of contact with the solution. The protruding part is scheduled to be cut approximately in half to prevent it from touching the pool wall. These adjustments are illustrated in Figure 50.

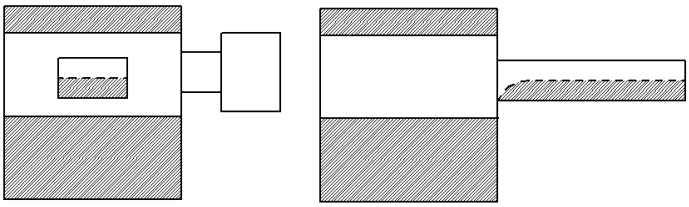

*Figure 50: Front and side view of the vertical locking piece. Shaded areas were removed or are scheduled for removal to allow for extra movement range. Original schematic by D.Sc. M. Aspiala, edited for this publication.*

For the calibration of the shovel height, three things need to be known: the position of the new MP-20 actuator, the corresponding position of the shovel, and how that position is related to the position of the needles. The MP-20 actuator has a position range from 0 to 26.44 mm with 0 being not extended and thus the furthest upwards. The V273.430 needle array actuator position range is reported as -10 to +10 mm with -10 being the furthest upwards. The setup was assembled in such a way that full extension of the MP-20 actuator corresponded to the lowest position of the shovel. In this way, no damage to the setup could occur from over-extending the MP-20 actuator while the shovel is out of movement range. By trial and error, it was determined that calibrating the setup as it was done in the original procedure, with the calibration piece for vertical and horizontal calibration and the needles in position -10 mm, while the MP-20 was extended 15 mm resulted in an adequate situation where the shovel could be moved upwards far enough for the pool to be removed, while collision between the locking piece and the pool was impossible, even at the

furthest shovel extension. By running the ExperimentalController VI with a bed height setting of 2 mm, a bubble size of 1 mm and a squeeze of 0, it was found that in this situation the VI set a V-273 actuator position of 9.24 as the 'point of contact'. As the squeeze was set to 0 mm, the tips of the 1 mm sized bubbles would exactly touch the particle bed at an actuator position of 9.24 mm and so the needles would touch the bed at the (impossible) position of 10.24 mm. Using the dimensions of the calibration piece and the shovel itself, it was calculated that when the calibration piece is used, the shovel is located 9.3 mm below the tips of the needles. As the default calibration position of the needles is -10 mm, this meant that an MP-20 position of 15 mm puts the shovel at a height that corresponds to a needle position of -0.7 mm (9.3 mm below the -10 mm position). It was then possible to derive that in order to reach the location corresponding to a 10.24 mm position of the V-273 actuator, the MP-20 needed to extend another 10.94 mm, from -0.7 to +10.24 mm, resulting in a final MP-20 position of 25.94 mm. Using the knowledge that an MP-20 position of 25.94 creates a particle bed of 2 mm the original VI could be adapted to incorporate the new actuator position values. For clarity, a schematic depicting the setup is shown in Figure 51.

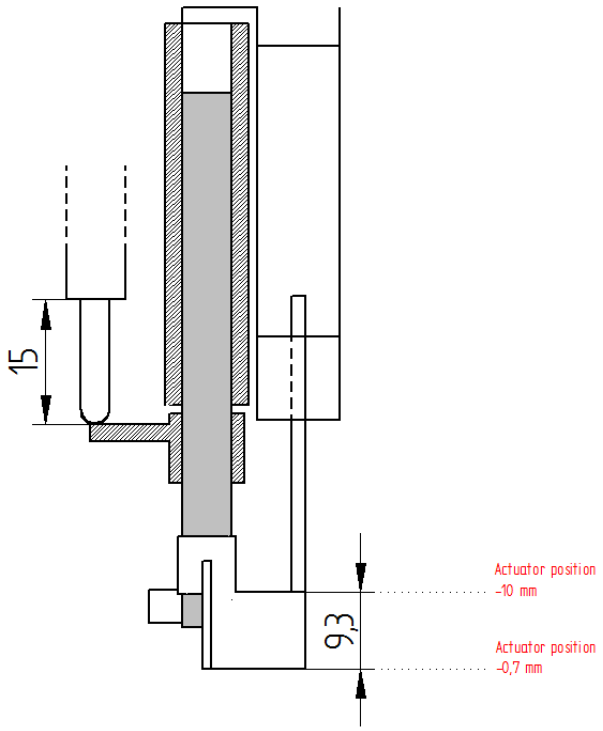


*Figure 51: Schematic showing the relevant positions and dimensions necessary for creating the new calibration setup. On the left, the MP-20 actuator, extended 15 mm. In the middle is the shovel with the attached calibration piece. On the right, the needles at position -10 mm, with the tips touching the calibration piece. The dotted lines show where the needle tips would be when the V273.430 actuator is set to the respective vertical extensions that are shown in red. Original schematic by D.Sc. M. Aspiala. Edited for this publication.*

### 3.3.5 A new ShovelController VI.

Due to the MP-20's vastly increased speed and movement range, the ShovelController VI that is used in the creating of the particle bed could be altered. The movement of the shovel is shown schematically in Figure 52. The vertical movements of 2 mm were originally performed at a velocity of 0.1 mm/s while the horizontal movement velocity was 1 mm/s. The 3rd part of the movement had to be performed slowly to prevent stirring up the liquid which could disturb the particle bed. This meant an entire shovelling cycle took 200.8 s. Due to the improved speed of the MP-20 actuator, the shovel velocity could now be changed to 5 mm/s during the vertical movements. The maximum velocity of 12 mm/s was not used to minimize disturbance to the particle bed. In addition, the shovel could now be lifted 18 mm, so it is completely out of the water during the 3rd part of the cycle. As there was no longer contact between liquid and the shovel, the movement speed for the 3rd part of the motion could be increased from 1 mm/s to 8 mm/s without stirring up the liquid or the particle bed. Due to these improvements, a single cycle now only requires 101.25 s. As multiple shovelling cycles are necessary for the creation of each particle bed this resulted in a significant reduction of the time needed for the particle-bed creation.

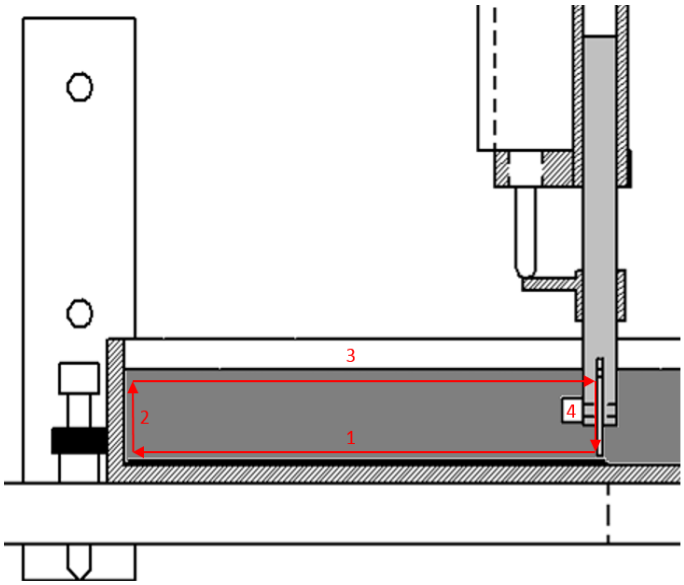


*Figure 52: Schematic depiction of the movement of the shovel during a shovelling cycle.*

### 3.3.6 Glass collection bin

A collection bin made from glass had been ordered from Finnish Specialglass before the start of this thesis. It was finally completed during the maintenance break. The plastic collection bin had several corners and microcracks into which particles could get stuck, which could make their retrieval after completion of the measurements difficult. Unfortunately there were several problems with the design of the glass collection bin that made it unusable in the experiments. First of all, due to the hydrophilic nature of the glass, there was liquid creeping up between the side of the pool and the back of the bin. This caused a permanent state of overflowing and leakage, even when the water level was relatively low. Secondly, it was found that the holes of the new metal cover plate had been cut approximately 0.05 mm too narrow. Consequently, some of the larger bubbles were unable to enter the collection bin, instead bouncing off the cover plate and detaching. This is problematic for the collection of the particles. The plate could not be switched out for the old one as the glass bin is 0.13 cm narrower than the old one, due to which the old plate doesn't fit. Lastly,

there was on the glass collection bin nothing to stop the cover plate from sliding all the way downwards as depicted in Figure 53. In addition, the plate could be moved sideways. This movement blocker and the grooves on the sides that are present on the plastic bin makes sure that the cover plate is always in the same location. This is important as the holes are just narrow enough to allow the needles to fit through them. Any variation in their locations causes the needles to crash into the metal cover, which can damage both the needles and the V-273 actuator. Due to the absence of a stopper on the glass plate the exact position of the cover has to be determined manually. This is inconvenienced by the fact that there is room for sideways movement. Due to all these factors, the glass bin was not used in any of the experiments described in this work. Some adjustments will have to be made to the design of the glass bin or the new cover plate before their use is both safe and convenient.

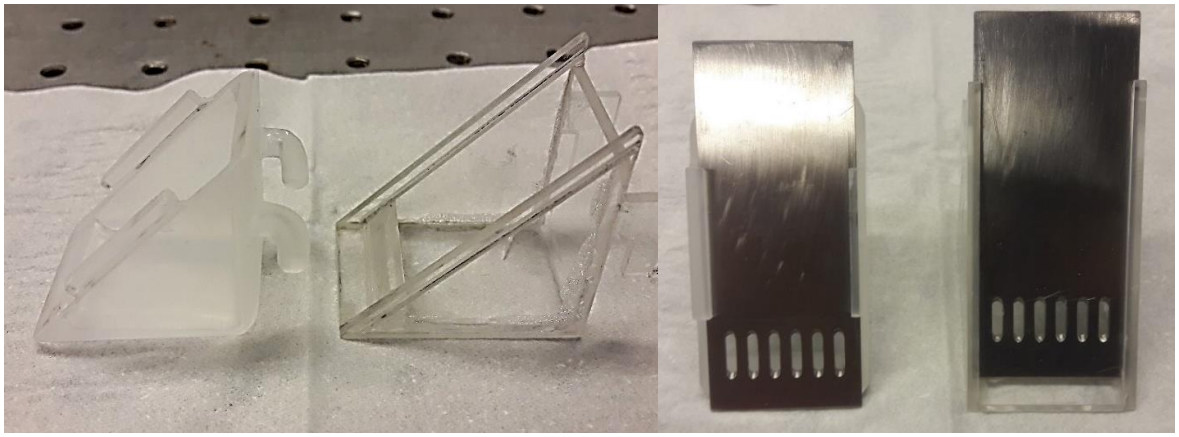

*Figure 53: Two photographs comparing the new glass bin (left) and the old plastic bin (right). As can be seen in the left photograph there is on the glass bin nothing to block the cover plate from sliding all the way downwards as is shown in the right photograph.*

# 4. Methodology design and development

There have been four main rounds of experiments with ACTA. Each round consisted of two days of experimenting. On each of these days, four or five measurements were performed on one sample type. The samples consisted of either chalcopyrite particles, or mixtures of quartz and chalcopyrite particles. The performed experiments are shown in Table 2. In light blue colour is shown the trial name that is used in the rest of this work to refer to the various experiments. In addition to these experiments, there were some small-scale tests for which ACTA was not used. These tests were performed to gain a better understanding of how to treat the samples and to find ways to improve the procedure. They are described as part of the experimental round during which they were performed.

*Table 2: A list of the types of samples and experimental conditions used in each of the rounds of experiments. Mixtures consist of a certain weight percent of chalcopyrite (Cp) particles mixed with quartz particles. Light blue indicates the name with which each series of experiments will be referred to.*

| Experiment name | Round | Day | Date performed | Number of measure-ments | Sample type | Cp content of samples (wt%) | KEX conc. (g/t solid) |
|---|---|---|---|---|---|---|---|
| 1-1 | 1st | 1st | 23-3 | 4 | Mixtures | 1% | 30 |
| 1-2 | 1st | 2nd | 24-3 | 4 | Mixtures | 5% | 30 |
| 2-1 | 2nd | 1st | 28-3 | 4 | Pure | 100% | 30 |
| 2-2 | 2nd | 2nd | 31-3 | 4 | Pure | 100% | 28.8 |
| 3-1 | 3rd | 1st | 18-5 | 5 | Pure | 100% | 3000 |
| 3-2 | 3rd | 2nd | 23-5 | 5 | Pure | 100% | 3000 |
| 4-1 (Cancelled) | 4th | 1st | 29-6 | 5 | Mixture | 10% | 3000 |
| 4-2 (Cancelled) | 4th | 2nd | - | 5 | Mixture | 10% | 3000 |

## 4.1 Sample preparation procedure

### 4.1.1 Round 1 and Round 2 (2-1)

Measurements were performed on samples of chalcopyrite and quartz particles. At the start of this work, three sets of four samples each were prepared with respectively 1, 5, and 100 wt% chalcopyrite. The 1%, 5% and 100% samples were used respectively in the 1-1, 1-2 and 2-1 experiments to measure the attachment probability for four different contact times. Each samples consisted of chalcopyrite and quartz particles in the 106-125 µm size range. The range was deliberately chosen to be as narrow as possible to minimize the influence of particle size on the measurement results. The mixed samples had a total mass of 6 g, while the 100% chalcopyrite samples had a total mass of 8 g. These values were based on the minimum mass of quartz and chalcopyrite needed to create a complete particle bed plus 1 g to compensate for any unforeseen material losses. For a complete particle bed with chalcopyrite particles, more mass was needed than for a bed consisting only of quartz due to the higher density of chalcopyrite.

Chalcopyrite ore originating from Durango, Mexico was obtained from Ward's Science. The size of the rocks varied from small shards to rocks of several centimetres. Real ore was chosen for these experiments in favour of synthetic minerals as the eventual goal is to use ACTA as a diagnostic tool in actual flotation plants. A consequence of this choice is that there are other minerals besides chalcopyrite present in the ore. Some of the purchased chalcopyrite was surrounded by grey-coloured waste-rock and on the surface of some pieces a purplish shine could be seen that was reminiscent of bornite. Other minerals that are likely to be present are pyrrhotite and pyrite. SEM analysis of one of the collected mass samples revealed traces of lead and antimony. For this thesis however, the mineral is assumed to be pure chalcopyrite. A few examples of the various rocks that were received are shown in Figure 54.

*Figure 54: Several rocks from the chalcopyrite ore obtained from Ward's Science.*

The larger rocks were broken with a hammer. The material of approximately three or four rocks was then placed in a Fritsch Pulverisette 09.003 ring mill and comminuted by dry grinding for approximately 4 s. The resulting material was sieved through a 360 µm RETCH sieve by manually shaking it for 30 s. The oversize was then returned to the ring mill for another 4 seconds of grinding. This process was repeated until virtually all material could pass through the 360 µm sieve. A sieving stack was then built with sieves of 106, 125 150 and 250 µm. The chalcopyrite was deposited in the top sieve and the stack was placed in a RETSCH AS300 Electromagnetic Sieve Shaker. The device was set to interval sieving for 20 min, with an amplitude of 8.0 mm/"g" and sieving intervals of 50 s. After sieving, the particles in the 106 µm to 125 µm size range were placed in a 100ml borosilicate glass vial. The undersize was discarded and the oversize was placed back into the ring mill for another 4 seconds of grinding. Additional chalcopyrite rocks were added if there was a small amount of oversize material. This process was repeated until around 12 g of chalcopyrite particles between 106 µm and 125 µm were collected. The 100 ml flask was filled with argon gas and stored in a fridge at 6 °C to prevent oxidation of the mineral surface.

Quartz particles with a size range of 100 to 600 µm were obtained from Sibelco. Originally, the quartz was treated according to the chalcopyrite procedure described above, but this resulted in very low yields of quartz in the desired size range. As only small amounts of particles could effectively be sieved at one time, countless rounds of sieving would have been needed to produce the necessary amount of quartz. To save time the quartz was therefore no longer comminuted. Instead the particles were immediately sieved, with both oversize and undersize being discarded.

Aside from the faster preparation of samples, the use of unground quartz had as benefit that there was much less dust in the solid samples. This only became apparent however during some of the small scale tests that were performed later.

When a sufficient amount of quartz was collected, the mixtures were prepared by weighing out four times 5.4 g and 5.7 g of quartz in 20 ml borosilicate glass vials for the creation of respectively the 1% and 5% samples. The scale used for weighing the material was a Mettler Toledo XS204 balance with a precision of 0.1 mg. The collected chalcopyrite was then split into fractions using the 'quartering' sampling method. From these fractions the necessary amount of chalcopyrite, either 0.06 or 0.3 g, was taken and added to the prepared vials with quartz to create the 8 final mixtures, each weighing 6 g. The remainder of the chalcopyrite was recombined and split again into four fractions from which four times 8 g was taken to create the 2-1 samples. All samples were then stored under argon atmosphere in a fridge at 6 °C to prevent oxidation of the mineral surface. Parafilm M® was used to ensure the vials were sealed airtight.

The sieves were cleaned by placing them in a sonicator bath filled with tap water for 30 min, followed by rinsing with tap water and drying overnight in an oven at 50 °C. After grinding chalcopyrite, the ring mill was cleaned by filling about half the available volume with the Sibelco quartz particles. The mill was then set to run for 30 s. After grinding, the mill was opened and the ground quartz mixed with chalcopyrite waste was discarded. This was repeated until the ground material had a white colour, indicating little to none of the black coloured chalcopyrite dust was left. The mill and its components were then rinsed with hot tap water and dried using microfiber papers. If any dust was visible on the microfiber paper the rinsing was repeated.

### 4.1.2 Round 2 (2-2)

As will be presented in Section 5.2, one of the possible reasons for the stochastic results of the 1-1, 1-2 and 2-1 experiments was variations in the chalcopyrite content of each sample. To minimise variation, it is therefore necessary that the material is split according to a correct sampling procedure. During the experiments of round 1, there were clear differences in the turbidity of the water to which the various samples had been added. This indicates that that the samples were not equal to one another and that they therefore had not been properly prepared.

Another issue with the previously used method was that creating samples of exactly 6 and 8 g took significant amounts of time. Creating samples with exactly the same mass was done as it would make for easy addition of the same amount of collector to all samples and therefore equal sample treatment. The result of this approach was however that the samples were now not equal to begin with as material often had to be removed from the split fractions to obtain the desired mass, which is not in accordance with proper sampling procedures. Therefore another approach was used for the 2-1 samples.

Chalcopyrite rocks were comminuted with the ring mill. Special care was taken to only grind those parts of the rocks that were golden, minimizing the amount of obvious waste rock being added to the mixture. Once more than 35 g had been collected the material was split into 20 fractions using a spinning riffler with a Fritsch Laborette 24.002 vibratory feeder. The created fractions were not all equal in weight but can from a sampling point of view be considered equal. As the mass of each fraction could not be controlled, care was taken to collect more chalcopyrite than was technically

*Table 3: Mass of each sample in order of use in the 2-2 experiment.*

| Sample Mass (g) |
|---|
| 8.8834 |
| 9.0832 |
| 9.1597 |
| 8.7944 |

necessary for the creation of the particle beds to ensure each of the samples would contain enough material. Five of the 20 created fractions were then combined in a glass vial to create each of the four samples. As is shown in Table 3, the mass of the samples now varied from 8.79 to 9.16 g, which was more than the 8 g required in the experimental procedure. The experimental method was altered to ensure each sample was conditioned with the same amount of collector per mass of solid. The rest of the preparation and sample storage was performed in the same manner as for the 2-1 samples.

### 4.1.3 Round 3

As the method used for the 2-2 samples had proved successful it was repeated for the experiments of round 3. During each experimental day in rounds 1 and 2 at least one out of the four measurements went wrong. This caused difficulties in interpreting the results due to a lack of data points. For round 3, five samples were created for each experimental day. This would allow a measurement to be repeated. The samples from round 2 had been created from two different batches of chalcopyrite. To allow for the 3-2 experiment to be a true repeat of the 3-1 experiment, all 10 samples were created from one prepared batch of 87.77 grams of chalcopyrite. With the spinning riffler this material was split into 20 fractions, and 2 of those fractions were combined to create each of the 10 samples. As is shown in Table 4, the mass of the samples ranged from 8.45 g to 9.18 g, so each sample contained more than the required 8 g of chalcopyrite.

*Table 4: Mass of each sample in order of use in the experiments of round 3.*

| Sample Mass (g) |
|---|
| 8.4532 |
| 8.8386 |
| 9.1752 |
| 8.3929 |
| 8.8781 |
| 8.9686 |
| 8.5348 |
| 8.8608 |
| 8.7199 |
| 8.9564 |

### 4.1.4 Round 4

*Table 5: Mass of chalcopyrite (Cp) in each of the samples prepared for round 4 in order of weighing.*

| Sample Cp Mass (g) |
|---|
| 0.7111 |
| 0.7464 |
| 0.7526 |
| 0.7582 |
| 0.7463 |
| 0.7754 |
| 0.7430 |
| 0.7537 |
| 0.7480 |
| 0.7735 |

Ten mixtures of 10 wt% chalcopyrite were prepared from one batch of chalcopyrite. In contrast to round 1 the quartz was once more comminuted because a size range of quartz particles from 53 µm to 180 µm was desired while the available quartz particles had a lower size limit of 100 µm. This larger size range was chosen in an attempt to minimize the segregation of the chalcopyrite and quartz particles during particle bed making. The increase in dust in the samples that the grinding would cause was expected to be negated by the filtering step that had by then been added to the measurement preparation procedure as described in Section 4.2. Around 80 g of quartz was collected from the 53 µm to 180 µm sieve fractions. In the same manner as in round 3, around 7.5 g of chalcopyrite particles between 106 µm and 125 µm were collected and split with the spinning riffler. Each of the samples weighed between 0.711 g and 0.776 g as can be seen in Table 5. Quartz particles were then added to each mixture so that their respective contents of chalcopyrite were 10 wt%. The mass of each completed mixture was therefore between 7.11 g and 7.76 g, well over the required mass of 6 g. To reduce the time needed for creating these samples, the added amount of quartz was not always exactly equal to the calculated amount. Instead, a maximum deviation of 0.5 mg from the calculated amount was

considered acceptable. The resulting difference in wt% chalcopyrite between samples was considered negligible and therefore so were the effects on the attachment probability.

## 4.2 Measurement preparation procedure

This section will cover all the steps between taking the prepared samples from the fridge and the start of the ACTA measurement. The exact details of particle bed creation are not of importance for this work and will therefore not be mentioned.

### 4.2.1 Round 1

During the first few measurements, several changes were made to the procedure, as certain steps were found to be impractical or ineffective. For the very first measurement, the times for each step of the procedure were recorded and each subsequent sample was then treated according to the exact same schedule. This was done to ensure all samples had the same conditioning time and had been submerged in water for the same amount of time before starting the measurements.

*Preparation*

The evening before start of the experiments, a 20 ml solution of 0.192 g/l potassium ethyl xanthate (KEX) was created. The solution was stored in a fridge at 6 °C for later use. Unless specifically mentioned otherwise, ultrapure Millipore water was used for the entire procedure.

*Rinsing and conditioning*

During the experiments, the turbidity of the water was found to increase when the solid mixtures were added due to the presence of dust in the samples resulting from the comminuting of the material in the ring mill. Examples of this increase in liquid turbidity after the addition of quartz and chalcopyrite particles can be seen in Figure 55. Water with a high turbidity causes problems with the acquisition of bubble images. Furthermore, the presence of fine suspended particles could have an influence on the attachment probability. Waiting for the fine particles to settle was not an option due to the experimental schedule and the fact that both in making the particle bed and during ACTA measurements the water will be stirred up again. It was therefore decided to clean the samples.

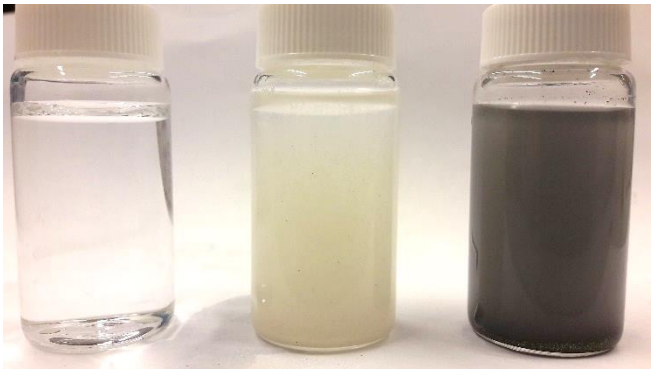

*Figure 55: Examples of water after the addition of unrinsed quartz particles (m) and unrinsed chalcopyrite particles (r). Clear water (l) shown for comparison.*

At the start of the measurement preparation, the vial containing the 6 g solid mixture sample was taken from the fridge and the solid mixture was placed on a 20 µm RETSCH sieve. The sample was then rinsed by continuously dripping water on top of it and shaking the sieve for 5 min. The water and the fine suspended particles would leak through the sieve apertures while the larger particles remained on the sieve. After rinsing the sample was removed from the sieve by spraying water through the sieve from the other side and collecting the liquid and solid particles in a 400 ml beaker. The time reserved for this transferring step was 2 min. Water was then added to the 100 ml mark and 0.9375 ml of the 0.192 g/l KEX solution was added so the concentration of KEX was 30 g/t of solids. Using a 4.5 cm magnetic stirrer the mixture was then stirred for 15 min at 450 rpm. When

the magnetic stirrer was removed, some particles were found to have attached to the magnetic stirrer. These particles were removed by spraying some of the conditioning liquid on the stirrer with a 5 ml Eppendorf research plus pipette while holding it above the beaker. The beaker was then taken to the prepared ACTA device where between 50 to 70 ml of the liquid was transferred to the ACTA pool by pouring from the beaker. The 5 ml pipette was then used to transfer the sample particles to the pool according to the procedure for particle-bed preparation. If necessary, after completion of the particle bed more liquid was added to the pool to obtain the minimum required operating level.

The conditioning liquid had varying levels of turbidity for the different measurements, thought to be caused by incorrect sample preparation as was described in Section 4.1. It also indicated that the rinsing was inefficient. The fact that the differences in turbidity were in fact not caused by sample inhomogeneity, but were caused by the rinsing procedure being unreliable could not be discounted. Even though it contained dust from the solid samples, the conditioning liquid was used to fill the pool rather than clean water. This was done to prevent desorption of xanthate from the particles, and because a future goal is to use ACTA to measure actual process plant samples. To achieve that, measurements have to be performed in such sub-optimal conditions. These experiments with opaque liquids could give an indication about what kind of water qualities can be used in performing measurements with ACTA.

For the very first measurement, the time between conditioning and completion of the particle bed took close to 40 min. Even though the making of the particle bed went significantly faster in subsequent attempts, the 40 min time period between completion of conditioning and start of the measurement was used for all measurements to ensure equal sample submergence time.

*Removing floating particles*

After the conditioning of the liquid, small quantities of floating chalcopyrite particles were visible in the beaker. Their amounts varied between measurements. During making of the particle bed they could end up in the ACTA pool. Photographs of the floating particles can be seen in Figure 56. These floating particles appeared after situations when the solids were vigorously stirred up, such as during the mixing of the conditioning solution, when liquid was added into the beaker, or when the particles were moved during the making of the particle bed. Their nature and their effect on sample homogeneity will be discussed in more detail in the subsection regarding Round 4 and in Section 5.2. Attempts were made to submerge the floating particles by sucking them up with a pipette and redepositing them under water. In most cases, this was unsuccessful. Therefore, care was taken to stir the particles up as little as possible during the making particle bed to prevent appearance of new ones. If floating particles were present in the pool after completion of the bed,

*Figure 56: Photographs of floating chalcopyrite particles encountered during the measurement preparation. Left: In the beaker after conditioning of the liquid. Right: In the ACTA pool during the making of the particle bed.*

they were removed from the pool to prevent them from getting into the needle array when it submerges during measurements.

*After the measurement*

After completion of the ACTA measurement, the attached particles were collected by carefully closing off the metal cover plate with a plastic lid to prevent loss of particles with outflowing water. The sample collection bin was then removed from the pool and emptied into a Merck analytical stainless steel filter holder prepared with a 8.0 µm nitrocellulose MF™ membrane filters. The collection bin and its covers were rinsed with water. This water was collected in the filter holder to ensure that all particles were collected. With a syringe, a vacuum was applied to the filter holder after which the filter and any collected particles were carefully removed from the filter holder and placed inside an upside down polypropylene cap from a 20 ml glass vial. The cap containing the filter was then placed into a desiccator overnight to remove any remaining moisture. Further details on the procedure used for the preparation of the filters and the measuring of the collected mass can be found in Section 4.4. After collection of the attached particles the remainder of the particle bed was disposed of.

*Cleaning*

Any parts of the ACTA that had come into contact with the conditioning liquid as well as all other materials like the used glassware and the magnetic stirrer were rinsed with water multiple times and wiped down using microfiber papers before the start of the next measurement. In between measurements, the sieve used for rinsing the samples was cleaned in a large sonicator bath filled with tap water for 20 min followed by rinsing with Millipore water. As the same concentration of collector was used in all measurements, there was between measurements no need for more intensive cleaning.

After completion of all measurements, a more intense cleaning was performed. The rinsing sieve was placed in large sonicator bath for 30 min, followed by rinsing with ultrapure water and drying overnight in an oven at 50 °C. All glassware used in the experiment and the measurement preparations was rinsed with water several times, followed by rinsing with ETAX A 94 wt% ethanol followed by more rinsing with water. The glassware was then placed in a sonicator bath and left there for 30 minutes after which it was rinsed again using water and placed upside down in a dry rack.

The detachable metal ACTA components that had come into contact with the conditioning liquid such as the shovel and the sample collection bin cover were rinsed with water and then placed in a beaker filled with ethanol. The beaker was subsequently placed in the sonicator bath and left for 30 minutes. The pieces were afterwards rinsed with water followed by drying with microfiber papers. The plastic pieces of ACTA such as the pool and the sample collection bin were rinsed with water followed by rinsing with a small amount of ethanol and rinsing with more water. Only small volumes of ethanol were used to prevent any effect on the glue holding the pieces together. After rinsing with water the pieces were wiped dry using microfiber papers and placed upside down on more microfiber papers to prevent any contaminating substances getting into the pool or collector bin.

Those parts of the machine that have been in contact with the solution but are not easily detachable from the ACTA device such as the shovel holder and the needles were cleaned with first with water,

then with ethanol and afterwards again with water by wetting a microfiber paper with the respective liquid and carefully wiping everything down. The insides of the needles were cleaned by dripping water into the air hose inlet with a 1 ml Pasteur pipette. More water was then sprayed from the bottom to clean the optical fibre surface. After this, more water was dripped from the air hose entry and an air hose was attached to each needle. The pump was then turned on and air was blown into each needle to remove the liquid from inside them. A microfiber paper was used to collect the droplets of water coming from the bottom. Pumping continued until no more liquid dripped from the needles. This entire process was then repeated with ethanol and another time with water. This ensured the removal of any possible xanthate residues or particle dust on the inside of the needles and on the optical fibre surface.

*Replacing the sieve and the magnetic stirrer*

After the first measurement, the 20 µm RETCH sieve used for the rinsing of the samples was replaced because the 20 µm sieve apertures were too small to effectively allow the rinsing water to pass through. This resulted in ineffective cleaning of the sample. In the following measurement, a sieve with a 50 µm aperture was used but this caused the same problem. During the third measurement a 106 µm sieve was used which resulted in a relatively clean conditioning liquid. The 106 µm sieve was from then on a standard part of the procedure. In the first six measurements a Teflon coated magnetic stirrer of 4.5 cm in length was used. On closer inspection of the conditioning process, it was found that the solution was not stirred effectively enough as there was a build-up of particles along the edges of the beaker. To achieve better mixing of the conditioning solution the stirrer was replaced with one of 6 cm length for the remaining two measurements.

*Segregation issues*

During the measurement preparation, it was noticed that due to differences in density, the quartz particles settled at a slower rate than the chalcopyrite. This occurred each time the particles were allowed to settle after being mixed or stirred such as in the conditioning beaker, in the pipette tips when they were transported to the pool, and when they were deposited in the ACTA pool to create a particle bed. The result of this different speed of settling can be seen in Figure 57 for a quartz and chalcopyrite mixture in a 20 ml vial just after being shaken. The darker chalcopyrite can clearly be seen to have collected at the bottom of the vial with the quartz settling on top. This phenomenon resulted in an inhomogeneous distribution of the chalcopyrite in the particle bed. Alternating patches of darker chalcopyrite and lighter quartz could be seen on the surfaces of the particle beds, like in the example in Figure 56 (right). Clear differences in the chalcopyrite distribution could also be seen between the beds of the different measurements. The effects of this inhomogeneity on the interpretation of the results will be discussed further in Section 5.2.

*Figure 57: Mixture of quartz and chalcopyrite particles in a 20 ml vial that has settled after it was shaken. Image brightness has been increased for illustrative purposes.*

### 4.2.2 Round 2 (2-1)

*Changes to the sample conditioning*

Several changes were made with respect to the conditioning procedure that was used in round 1. As the samples weighed 8 g instead of 6 g, 1.25 ml of the 0.192 g/l KEX solution was added to

achieve the xanthate concentration of 30 g/t of solid. In addition, the magnetic stirrer was replaced by an IKA® RE16 overhead stirrer with a stainless steel agitator set to 500 rpm. As it was non-magnetic, this stirrer did not have any particles getting attracted to it. It had the added benefit of being easier to remove from the liquid after the conditioning was completed. Similarly to the procedure with the magnetic stirrer, the agitator was rinsed with process liquid to ensure no particles were stuck to it after conditioning was completed. In between measurements, the agitator was rinsed with water and dried using microfiber paper.

*Addition of a filtration step*

During the first measurement of this round, there was a problem with the high turbidity of the water. The conditioning water was completely black and as there was no visibility the particle bed could not be made. The rinsing procedure had up until this point seemed to work relatively well, but the experiments of round 1 had been performed with mixtures of chalcopyrite and quartz. As shown in Figure 55, adding quartz particles to the liquid gave it a cloudy beige appearance which one could still see through relatively well once it was placed in the ACTA pool whereas chalcopyrite turned it completely black and lowered visibility immensely. As this was the first measurement with more than 0.3 g of chalcopyrite per sample, only now did the ineffectiveness of the rinsing step become evident. Preparing the particle bed with zero visibility was impossible and the quality of the bubble photographs could not be guaranteed. Therefore the liquid was removed from the pool and filtered through a 185 cm diameter Munktell general purpose filter paper. As can be seen from the comparison in Figure 58 this removed a lot of the black fine suspended particles from the water. For the remainder of the 2-1 experiment both the rinsing and the filtering were used to ensure equal sample treatment.

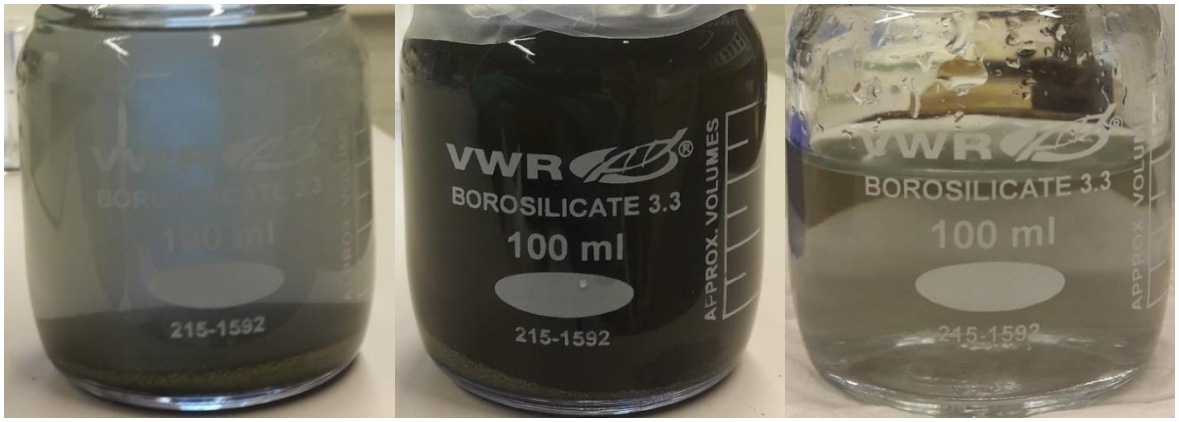


*Figure 58: Comparison image showing the conditioning liquid at various stages during the measurement preparation. Left: Just after xanthate addition. Middle: After 15 minutes of conditioning. Right: After filtration.*

The filtering was performed by using a 5 ml pipette to remove the liquid from the beaker and having it drip through the filter paper. The filtered liquid was collected in a 100 ml borosilicate vial. Care was taken to not remove any of the solid particles from the conditioning beaker and to make sure the particles were always submerged by a thin layer of water to prevent any exposure to the air. To reduce chance of spillage, the clear liquid was carefully pipetted into the pool rather than poured from the vial. The particle bed could then be created according to normal procedure by pipetting the solids from the beaker. After addition of the filtering step, the liquid in the pool during the measurements was in all cases significantly clearer than it had been in the experiments of round 1. The layer of unfiltered water in the beaker still had a high turbidity however, and some of this is transported into the pool during the making of the particle bed. The filtered water itself also still

shows a black colour. The presence of very fine suspended particles in the water therefore cannot be avoided entirely as can be seen in Figure 60. However, with the use of this procedure the turbidity did not reach such high levels that it significantly affected the measurement of the bubble sizes or made it impossible to create a particle bed. A comparison of the quality of the bubble photographs during an experiment with a 100% chalcopyrite sample can be seen in Figure 59 without the use of filtering (top) and with the use of filtering (middle). An image taken in clean water (bottom) is added for comparison. The middle image is made during the experiment shown in Figure 60. From this image, the importance of the use of the filtering step and the influence of even relatively small amounts of fine suspended particles can clearly be seen. The darker the surroundings are, the less effective the bubble size measurements will be. By changing parameters such as the image brightness and the contrast, images like Figure 59 (top) can still be used. However, with the current setup this would require manually editing the images and finding correct settings for each situation, which is highly impractical. The fine suspended particles also tend to settle on the camera viewing area over the course of the experiment, which then requires regular cleaning.

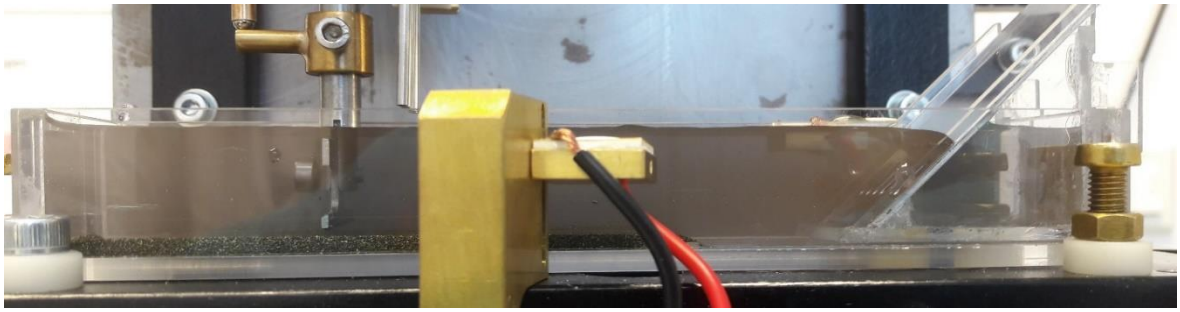

*Figure 60: Photograph of the ACTA pool during the making of the particle bed. Most of the liquid has been filtered. Some dust is still present in the water but not to such an extent that it impairs the making of the particle bed or creates problems for the image analysis.*

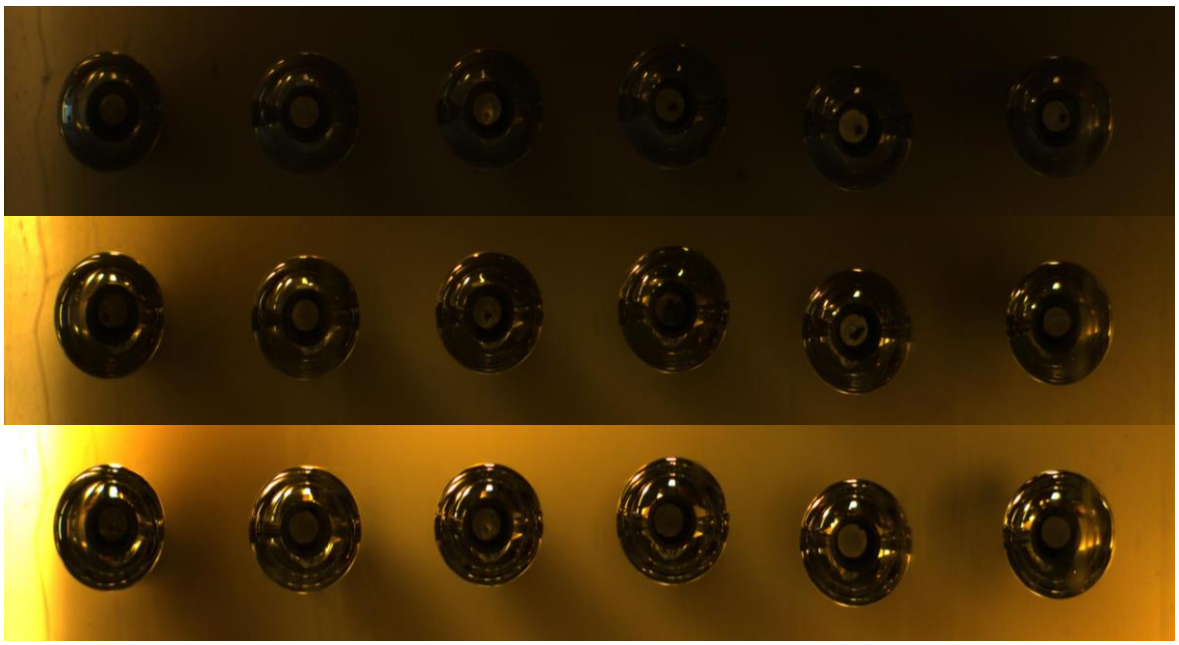

*Figure 59: Comparison of several bubble photographs taken during measurements. Top: 100% chalcopyrite particle bed, solids were rinsed but liquid not filtered. Middle: 100% chalcopyrite particle bed, liquid was filtered but solids not rinsed. Bottom: Image taken in clear liquid.*

*Implementation of a waiting period*

As a result of the experience obtained in the previous experiments, the process of creating the particle bed was performed much faster than during round 1. To ensure equal submergence time of the samples, a waiting time of 10 min was implemented between the completion of the particle bed and the start of the measurement during the first measurement. This allowed for extra time in case of unforeseen problems during the following measurements. Including this waiting period, the measurement was started 40 min after completion of the conditioning. Within this time, the liquid was filtered and the particle bed was built. This schedule of 40 min was also used for the 2-2 experiment and all those in round 3.

### 4.2.3 Round 2 (2-2)

*Removal of the rinsing step*

There had already been serious doubts about the effectiveness of the rinsing step due to the fact that the liquid was often still opaque during the measurements of round 1. The repeatability of the procedure was also called into question due to the varying amounts of turbidity during those experiments, and the fact that it was difficult to perform the step in exactly the same way for every sample. It also turned out to be problematic to retrieve the solids from the sieves and collect them in the beaker without losing material. Lastly, as can be seen in Section 6.2, there was a severe problem with bubble formation during the final measurement of the 2-1 experiment. This problem was suspected to be caused by contamination of the sieve during its cleaning in the sonicator between measurements. The sonicator had previously been used by other lab personnel to clean equipment which might have resulted in contamination of the sieve with detergents. Due to all these issues and the fact that the addition of the filtering step during the 2-1 experiment had already made the rinsing essentially superfluous the rinsing step was removed in its entirety. Instead, the solids were conditioned straight after being removed from the fridge and the liquid was filtered after conditioning according to the procedure used during the 2-1 experiment.

*Calculating the KEX addition*

Due to changes in the sample preparation procedure, described in Section 4.1.2, the samples were no longer all exactly 8 g. Therefore, the amount of xanthate solution that was added had to be calculated for each specific sample. The evening before the experiments, a 15 ml solution of 0.273 g/l KEX was created. The weight of each sample was known (Table 3) so the exact amount of KEX solution that had to be added to achieve the desired xanthate concentration of 30 g/t solid could be calculated for each separate sample. The amounts of KEX solution to be added were rounded to increments of 0.005 ml as that was minimum possible volume change within the calibrated range of the 5 ml pipette. Admittedly, an error was made in the calculations for this experiment since the 96% purity of the used KEX was not compensated for in the calculation. This resulted in a xanthate concentration of 28.8 g/t solid, which is slightly lower than the intended 30 g/t solid.

*Floating particles*

During the experiments of round 2, more floating particles were visible than in the previous experiments. As there was also significantly more chalcopyrite in each sample this was not unexpected. Attempts were made to submerge the particles as much as was possible but were not often effective. Due to their large quantity, the floating particles were for the most part left as they were. If they were present in the ACTA pool, they were removed before the start of the measurement as was done during round 1.

### 4.2.4 Round 3

*Small scale trial*

During the maintenance break, the issue of the floating particles had been addressed. As will be explained in Section 5.2, these floating particles are a problem for sample homogeneity, especially for the mixed samples of quartz and chalcopyrite. Small scale tests were performed with chalcopyrite particles in 20 ml glass vials filled with liquid containing various concentrations of KEX ranging from 0 to 3000 g/t solid. Floating particles could be seen regardless of the concentration of KEX. When the vials were shaken in a calm way that did not cause a lot of mixing between air and water, all floating particles would sink even at KEX concentrations up to 3000 g/t solid. If they were then shaken in such a way that a lot of air was mixed with the liquid, the floating particles would reappear. This indicated that these particles were not floating as a result of being strongly hydrophobic as had initially been suspected. Instead, the particles were not wetted well enough, causing them to float on the liquid surface rather than becoming submerged. This is in line with the observations from the previous experiments where the floating particles appeared every time either the particles or the liquid were stirred vigorously, and thus the particles had come into contact with a liquid-air interface.

It was in realized during this trial that the chalcopyrite particles of round 2 had been conditioned with much less xanthate than those in round 1. The original xanthate concentration of 30 g/t of solid was chosen to resemble concentrations that might be used in the processing of actual ores in a flotation plant. The ore that is processed in real flotation plants however, might contain several percent of valuable materials but will hardly ever be 100% pure desired mineral. Therefore, when xanthate is used in the concentration of 30 g/t solid and the solids consist of only 1% or 5% of the actual valuable mineral, the concentration of xanthate per gram of mineral to which the xanthate will actually adhere is much higher than 30 g/t. This was not taken into account when, during round 2, the samples were changed from mixtures to 100% chalcopyrite. The concentration was kept at 30 g/t solid, as it had been for the 1% mixture. However, for that amount of xanthate there was now 100 times more chalcopyrite. It was theorized that this oversight would have resulted in much less hydrophobic material.

During the small scale tests, chalcopyrite samples of 1 g were examined in liquid with xanthate concentrations per gram of chalcopyrite equal to that of the 1-1 and of the 2-1 experiments. In both cases, the xanthate concentration had been 30 g/t solids but due to the differing chalcopyrite content of the samples, the concentrations were 3000 g/t chalcopyrite and 30 g/t chalcopyrite respectively. Under these conditions, a simple cling test was performed. Using a Pasteur pipette, small bubbles were created which were then pressed into the particle bed. Although it was more a quick visual inspection than a true systematic test, the results were clear. For the 3000 g/t chalcopyrite concentration the particles easily attached to the bubbles and each other, forming chains of particles of which the uppermost one was attached to the bubble. For the 30 g/t chalcopyrite concentration of xanthate there were occasionally attached particles when high bubble compression was used, but the chains of particles were never seen.

*Changes to the sample conditioning*

To minimise the amount of floating particles and improve the ease with which they could be submerged the method of conditioning the samples was changed for round 3. The shaking needed to submerge the floating particles was not easily performed with a 400 ml beaker that

could not be closed off in any way. The use of 100 ml borosilicate glass vials with polypropylene caps allowed for shaking and could still fit the necessary amount of liquid. They did however not allow for the use of the overhead stirrer. Its replacement had already been considered as it had a dead zone right underneath the agitator where particles piled up, indicating that the solution was not properly mixed. Magnetic stirrers were an option but were considered impractical. Instead, the vials were filled with 100 ml of liquid and the calculated amount of KEX solution to achieve a concentration of 3000 g/t of solids. The increase in xanthate concentration to 3000 g/t of solids was implemented to ensure the chalcopyrite was sufficiently hydrophobised, and that it was as conditioned with the same relative amount of xanthate as the chalcopyrite in the 1-1 experiment.

After addition of the solid sample, the cap was screwed on the vial and closed off with Parafilm M®. The vial was then attached to a Kisker tube revolver (Cat. No. 79000) and then rotated at 35 RPM for 15 minutes. Initially Parafilm M® and a foam piece were used to secure the bottle in place. This setup is displayed in Figure 61. In later attempts, basic duct tape was used to secure the vial. After conditioning, any floating particles were submerged by gently shaking the vial. The rest of the preparation was similar to the procedure used in the 2-2 experiment, with the liquid being filtered before the making of the particle bed. Although this did not entirely prevent the presence of floating particles as they could also appear during the creation of the particle bed, it did significantly lessen their numbers. Another benefit was that no external objects needed to be introduced into the liquid for the conditioning of the samples.

The upwards trends seen in the measurement results of round 3 indicated that the improvements made to the experimental method have had a positive effect on the reliability of ACTA measurements.

*Figure 61: Photograph of the conditioning setup. A 100 ml vial containing the solution and the solid sample is attached to a tube revolver, which is then set to rotate for 15 minutes at 35 RPM.*

### 4.2.5 Round 4

*Particle bed segregation*

As experiments with mixtures were once more planned for round 4, the problems with particle bed inhomogeneity caused by the different settling speeds of the quartz and chalcopyrite had to be solved. Tests with mixtures showed that manually mixing the solids with a raking tool once they had been deposited in the ACTA pool resulted in a seemingly more homogenous distribution of the chalcopyrite. Proof for this would have to be obtained from the ACTA measurement results.

*Chalcopyrite clusters*

Before the start of each measurement, the temperature and the moisture content of the surrounding air would be recorded to determine any possible fluctuations over the course of the day and investigate possible influences on the measurement results. A raking step was added to the procedure, during the particle bed making in an attempt to obtain better mixing of the chalcopyrite. Aside from this change, the 10 wt% chalcopyrite mixtures used in this round were to be treated according to the same procedure as was used for the round 3 samples. Only one sample was in fact prepared because, aside from the segregation due to density differences, another phenomena was noticed. After conditioning, clusters of chalcopyrite particles had appeared on top of the settled mixture. Photographs depicting these clusters can be seen in Figure 62. Simply shaking the solution as had helped with removing the floating particles was not effective in removing these agglomerates and in fact only seemed to worsen the problem. As is explained in Section 5.2, this phenomenon would cause the same issues for interpreting the results as did the floating particles and the settling segregation. When it was realized that any results obtained from measurements with these mixtures would be useless, the focus of this round shifted from performing experiments to attempts at removing these clusters.

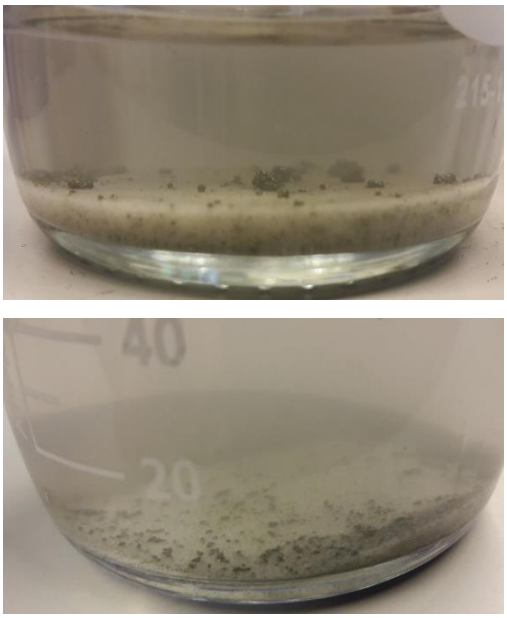


*Figure 62: Photographs showing the agglomerates of chalcopyrite particles that appeared after conditioning.*

After closer examination, these clusters were found to consist of hydrophobic chalcopyrite particles adhered to air bubbles. These clusters were too heavy to float and settled on top of the mixture. The available options to remove them were quite limited. Altering the chemistry or physical environment of the system was not an option, which only left mechanical treatment. Several options were tried including tapping, shaking, rotating, and sonicating the sample. None of these options were particularly effective, while some only caused the formation of more clusters as new bubbles were introduced into the solution. Especially sonicating severely worsened the issues due to significantly increasing the segregation caused by density differences. The bigger agglomerates could be manually broken apart with a tool such as small tweezers, but this was impractical and did not work for the many smaller specimens. The ease with which they reformed at the slightest introduction of bubbles into the liquid also inconvenienced the process.

As the clusters formed from air bubbles, an attempt was made to perform the conditioning without having any air present in the 100 ml vials. The vial was filled to the brim with liquid and closed before starting the conditioning. In addition, a slower rotational speed was used. This approach was abandoned because there was spillage of the conditioning liquid which was both messy, and meant there was no guarantee that the correct amount of KEX was present in the vial. In addition, it was impossible to entirely remove the air and so the clusters formed regardless. It is also possible that some of the smaller agglomerates did not contain air bubbles but rather were only chalcopyrite particles that would sooner adhere to one another than mix with the more hydrophilic quartz. Other attempts focussed on making sure all chalcopyrite was sufficiently wetted by slowly adding liquid to the solid sample and stirring it well before addition of more water. An attempt was made to condition the samples with the overhead stirrer that was used in round 2 to see if this caused less air to be mixed in with the solution but no clear effect was noticed except the reappearance of many floating particles. Increasing the xanthate level to 4000 g/t of solids did not have the desired effect. Neither did lowering it to 300 g/t. In the absence of xanthate the agglomerates did not form. Unfortunately no conclusive solution has yet been found for this problem.

## 4.3 Measurement settings

This subsection will describe the parameters that were used in the various measurements. Only those parameters that can influence the induction time as described in Section 2.4 will be mentioned. Regarding the device parameters, the only differences between experimental rounds were the various contact times, as this was the variable under examination. All other settings were kept constant for all the experiments. Both the approach velocity and the velocity of retraction were set to 50 mm/s. The approach distance was 0.5 mm and the bubble compression was set to 0.1 mm. Figure 63 schematically explains these parameters. The values were chosen either because they were similar to settings used in experiments described in literature, or simply because they gave adequate results within the tested range of hydrophobic particles and contact times. It is important to note that as the results obtained from ACTA measurements are comparative, the actual values used are of little consequence as long as they are kept constant and the attachment probabilities obtained are not consistently too high or too low to be of use (Verrelli and Albijanic, 2015).

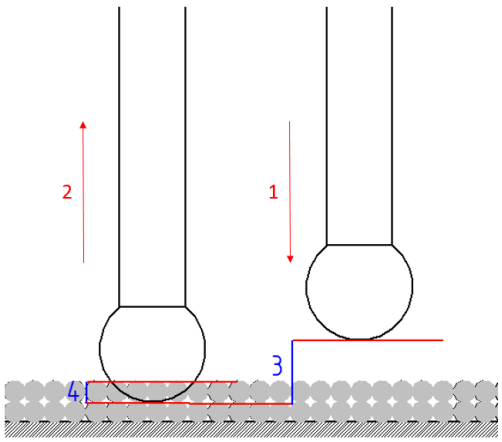


*Figure 63: Schematic depiction of a bubble being pressed into a particle bed (bubble deformation is not depicted for illustrative purposes) and the various relevant parameters. 1: Velocity of approach. 2: Retraction velocity. 3: Approach distance. 4: Bubble compression. Original schematic by D.Sc. M. Aspiala. Edited for this publication.*

Four or five measurements were performed during each experiment day, during which the contact time was the changing variable. The contact time set points for the various experiments are shown in Table 6. The created bubbles vary in size, and so their actual contact time will often vary from the set value. In addition, small variations in the movement of the V-273 actuator also influence the true contact times. An average contact time is therefore determined for each measurement based on the bubble size measurements and V-273 movement data. The average percent error between the set value and the average actual contact time for all performed measurements was calculated

to be 3%. From this calculation the two measurements with a set time of 5 ms were excluded as in those cases the difference between set and actual contact time values was larger, as the operating limits of the device were approached. More information on this subject can be found in Section 5.1.

During the 2-1 and 2-2 experiments, measurements for certain contact times were repeated when a problem had occurred. The contact time set points in the pure chalcopyrite experiments were different than those used for the mixtures. It was expected that with the significant increase in the amount of hydrophobic materials, measuring relatively long contact times such as 200 ms or 290 ms would result in consistently high attachment probability. This would have prevented the detection of any trends. With the current setup of ACTA, contact times can be set between 20 ms and 390 ms.

*Table 6: Table detailing all contact time set points per experiment day in order of measurements (l-r). *Large difference between true contact time value and set value due to device operating limits.*

| Experiment | Contact time set points (ms) | | | | |
|---|---|---|---|---|---|
| **1-1** | 200 | 20 | 110 | 290 | - |
| **1-2** | 20 | 110 | 200 | 290 | - |
| **2-1** | 20 | 50 | 80 | 80 | - |
| **2-2** | 20 | 50 | 80 | 20 | - |
| **3-1** | 20 | 50 | 80 | 110 | 5* |
| **3-2** | 20 | 50 | 80 | 110 | 5* |

## 4.4 Collected mass measurement procedure

During an ACTA measurement, the attached particles get collected in the collection bin. The water is filtered out and the particles are stored for further analysis. For this thesis, only chalcopyrite is used as hydrophobic particles so the obtained samples were not analysed further. There are several options for storing these samples. Two that were considered are instantly preserving the filter and the collected particles with epoxy and then grinding the surface down to allow for analysis of the particles. This has as a benefit that no particles can be lost and the sample is relatively easily used for analysis by scanning electron microscope (SEM). The other option is to store the filters with the particles as-is, only removing the moisture from them by placing them in a desiccator. A downside is that once dried, the particles tend not to remain on the filter and they are easily lost. With this method of storage however, no epoxy is needed, the collected mass can be weighed and particles could be analysed for size and even with SEM, although this might be more difficult if they move around during transporting of the filter. The second method is the one currently in use, with the samples being stored in 20 ml borosilicate glass vials. The procedure and its changes are described below.

### 4.4.1 Round 1

The day before the experiment several 8.0 µm nitrocellulose MF™ membrane filters were placed in a Petri dish. This Petri dish was stored overnight inside a desiccator to remove any moisture from the filters. While the measurement was running, one filter was removed from the desiccator. The filter was placed in an upside down polypropylene cap from one of the 20 ml glass vials for convenient transportation. The combined mass of the cap plus the filter, and separately that of a 20 ml glass vial were then measured and recorded. Both the cap and the vial had been marked with the number of the respective measurement. The filter was then placed inside of a Merck analytical

stainless steel filter holder and the sample was collected as has been described in Section 4.2. After collection of the particles the filter was removed from the holder and placed inside of the glass vial. Extreme care had to be taken during the transfer of the filter to prevent the loss of particles. The shape of the filter holder makes this difficult. The losses can however be minimized or negated entirely by having the filter still be slightly moist when it is removed. When a very strong vacuum was applied and nearly all water was removed, the particles tended to be loose on the filter and were lost more easily. A slightly wet filter resulted in a cake of particles that could relatively easily be transported without loss of material. The open vial with the filter in it were then placed in the desiccator. The following day the cap was screwed on and the vial, cap, and dried filter plus collected particles were weighed again. The mass of collected particles could now be determined by subtracting the weights of the filter, cap, and vial that were measured the day before.

The calculated collected masses of the round 1 measurements can be seen in Table 7. As negative masses were calculated it is clear that there must be an error in the procedure. It was theorized that the impossible results from the mass measurements were caused by the inclusion of the vial and its cap in the measurement procedure. Both are significantly heavier than the filters that weigh approximately 4.5 mg, and the mass of the collected particles. The respective weights of the vial and the cap are approximately 15 g and 1.7 g. In addition, in the measurement after collection of the particles, the masses of the vial and the cap were determined after overnight drying in the desiccator. They had however not been stored in the desiccator before the first measurement. All this can cause measurement errors, as is demonstrated by the negative mass. Another problem was that storing the samples in the glass vials made them difficult to retrieve for potential further analysis. The shape of the vial does not allow for easy retrieval of the filter. Furthermore, once dried up, the particles were less attached to the filter and it was near impossible to move a filter without the particles getting detached and scattered.

*Table 7: Mass of the collected particles for each of the measurements in the 1-1 and 1-2 experiment series.*

| **1-1 Mass collected** | **1-2 Mass collected** |
|---|---|
| 3.0 mg | -6.1 mg |
| -5.4 mg | -3.9 mg |
| 4.2 mg | 0.8 mg |
| 1.4 mg | 2.8 mg |

### 4.4.2 Round 2 (2-1)

Clearly, measurement errors had occurred in round 1. It was therefore decided that in round 2, before collection of the particles, only the dried filter would be weighed. After collection of the particles, the filters were again placed in a vial cap for overnight storage in the desiccator. Once dried, only the filter and the collected particles were weighed. Although this technique should in theory result in the least amount of error, there were massive losses of particles during the transporting of the very thin filter to the scale.

### 4.4.3 Round 2 (2-2)

A container was deemed necessary, both for easy transportation of the filters and to ensure no particles were lost before the weighing step. The vial caps were chosen for this as they are light, not too big and there was a large supply. It also makes it easy to store the filters in glass vials afterwards. The vial caps were now marked with the measurement numbers and stored in the desiccator together with the filters the night before the experiments. Therefore, both the cap and the filter were dried when their weight was first determined. This removed measurement errors

caused by potential effects that storing the caps in the desiccator overnight might have on their weight. Before collection of the particles, a filter and a cap were removed from the desiccator and weighed together. After collection of the particles, the filter was placed back in the cap and stored in the desiccator once more. The day after measurements the cap with the filter as shown in Figure 64, could then easily be transported to the scale and weighed. The collected mass could be determined from the difference between the two measurements. By using this method, no particles were lost in the transporting of the samples to the scale. After some measurements, it was found that when the glass vials were screwed onto the caps while still upside down and stored in a box made for storing these vials, the filters could more easily be used in further analysis. The filters can much more easily be removed from the caps than from inside the glass vials so there is less chance of losing material in the process. With the use of this method, there were no more cases of negative calculated mass. This method was used for all subsequent experiments.

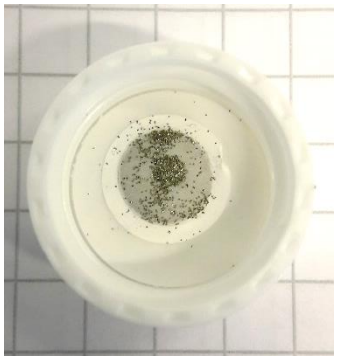

*Figure 64: Nitrocellulose membrane filter with collected chalcopyrite particles stored in the polypropylene cap of a 20 ml vial.*

# 5. Data analysis and sources of error

## 5.1 Data processing

During each measurement, ACTA records a large amount of data in four distinct sets. The first set is the radius and estimated height of each bubble. The second is the recorded V-273 movement of each cycle. The third, after manual inspection of all pictures, is a table detailing at which bubbles attachment has taken place. The fourth set of data is the mass of the collected particles. From these sets of data and their various combinations much can be learned, but it should be processed in a consistent way to make it clear and easily accessible.

For the analysis of data during this thesis, no distinction is made between the attachment of one or multiple particles. Neither is the type of mineral taken into account. Although in most cases the images are clear enough to distinguish between one or multiple attached particles their exact amount can be hard to determine, especially when many attached particles are small and clustered together. For simplicity, and to prevent counting errors, a binary approach is therefore used in these initial stages of device operation. Attachment is defined as the attachment of one or more particles to a bubble. A value of 1 is entered to the attachment table in case of attachment and a value of 0 is used in case of no attachment. Similarly, no distinction is made between the attachment of quartz or chalcopyrite particles. The difference between both minerals can in some cases be seen quite clearly as especially the larger quartz particles appear transparent while the chalcopyrite particles do not. Distinguishing between the two minerals is however a process that is prone to user error. It also becomes more difficult for smaller particles. In addition, it would not be possible to do this for two minerals if neither is transparent. In such a case all particles would appear black against a green background. Therefore, in case of mixed samples, information on the attachment probabilities of specific minerals will have to be obtained from baseline measurements with pure mineral samples and from analysis of the collected material.

For each experiment, the measured bubble sizes are sorted in a histogram with upper limits between 1.65 mm and 1.95 mm and bin sizes of 0.05 mm. For the creation of bubble size distributions these histograms are used rather than the exact measured values. This is done to compensate for the possible measurement errors in the process of determining the bubble heights. For each set of measurements that are to be compared a histogram is made. It shows the frequency of attachment relative to the height of the bubble. An example of this is shown in Figure 65 for the results of round 3. This figure is used to determine the upper boundary for the acceptable bubble size. The limit will vary per set of experiments due to differing experimental conditions. The limit is chosen as the largest size before the first occurrence of 100% attachment probability. In this example that would be 1.85 mm as all bubbles larger than that in the 3-1 experiment had particles attached to them. The lower limit is chosen as the smallest bubble that can still contact the particle bed. This value depends on the expected bubble size specified in the operating code and the chosen bubble compression. The value has been varied between experiments but was for round 3 set to 1.76 mm. With a compression of 0.1 mm any bubble smaller than 1.66 mm could in theory not have touched the particle bed. All subsequent calculations are performed only with those bubbles that are inside the size boundaries.

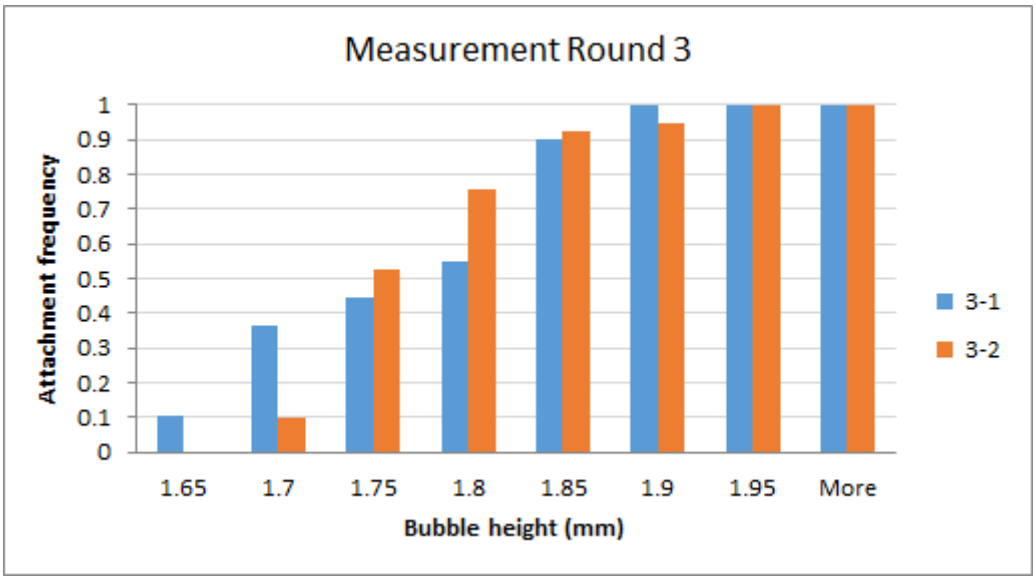


*Figure 65: Histogram showing the attachment frequency relative to bubble size for the results of the Round 3 measurement days.*

This size check prevents bubbles from falsely influencing the attachment probability. Excessively large bubbles will have a 100% attachment probability due to extreme compression. Small bubbles that cannot reach the bed and needles at which no bubble is formed don't have any chance of a particle attaching. Neither of these cases contributes to an accurate measurement of the attachment probability and their excessive occurrence can skew the results. Their inclusion would make comparisons of the results between different measurements and experiments unreliable. If in later versions of the device the bubble size distribution does not shift as much between measurements, this step can perhaps be eliminated.

The attachment probability is calculated by dividing the number of bubbles with attached particles within the size boundaries by the total number of bubbles within the boundaries. Due to the fact that the created bubbles show a size distribution which tends to shift between measurements, the average bubble size might differ from the expected value. In this case, the time of contact with the particle bed differs from the set value. The average contact time of each measurement is determined from the calculated average bubble size and the V-273 movement data. For practical purposes, the movement of each cycle is assumed to be the same as the movement of the first cycle. As is described in Section 5.2, this assumption is for all intents and purposes correct. The attachment probability can then be plotted against a number of variables such as the contact time or the bubble compression. All data can also be examined per separate needle, per bubble size or per ACTA cycle.

## 5.2 Possible sources of error and uncertainty

### 5.2.1 Particle counting

Some of the measurements described in this work were performed in water that had a high turbidity due to the presence of fine suspended particles. During this thesis, the turbidity of the water never inconvenienced the manual counting of the particles. In hypothetical future situations in which very turbid waters and small particles are used, the detection might become more problematic. It cannot be denied that an occasional mistake may have been made as it remains a process based on human judgement and one is dependent on the quality of the photographs.

However, the photographs were for the most part very clear and the particles consistently appear in the same location on the photographs as has been mentioned in Section 3.2. This makes detecting them a simple, albeit lengthy, task. A single bubble constitutes 0.2525% of all created bubbles in a full measurement run. Multiple bubbles would have to be miscounted to cause any significant impact to the measured attachment probability. Such large mistakes are highly unlikely to have occurred. The possible error in the results obtained during this work that might have resulted of miscounting particles are also expected to be negligible when compared to the other factors that currently influence the results.

### 5.2.2 Bubble height calculation

Due to the presence of the collection bin, it is impossible to take a photograph showing all six bubbles from the front. Therefore, their height has to be calculated from the measured radii based on the relationship that was derived in the calibration experiment described in Section 3.2. The resolution of the front view photographs was only 2 MP which meant the photos were not as sharp as they could have been and although the sizes were determined in a consistent manner, it remained a process in which human judgement was required. This will always be prone to error. The derived relationship shown in Figure 43 fits the data relatively well, with an $R^2$ value of 0.9942. However, it remains an approximation and not all data points can be seen to fit equally well. The most aberrant point has a radius of 1.007109 mm and a height of 1.69 mm. According to the derived relationship such a bubble would have a height of 1.72 mm. This difference of 0.03 mm is significant on the scale that is being examined in this work. Most of the 39 other data points can be found closer to the derived relationship so it is possible the aberrant value is a result of a false determination of the height. The fact that the occasional bubble does differ that much from the estimated relationship can however not be discounted. To compensate for these uncertainties regarding the true bubble height the bubbles are sorted in size classes of 0.05 mm width before any bubble size-based trends are examined. Perhaps the calibration can one day be repeated, with better quality photographs and even more bubbles to further specify the relationship between bubble radius and height.

### 5.2.3 Bubble radius measurement

The measurement program analyses the images based on parameters which were found to be successful in finding the edges of bubbles in several photographs with different qualities of lighting and bubble sizes. Not all bubbles will be measured perfectly since they all differ in size and shape. This results in different reflections of light on each bubble. Nor will all bubbles in reality be perfectly spherical. All this means that the measured radius is an approximation. As can be seen in Figure 66, a bubble might in reality be slightly bigger or smaller than the estimated size. It is hard to be certain which is the case as the red line overlaps with the bubble at some locations but in other places it is outside of the edge. In addition, it is hard make a definitive statement on this because what might be perceived by the user as being the bubble edge might just as well be a reflection of light. Visual examination of the collected photographs seems to indicate that most bubbles might in reality be slightly larger than estimated by the program. This is however, purely an educated guess by the author based on having examined multiple hundreds of these images during this work. In theory, the parameters could be set a bit less strict to also detect vaguer edges. Whether this would be useful can be debated however as doing so might cause other objects and pixels to be falsely detected as the bubble edge.

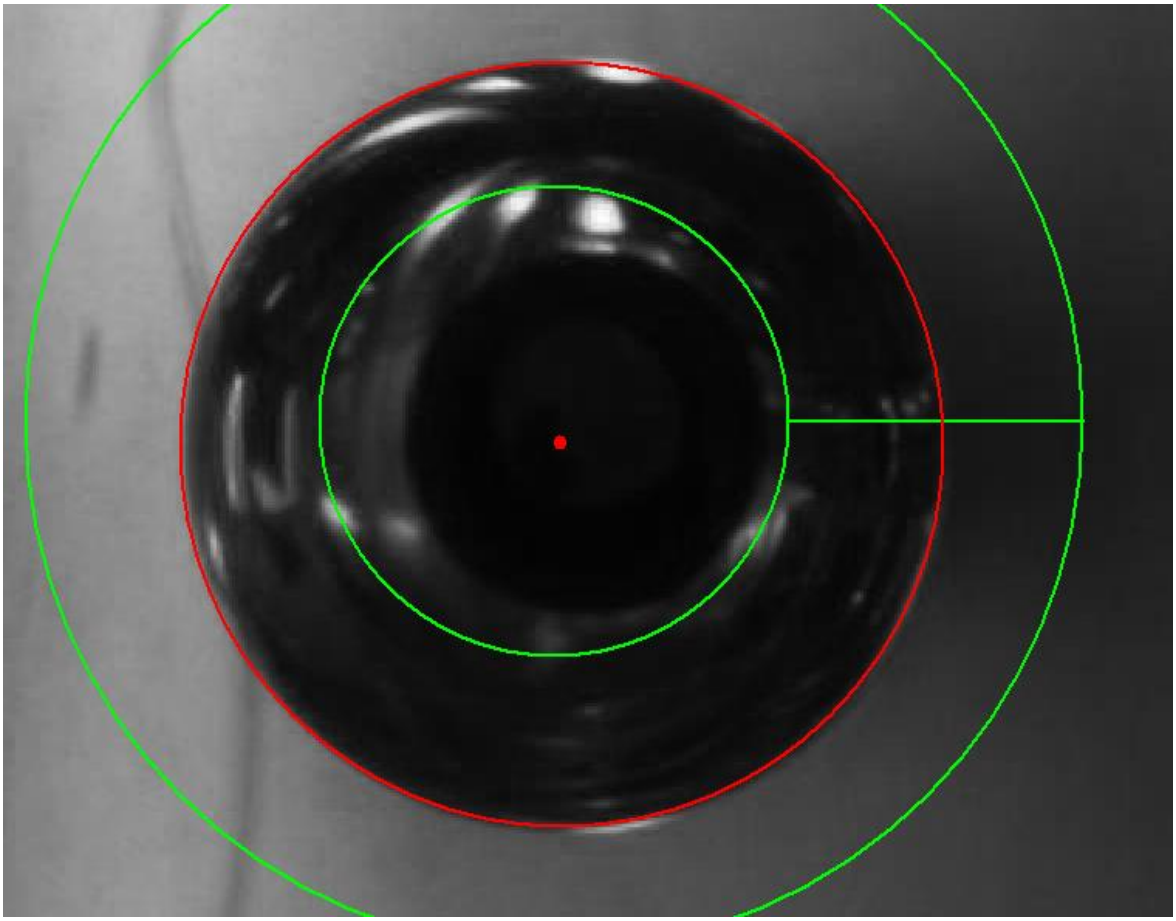

*Figure 66: Example of a processed bubble photograph. The red line shows the estimated bubble size. Green lines show the area in which the image was analysed to find the bubble edge based on the set parameters.*

A quick calculation can be performed to give an indication of the amount of measurement error this issue might cause. Due to calibration file's compensation for lens distortion and needle height the exact real world length of one pixel in the photograph depends on its location. On average, a pixel in the area of the image where the bubbles are found equals approximately 0.0087 mm. Based on the photograph in Figure 66 it is assumed that the measured radius in pixels is about 2 pixels smaller than the 'true' radius. That means the bubble would overall be 4 pixels, or 0.0348 mm, wider than estimated. Due to the nonlinearity of the radius-height relationship, the difference with the calculated height an extra 2 pixels in radius will cause depends on the size of the bubble. Nearly all bubbles that are created have an estimated radius between 0.97 mm and 1.17 mm. this corresponds to heights of 1.65 mm and 2.01 mm. In the 10 most recent measurements, these values have been outside the set bubble boundaries. If these bubbles would in reality be 4 pixels wider their heights would be calculated as respectively 0.034 mm and 0.029 mm larger than now. As these were 'extreme' sized bubbles the difference 4 pixels would make for all relevant bubbles will be somewhere between 0.034 and 0.029 mm. These differences are significant on the scale that is being examined in this work. In an attempt to compensate for these uncertainties regarding the true bubble height the bubbles are sorted in size classes of 0.05 mm width before any bubble size-based trends are examined. This might not be sufficient however, especially if the difference would be more than 4 pixels as then the discrepancy between estimated and actual height would become even larger.

It is good to keep in mind that the determination of bubble size by ACTA is not necessarily meant to be perfect. Rather it is used to identify smaller from larger bubbles to help in the detection of trends for plots such as that in Figure 65. If with the current search parameters the first pixels of the bubble's true edge are not detected by the program due to the edge not having sufficient contrast, this is likely to happen to nearly all bubbles. If all bubbles are detected slightly smaller than they truly are, that would not be a significant problem for the current purposes with which the device is used. These assumptions are only valid however, if no large differences occur in the lighting conditions of the bubbles between measurements. Ensuring even better detection is therefore obviously still preferential. Not much more can be done about this in the current setup of the device however, but in a future project based on further improving the ACTA code, a better detection system might be created. In addition, if the camera is ever upgraded, sharper images could help with the measurement precision. For the current purposes, the code that was developed during this thesis seems to serve acceptably.

The lighting conditions and search parameters in the latest series of experiments have been essentially the same. No significant differences were seen in the turbidity of the water. Visual examination of the photographs revealed no clearly apparent variations in the quality of the photographs or that of the fitted circle between the measurements. It therefore seems unlikely that the bubble detection program could be the cause of the apparent shifts in the bubble size distributions.

### 5.2.4 Calibration grid height

The calibration grid is placed at a height where the average bubble's centre is expected to be. As bubble sizes vary, so do the positions of their centres, of which the circumference is measured. For larger bubbles of which the centre is closer to the camera this means the calibration grid was further from the camera than the circumference that is being measured. These bubbles are therefore perceived as having bigger radii than they have in reality. Similarly, smaller bubbles are measured as having smaller radii. From this radius, the height of the bubble is calculated according to the relationship shown in Figure 43. The effect of having the calibration grid closer or further to the camera than the object to be measured was examined as is shown in Figure 67. A photograph of six bubbles was analysed with 5 different calibration photographs. One was taken at the original location while the other four were taken either 1 or 2 mm above or below its normal position.

Trial experiments revealed that if the search parameters remain unchanged, the bubble measurement program will always find the exact same size on re measuring a photograph. The calibration grid images themselves have a standard deviation of 0.00013 mm according to the program used to create them. This means that the differences in size shown in Figure 67 are caused by changing the grid position. The slopes are all linear and for the most part very similar. There are small differences that can be attributed to the qualities of the individual calibration grid photographs. These varied slightly because the more the object to be photographed deviates from the expected position, the more it becomes out of focus on the photograph. The steepest slope measured here was -0.013x. This means that if the grid was a millimetre behind the measured bubble it would appear to be 0.013 mm smaller than it really was. The difference will in reality never be so big. The needles are in the same location every time the photograph is taken. Therefore the difference between the position of the centre of a bubble with height 2 mm and one of 1.76 mm height is only 0.12 mm. If the grid was located at the centre of the 1.76 mm bubble the grid would

be 0.12 mm behind the measured centre of the 2 mm bubble. Due to the difference this causes in its apparent radius, this would make the bubble appear as being as having a height of 2.00156 mm. Such a difference can be considered negligible.

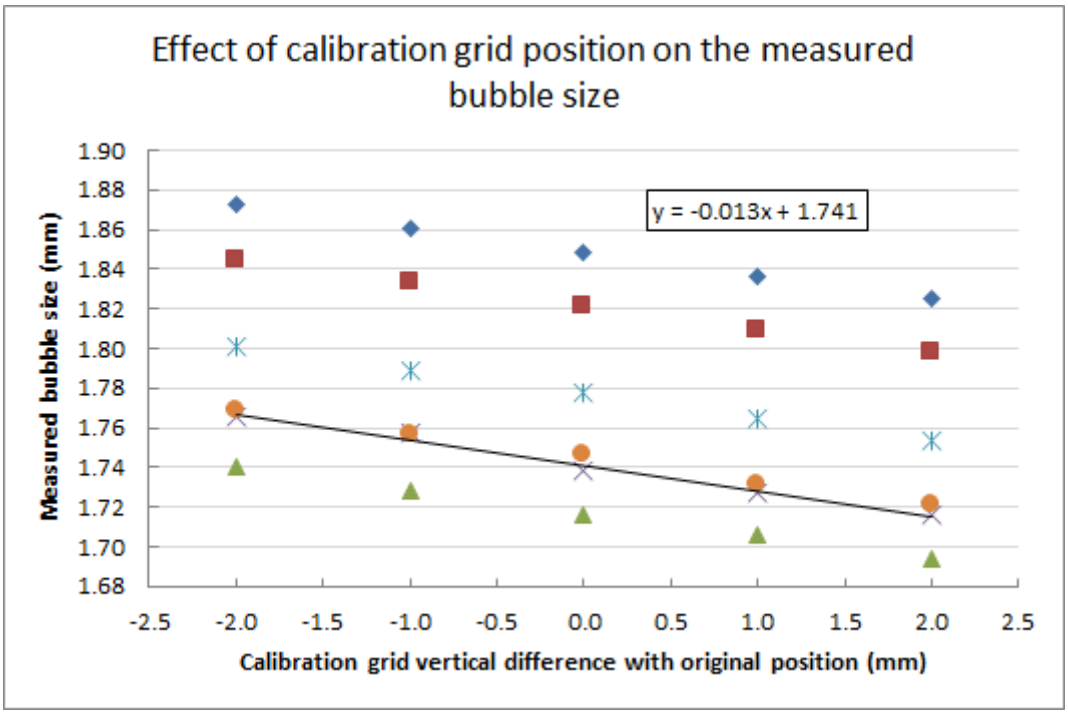


*Figure 67: The height of a set of 6 bubbles measured based on 5 different calibration grid images. The grid images were taken at the original position (0) and respectively 1 and 2 millimetres closer (+) and further away (-) from the camera.*

### 5.2.5 V-273 Movement precision

In theory, errors could occur if the V-273 actuator would not make the exact same motion every single cycle. A lower final position would cause a different amount of bubble compression. A different movement of approach or retraction would cause a different contact time. One data point is recorded every $3.03999 \cdot 10^{-4}$ seconds. The recorded movement data of all 66 cycles of the 80 ms measurement of the 3-1 experiment was compared and the standard deviation of each recorded data point was calculated. The results are shown in Figure 68. The position values of the 1st cycle are also plotted on the secondary Y-axis for illustrative purposes. It can be seen that the standard deviation is highest around the moments that movement is initiated. This is most likely the result of the movement starting one or several data points earlier or later between various cycles. Even there however, the highest standard deviation noted is 0.0004 mm. This assumption is confirmed when the cycles are examined individually. Had bubbles been attached of the expected size of 1.76 mm, they would have touched the particle bed the moment the actuator reaches an extension of 8.48 mm. For all 66 cycles, the time the actuator spent further extended than 8.48 mm (and thus the time the bubble would have been in contact with the bed), was exactly 262 data points. This means that if there were any differences in contact time caused by variations in the movement of the actuator, they were less than 0.3 ms. Differences are present between each set of recorded data due to slight variations in the exact moment the movement is initiated. But once movement was started the actuator made nearly the exact same motion during each cycle. As can be seen from Figure 68 the standard deviation for the position at maximum extension is below 0.00005 mm.

This shows that the V-273 actuator consistently moves to near-exactly the same final position. This repeatability is the result of pre-loading a movement graph rather than sending the position commands live during the movement. A significant variation in contact time or bubble compression occurring due to the V-273 actuator is therefore highly unlikely. If it occurs at all, it will most certainly be overshadowed by the differences in both these parameters caused by the varying size distribution of the created bubbles.

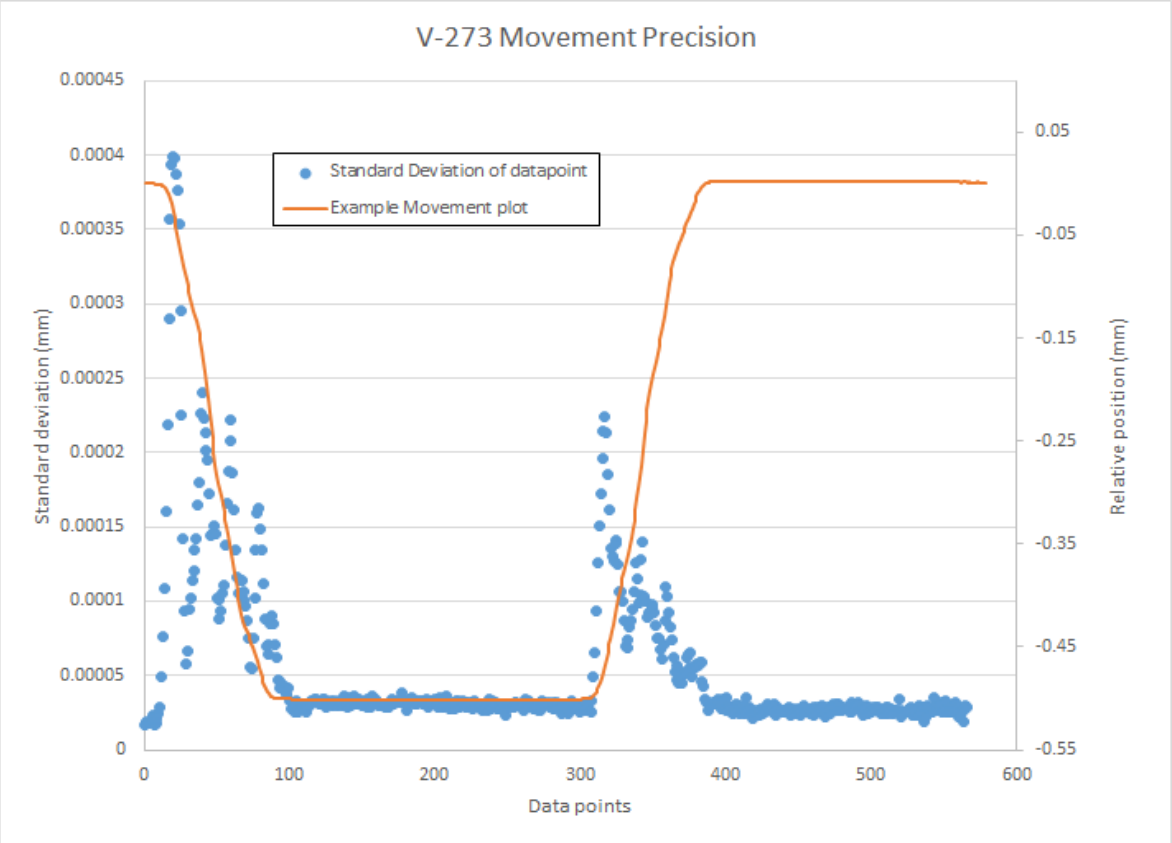


*Figure 68: Standard deviation of each data point of the recorded V-273 movement data of all 66 cycles of the 80 ms measurement of the 3-1 experiment. The actuator position for each data point recorded during Cycle 1 is plotted on the secondary Y-axis for illustrative purposes.*

### 5.2.6 Particle bed height

There are several ways the particle bed could have varied in height between measurements. As the MP-20 actuator possesses a uni-directional repeatability of 0.3 µm, it seems unlikely there could have been significant variation in particle bed height without recalibration of the shovel. A repeatability of 0.3 µm means the MP-20 should have moved the shovel essentially to the same position each time it is lowered. It has to be noted that in recent weeks, due to the shovel tube not being as well attached as it used to be, the shovel became slightly looser than after its first installation. As a result of this, the shovel could be twisted away from its calibrated position more easily. This issue still has to be fixed and means the shovel could have been moved while it was being cleaned. In the procedure for future experiments, the cleaning of the shovel between measurements is removed to ensure no change occurs to its position. The shovel could also be rotated past a 90° angle with the pool wall, which before was not possible. When this occurs, the shovel is no longer aligned parallel to the array of needles.

Differences in the particle bed height between two experiment days are possible due to recalibration of the shovel. Both the height and the tilt could have varied between the experiments. Although the calibration procedure was followed correctly on both days, the calibration piece is made of Teflon, which is a relatively soft material, and the needles are only just touching it as is seen in Figure 69. The fact that the shovel can be rotated past 90°, which is the original calibration position, introduces some arbitrariness to the calibration procedure, which means in theory differences could occur to the exact tilt and the height of the shovel. Large differences seem unlikely, but the true extent of the effect of particle bed height on the attachment probability has not been researched yet. Considering the fact that bubble compression affects the contact time, the contact area, and the applied pressure, it may reasonably be expected to be a significant influence.

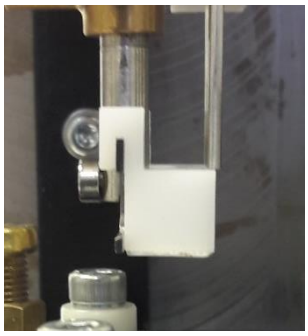

*Figure 69: Photograph of the needles touching the calibration piece.*

### 5.2.7 Segregation and the homogeneity of the particle bed

During rounds 1 and 4 there were several issues due to the use of mixed samples of quartz and chalcopyrite. Even if the mixtures were all prepared to have exactly 1 wt% and 5 wt% chalcopyrite, the surface of the various particle beds that were created most likely did not contain these amounts.

Comparing the attachment probability from various ACTA measurements can only be done if the particle bed can reasonably be assumed to have been equal for each of the measurements. If a mixture with 5 wt% chalcopyrite is measured, the created particle bed should have that 5 wt% homogenously distributed through it. Otherwise it seems unlikely that the surface of the bed that will be in contact with the bubbles will consist of the correct amount of homogeneously distributed chalcopyrite. When some fraction of the chalcopyrite particles floats or forms clusters with air bubbles after conditioning, the remainder of the mixture does not have the same wt% chalcopyrite as it was before. When the amount that floats or clusters varies between measurements, the chalcopyrite content of the mixtures will vary between measurements. Aside from this, settling segregation causes an inhomogeneous distribution of chalcopyrite through the mixture and the created bed, with the chalcopyrite ending up in the lower layers. Thus the surface of the particle bed that is in contact with the bubbles will have a different chalcopyrite content than the originally prepared mixture. Adding to this, an inhomogeneous distribution of the chalcopyrite that did end up on the surface could clearly be seen in the experiments of round 1 as illustrated in Figure 56 (right). The surfaces of the particle beds were clearly different between measurements. All this makes it very unlikely that the particle bed surfaces that were presented to the bubbles during these measurements all had the same amount of homogeneously distributed chalcopyrite. This makes any measurement performed with mixtures essentially unreliable. As has been mentioned in Section 4.2, a raking step was thought to increase particle bed homogeneity but this was never put to the test due to the issues with the other segregation effects such as the floating particles and the clusters.

### 5.2.8 Bubble size distributions and the length of the needles

In an ideal device all needles would have the same length and the same tilt so when it is calibrated the shovel exactly aligns with all needles. In such a case all needles would have the same distance to the particle bed. This would improve the repeatability of the experiments and increase the

accuracy of the determined relationships between bubble size and attachment probability. In the current state, the shovel and the calibration piece are both straight, but aligned against a set of needles that is clearly not straight. This will cause some needles to be further from the bed than the rest. If all bubbles that were created had the same size, there would in principle be no problem with a needle being shorter than the rest because the measurements are meant to be comparative. The position of the needles is consistent, the calibration procedure is always the same and the needle positions don't change either. So in principle, although it would not be ideal, the situation would be the same for each measurements and therefore the results of different experiments could be compared to one another regardless of the needle positions.

The problem lies in the fact that there is a distribution in the size of the created bubbles that also tends to shift between measurements. At the shorter needles only the largest bubbles have chance of attaching to particles. Therefore, a bubble of a certain size created at Needle 1 will have a different probability of attachment than that same bubble at Needle 3. This causes problems in obtaining consistent results for the attachment probability of various bubble sizes and interferes with the repeatability of the measurements. Two measurements under the same conditions with the exact same bubble size distribution can have different attachment probabilities based on which needles the bubbles form at. How big this effect truly is, is yet unknown. In principle, examining the results per bubble size per measurement per separate needle is possible. However, in this case the number of bubbles is often insufficient for determining the probability with high certainty. The number of bubbles per size class tends to vary quite a lot due to the shifting bubble size distributions. This makes comparison of these very specific results problematic as one might be comparing 4 bubbles of a certain size made at a specific needle during one measurement against 50 similarly sized bubbles at the same needle for another measurement.

The fact that the needles have different lengths makes the impact of the shifting size distributions hard to estimate and interferes with the identification other causes of measurement uncertainty. It is therefore itself a source of uncertainty in these measurements.

# 6. Results and Discussion

## 6.1 Round 1

*Table 8: Contact time set points, average contact time, attachment probabilities, collected mass, weight percent chalcopyrite (Cp), and number of bubbles out of range for the experiments of round 1.*

| Experiment | Contact time set point (ms) | Average contact time (ms) | Attachment probability | Collected mass (mg) | Bubbles out of range |
|---|---|---|---|---|---|
| **1-1** (1 wt% Cp) | 200 | 198 | 0.27 | 4.2 | 2 |
| | 20 | 21 | 0.19 | 3 | 1 |
| | 110 | 108 | 0.56 | -5.4 | 7 |
| | 290 | 286 | 0.11 | 1.4 | 7 |
| **1-2** (5 wt% Cp) | 20 | 20 | 0.19 | -6.1 | 1 |
| | 110 | 106 | 0.17 | -3.9 | 5 |
| | 200 | 195 | 0.07 | 0.8 | 32 |
| | 290 | 285 | 0.54 | 2.8 | 12 |

The lower bubble size limit was 1.645278 mm while the upper limit was 1.95 mm. Measurement details and results are shown in order of measurement in Table 8. The attachment probability is plotted against the contact time in Figure 70. Increasing the chalcopyrite content of the mixture did not consistently result in higher attachment probability and neither did increasing the contact time. There are several possible explanations for these unexpected results. Firstly, there were many changes made to the experimental procedure during this round and therefore samples were not all treated the same way. Secondly, there is no guarantee the samples were all equal due to incorrect sampling during their preparation. Thirdly, the shovel had to be recalibrated in between each measurement, which can cause differences in the exact particle bed height. Lastly, the homogeneity of the particle beds varied between measurements due to the segregation of quartz and chalcopyrite particles. Even if the mixtures were all prepared to have exactly 1 wt% and 5 wt% chalcopyrite, the surface of the various particle beds therefore most likely did not consistently contain these amounts. In addition, according to the measurements, negative mass was collected. This indicates there were large measurement errors and although this was a useful run to become acquainted with the operation of the equipment, these results should be ignored.

Clear differences can be seen in the distributions of the measured bubble sizes that have been plotted in Figure 71. Due to the varying samples and measurement conditions, it is impossible to know for sure how significantly this will have affected the results. What causes these variations is still unknown. It could have something to do with chemical environment variations, physical environment variations, or be caused by heating or wear of device components such as the air hoses. From Figure 71 can also be seen that the 1-2 200 ms measurement had the largest number of bubbles under 1.65 mm. Interestingly enough, it is also the only measurement of this round where bubbles larger than 1.9 mm occurred. As shown in Table 8, this causes that particular measurement to have a relatively large number of bubbles that are outside the selected boundaries.

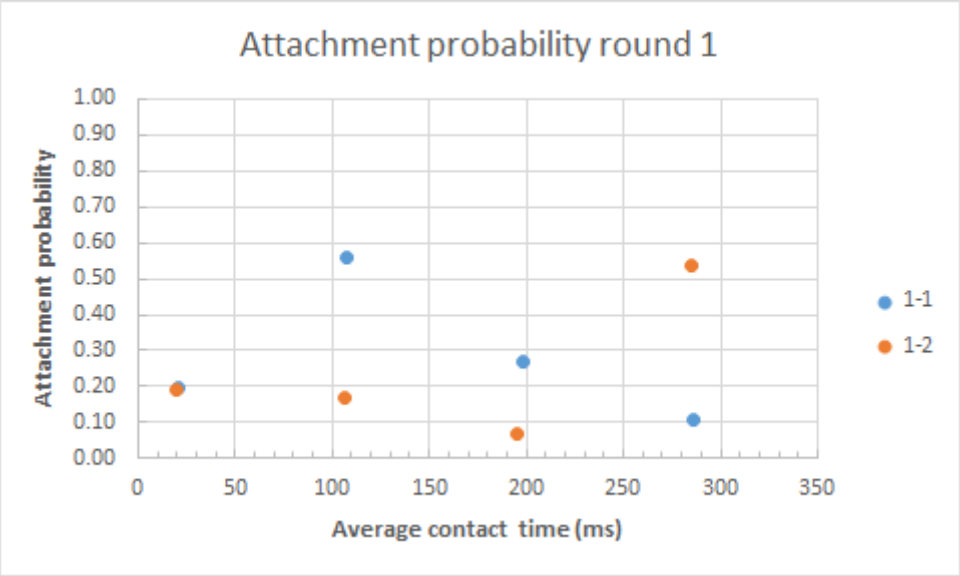


*Figure 70: Attachment probability plotted against the average contact time for the experiments of round 1.*

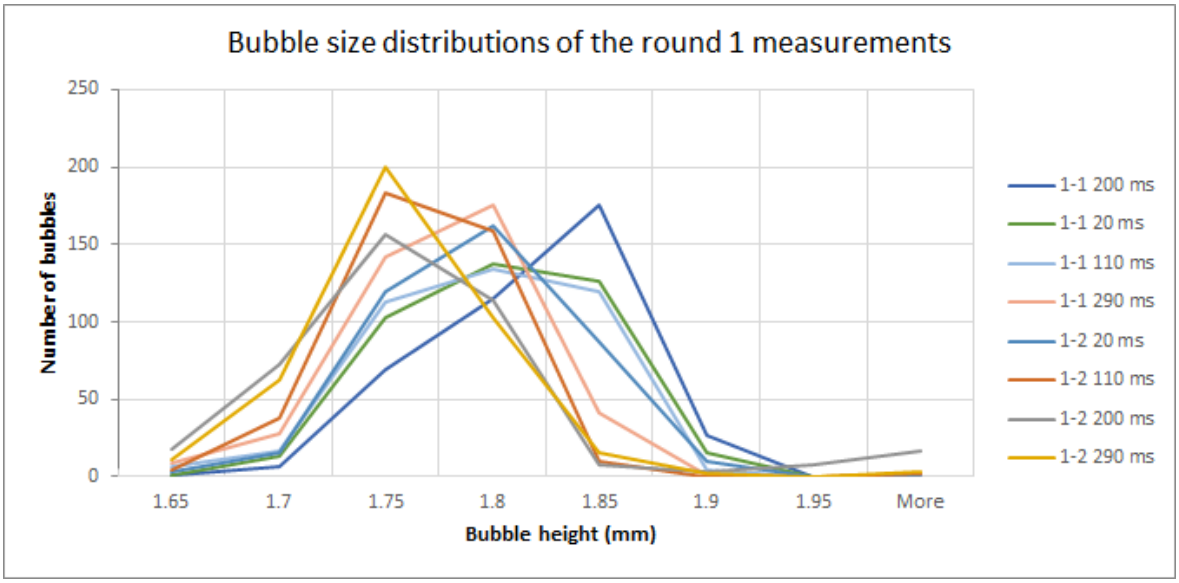


*Figure 71: Bubble size distributions of the round 1 experiments. Measurement names are given based on the experiment and the contact time set point. The names are listed from top to bottom in order of measurement.*

## 6.2 Round 2

*Table 9: Contact time set points, average contact time, attachment probabilities, collected mass, weight percent chalcopyrite (Cp), and number of bubbles out of range for the experiments of round 2. *During this measurement only 216 bubbles were created instead of the regular 396.*

| Experiment | Contact time set point (ms) | Average contact time (ms) | Attachment probability | Collected mass (mg) | Bubbles out of range |
|---|---|---|---|---|---|
| **2-1** (100% Cp) | 20 | 21 | 0.37 | 1.5 | 48 |
| | 50 | 48 | 0.56 | 0.4 | 8 |
| | 80 | 77 | 0.16 | 1.1 | 4 |
| | 80 | 78 | 0.78 | - | 147 |
| **2-2** (100% Cp) | 20 | 21 | 0.83 | 2.2 | 15 |
| | 50 | 47 | 0.41 | 1.4 | 21 |
| | 80 | 78 | 0.58 | 1.7 | 8* |
| | 20 | 20 | 0.77 | 2.6 | 17 |

The lower bubble size limit was 1.645278 mm while the upper limit was 1.90 mm. Measurement details and results are shown in order of measurement in Table 9. The attachment probability is plotted against the contact time in Figure 72. The expected trend of increasing attachment probability with increasing contact time cannot be confirmed from these results. In addition, both sets of data do not well resemble one another. The use of 100% chalcopyrite instead of quartz mixtures should have prevented any segregation issues resulting in inhomogeneous particle beds. The samples were however prepared from two different batches of chalcopyrite with two different methods, as described in Sections 4.1.1, 4.1.2, 4.2.2 and 4.2.3, which lessens their comparability. The unexpectedly high attachment probabilities for the 2-2 20 ms measurements and the unexpectedly low value for the first 2-1 80 ms measurement might indicate discrepancies in the particle bed height caused by recalibrating of the shovel in between measurements. As mentioned in Section 4.2, an error was made in the calculation of the amount of xanthate, resulting in the 2-2 experiment only having a xanthate concentration of 28.8 g/t solid.

Only three measurements with different contact times were performed each day. The 2-1 80 ms measurement resulted in an unexpectedly low attachment probability. The measurement was therefore repeated and the resulting probability together with the measured results of the 20 and 50 ms measurements seem to indicate an upwards trend. Due to the absence of a fourth contact time however, it cannot be stated with certainty that the first 80 ms measurement is an outlier. In addition, a problem with bubble formation occurred during the 80 ms repeat measurement. During the measurement, the problem worsened over time and prevented the formation of normal bubbles. Instead, small streams of microbubbles came from the needles, or the bubbles became immensely big due to a previous bubble not disappearing completely. The problem resulted in 147 cases where the bubble was out of either range, or non-existent. As was mentioned in Section 4.2.3, the problem is suspected to have occurred due to a possible detergent contamination caused by the process of cleaning the sieve that was used for rinsing the samples. Although it cannot be conclusively proven, this explanation is thought to be more likely than a mechanical issue because the problem became consistently less, and eventually disappeared, after several rounds of rinsing

the needles and the pool with water after completion of the measurement. In addition, the presence of a detergent seems a plausible explanation for the problems with bubble formation as it is known to interfere with surface tension. It is unknown what effect this possible detergent contamination might have had on the attachment probabilities of the good bubbles made in the early cycles of the measurement. Whatever the reason for the problems, the 2-1 80 ms repeat measurement data point, although included in the graph, is perhaps best ignored.

During the 2-2 experiment the first 20 ms measurement gave an unexpectedly high value. The measurement was therefore repeated after completion of the 50 ms and 80 ms measurements. Interestingly enough the result of the second attempt is very similar to the first one. The source of this discrepancy however, cannot be stated from this data set. The 2-2 50 ms and 80 ms results are respectively 0.15 and 0.20 pp lower than the measured attachments of their 2-1 counterparts. As it concerns only two data points however, nothing can be said with certainty about whether this is due to differences in bed height, bubble size distributions, the effect of having two different stocks of chalcopyrite, the lower concentration of xanthate, or if it is purely random. In addition, the 2-2 80 ms measurement consisted of 36 cycles instead of the regular 66 due to a mistake made by the author which caused the measurement to abort. Only 216 bubbles were therefore created, of which 8 were out of bounds as listed in Table 9.

The bubble size distributions plotted in Figure 73 clearly show the smaller amount of created bubbles in the 2-2 80 ms measurement and the possible contamination issues in the 2-1 20 ms repeat measurement. In all measurements, bubbles over the size of 1.90 mm have been created although all of them are considered out of range. In the round 1 experiments only one measurement had bubbles larger than 1.90 mm. The distributions seem to have shifted slightly to the larger bubble sizes when compared to the round 1 experiments. In round 2 all distributions reach their maximum in the 1.75 to 1.80 mm size range whereas this was only the case for four of the round 1 distributions. Again, clear differences can be seen between the shapes of the distributions, although perhaps less so than for round 1. Whether this is caused by changing environmental conditions such as moisture content of the air or varying temperatures or chemical changes such as solution pH is unknown. The phenomenon of the shifting distributions was not yet recognized at the time these experiments were performed so unfortunately none of these parameters were recorded. This increase in the amount of larger bubbles combined with the lower upper boundary causes more bubbles to be outside the limits even for measurements that were not cut short or contaminated. An extreme example of this is the 2-1 20 ms measurement of which 48 bubbles (12.1% of the total amount) is filtered out.

The data about the collected mass of the 2-1 experiment can be ignored. Massive losses of particles occurred before they could be measured due to problems with the procedure while the particles of the fourth measurement were not collected due to the contamination of the water. The results from the 2-2 experiment are plotted in Figure 74. Apparent differences between this graph and that of the attachment probability can be explained by the fact that attachment probability is noted as a binary 1 or 0. For every 1 there could in reality be multiple particles. Their size can also vary slightly from 106 µm to 125 µm. It can also not be denied that the occasional particle might have been lost, as the transfer of the filter from the filter holder into the vial cap remains a precarious process.

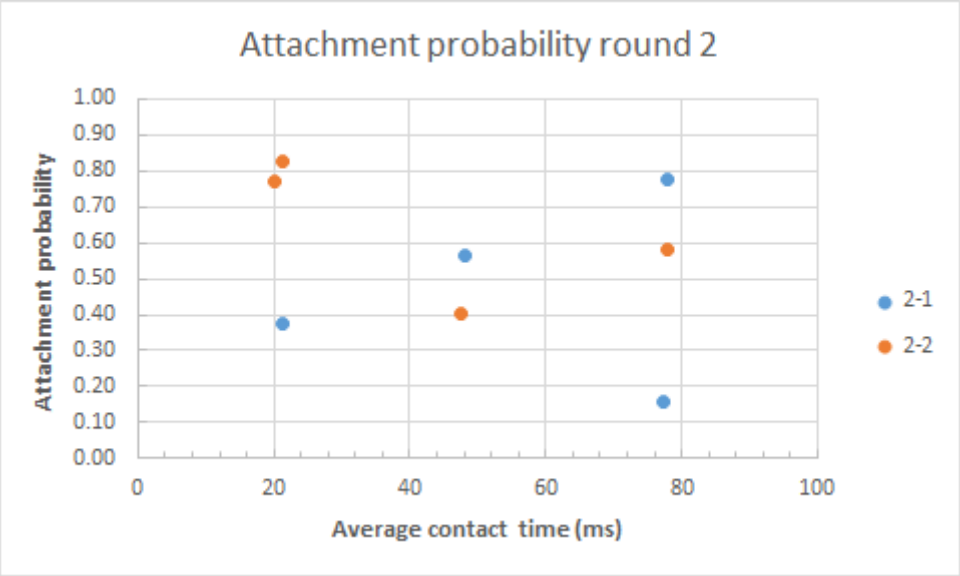


*Figure 72: Attachment probability plotted against the average contact time for the experiments of round 2.*

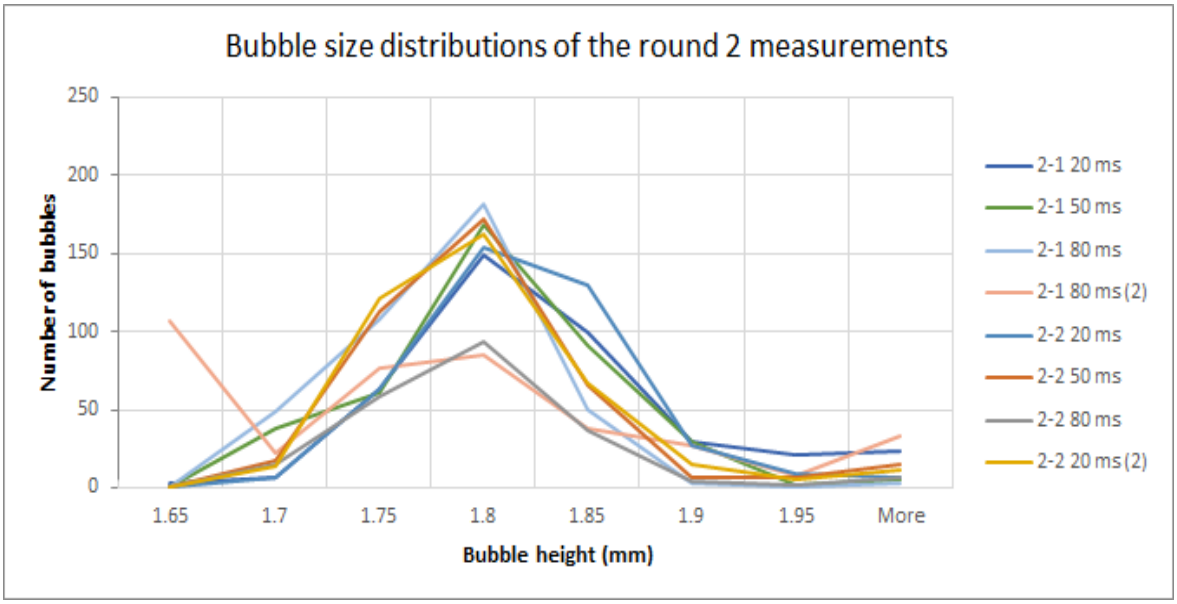


*Figure 73: Bubble size distributions of the round 2 experiments. Measurement names are given based on the experiment and the contact time set point. The names are listed from top to bottom in order of measurement.*

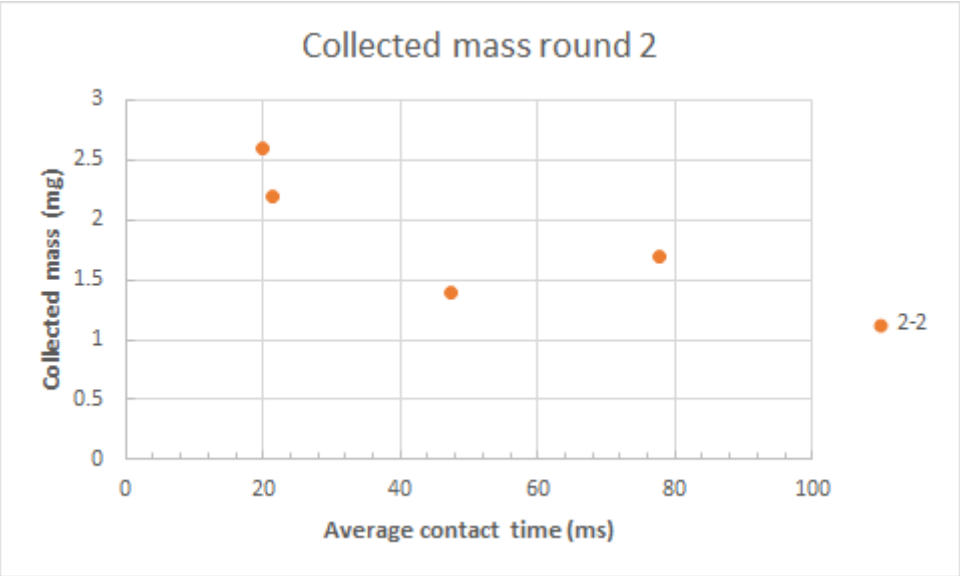


*Figure 74: Mass collected during the experiments of round 2.*

## 6.3 Round 3

*Table 10: Contact time set points, average contact time, attachment probabilities, collected mass, weight percent chalcopyrite (Cp), and number of bubbles out of range for the experiments of round 3. *The large difference between the set and the average contact time values is the result of device operating limits.*

| Experiment | Contact time set point (ms) | Average contact time (ms) | Attachment probability | Collected mass (mg) | Bubbles out of range |
|---|---|---|---|---|---|
| **3-1** (100% Cp) | 20 | 21 | 0.44 | 2.7 | 45 |
| | 50 | 51 | 0.57 | 2.9 | 21 |
| | 80 | 78 | 0.64 | 3.7 | 16 |
| | 110 | 107 | 0.77 | 5.2 | 50 |
| | 5 | 18* | 0.47 | 2.5 | 52 |
| **3-2** (100% Cp) | 20 | 22 | 0.67 | 2.7 | 66 |
| | 50 | 52 | 0.74 | 3.9 | 53 |
| | 80 | 81 | 0.77 | 4.4 | 70 |
| | 110 | 111 | 0.82 | 4.1 | 48 |
| | 5 | 18* | 0.71 | 3.3 | 51 |

The lower bubble size limit was 1.66 mm while the upper limit was 1.85 mm. Measurement details and results are shown in order of measurement in Table 10. The attachment probability is plotted against the contact time in Figure 75. The relatively high attachment probabilities were expected due to the use of the 3000 g/t xanthate concentration. The results of both measurement days seem to indicate the expected trend of increasing attachment probability with increasing contact time. Unfortunately, they do not show the same trend nor are the results of measurements at approximately the same contact time very similar between both days. Between the results that are the closest together, that of both 110 ms measurements, there still is a gap of 0.05 which quickly increases to 0.24 when the contact time set point becomes shorter.

The bubble size distributions are plotted in Figure 76. The largest individual differences so far can be seen in this round. Especially the distributions of the 80 ms and 110 ms measurements of the 3-1 experiment exhibit a clear shift to the smaller bubble sizes, setting them apart from the rest of the measurements. Overall, when compared to rounds 2 and 1 most of the distributions seem to have shifted yet again to the larger bubble sizes. Most still peak at the 1.75 - 1.8 mm size but a larger part of the distributions than in round 2 overlaps with the 1.8 - 1.85 mm class. It is unfortunate therefore that the attachment reached 100% for the 1.85 - 1.9 mm bubbles. Due to this, the upper limit is set at 1.85, resulting in a large number of bubbles being filtered out. In future experiments, this might be prevented by setting a lower bubble compression. The general shift to larger bubbles observed over the course of this thesis might have had something to do with the increasing amount of xanthate used although this cannot be conclusively proven. It could also have been the wear of the pump hoses or the climate outside. The individual variations between measurements that can be quite significant are also still unexplained.

The collected mass is plotted against the attachment time in Figure 77. For the most part it increases with increasing attachment time.

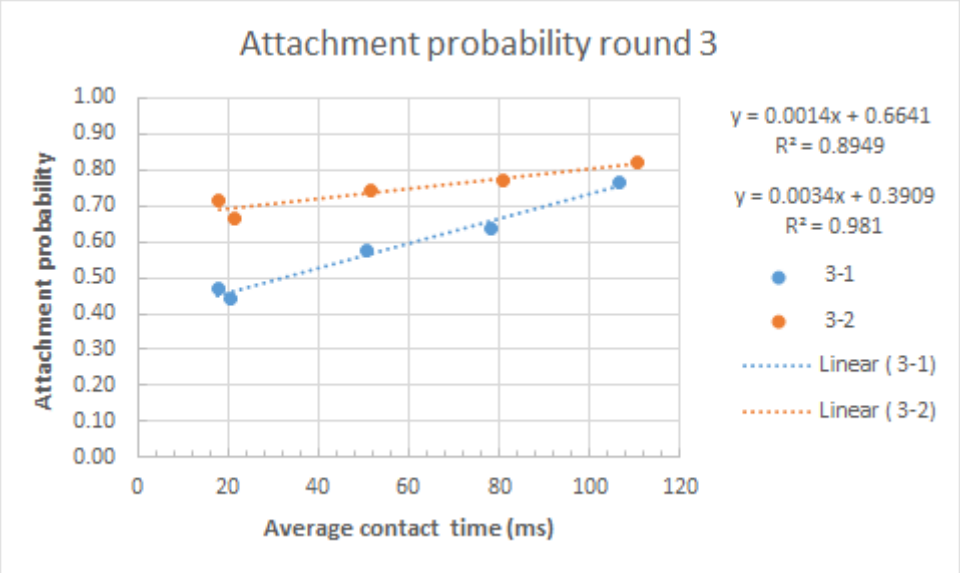


*Figure 75: Attachment probability plotted against the average contact time for the experiments of round 3.*

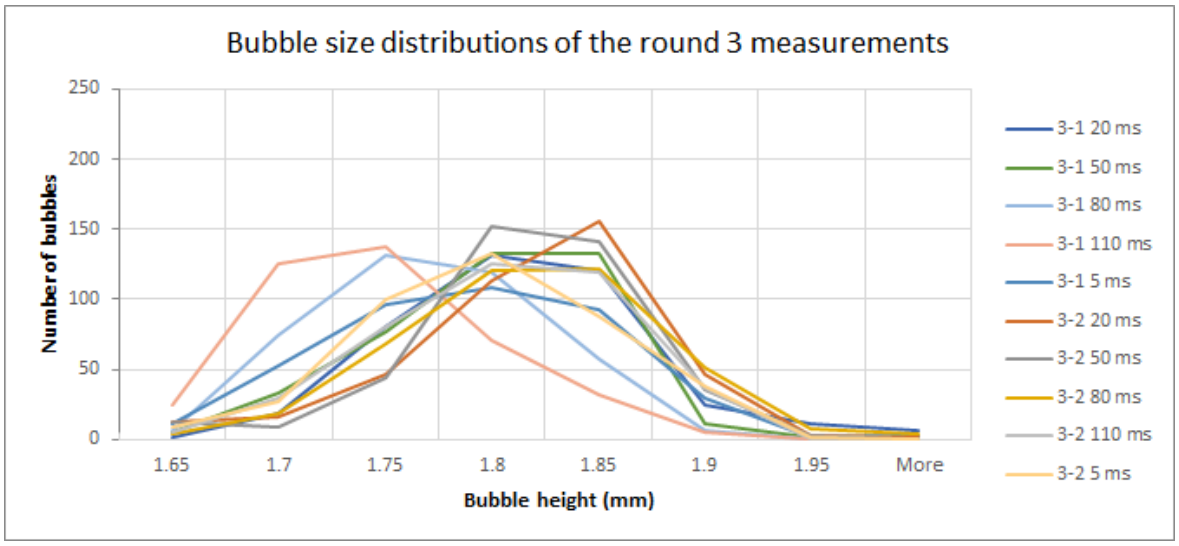


*Figure 76: Bubble size distributions of the round 3 experiments. Measurement names are given based on the experiment and the contact time set point. The names are listed from top to bottom in order of measurement.*

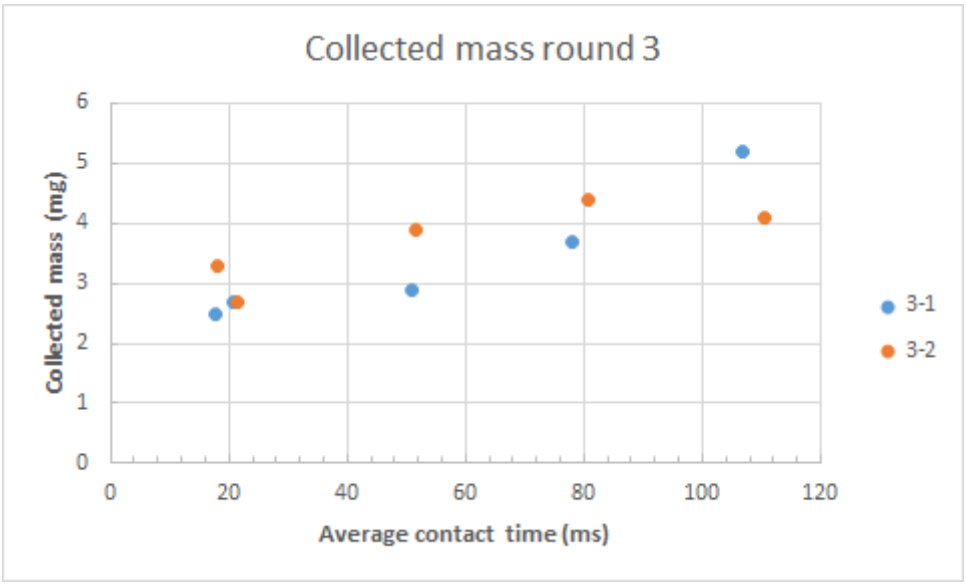


*Figure 77: Mass collected during the experiments of round 3.*

The presence of the attachment probability trends indicates that that the changes made to the device and the experimental method might have been beneficial to the repeatability of the measurements. Several things might have caused the discrepancy in the attachment probability between both days although none can definitively be confirmed. It is improbable that the large differences are caused by random measurement error. If the random error could be as much as 0.24 it seems highly unlikely that two clear upwards trends would be visible. Of all the measurements performed during this thesis the four that can be considered the most comparable are the 5 ms and 20 ms measurements of this round. This is because the 5 ms setting ended up being 18 ms due to device operating limits. In addition, the same stock of chalcopyrite was used to prepare the mixtures, and all samples were treated equally before the measurements. For 3-1 and 3-2 the differences between the 18 ms and 20 ms measurements were respectively 0.03 and 0.04. These results are very close to one another, even though there were three measurements

performed in between. It seems reasonable to assume these smaller differences are caused by measurement error or bubble size variations while the large 0.24 difference is caused by some condition being different between both days. This is however impossible to conclude based on the current set of data.

The effect of the shifting bubble size distributions on the attachment probability is unknown. As the distributions shift between basically every measurement, this makes evaluating the data problematic. The two distributions that are clearly the most different from the rest are that of the 3-1 80 ms and 3-1 110 ms measurements. But against all expectations, these two points are in fact the closest to their 3-2 counterparts. This is peculiar as it would be expected that smaller bubbles, with smaller contact times, compression, and contact area would have much smaller attachment probabilities than their larger sized counterparts. The most likely reason for the difference in attachment probability between the measurement days is differing particle bed heights. This could be due to an error in the calibration of the shovel, resulting in a systematic difference in bed height between both days. Another possibility is differences between the beds made on the same day due to variations in the movement of the actuator, or something else changing the shovel height. Even though the shovel did not have to be recalibrated between measurements it was calibrated at the start of each day. Due to the issues discussed in Section 5.2.6, this could have caused a systematic difference. Small variations within the day are less likely because the MP-20 actuator possesses a Uni-directional repeatability of 0.3 µm. It has to be noted that in recent weeks the shovel could be moved slightly more than it could be before due to the shovel tube not being as well attached as it used to be. This issue still has to be fixed and might have had an influence.

Whether there truly were differences in the heights of the beds cannot be determined from the data. In theory, the attachment probability could be examined by comparing the measurements with the same contact times from both measurement days. Plotting the attachment frequency per bubble size class for such a comparison as is done in the example plot in Figure 78 might in theory help in clarifying the obtained results. If there was a systematic difference in particle bed height between the experiments, this would be reflected in those plots. The movement of the needle array is based on the expected particle bed height and was therefore the same for both experiments in

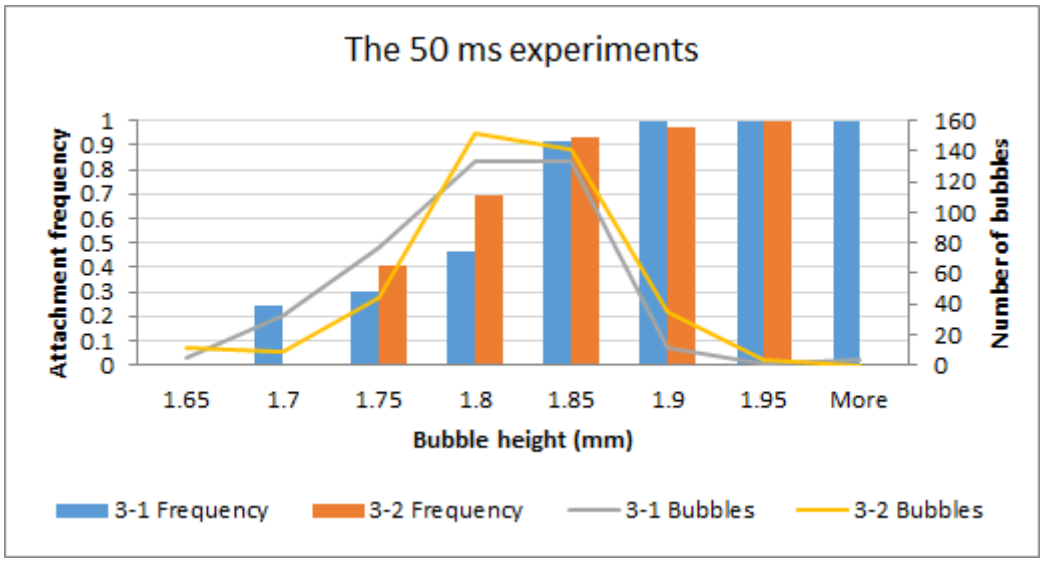


*Figure 78: The measurement results of the 50 ms measurements of both experiment days respective to the bubble size. Primary Y-axis: Attachment frequency. Secondary Y-axis: The bubble size distributions.*

round 3. If the bed height was in fact higher for the 3-2 experiment than for the 3-1 experiment, the 3-2 bubbles would have been compressed more than comparable bubbles in the 3-1 experiment. Increased bubble compression would cause a larger contact area with the particle bed and a longer contact time. In this case, the bubbles made during the 3-2 experiment could be expected to show a higher probability of attachment than those of 3-1 over the entire size range and for all contact times.

Although all these plots could be made, there are several reasons why their reliable analysis can unfortunately not be done with the currently available data. Firstly, although the contact time set point values might have been the same, the true contact times were not always similar. This would lower the comparability of the measurements. Secondly, the size distributions are different for each experiment, resulting in varying numbers of bubbles in each size class. Especially for the larger and smaller bubble size groups which contain less bubbles this makes reliable comparison problematic. Aside from that, there are clear differences between the average sizes of the created bubbles between the various needles. Figure 79 illustrates this for the measurements of the 3-1 experiment. Variations in the average size of the created bubbles can be seen between the six needles for the same measurement. Differences can also be seen for the average size of the bubbles made at one specific needle in different measurements. Even if the bubble size distributions were not constantly varying, the data plots of attachment probability relative to bubble size of the type shown in Figure 78 would be misleading due to differences in needle height. A bubble of a certain size will be compressed differently depending on the needle where it was produced. Due to this the attachment probability of a certain bubble size could still vary even if all other influences remained unchanged. In principle, the data could still be compared between both days by only examining one specific size of bubbles, made at one specific needle, from measurements with the same contact time set point. This would however be an immensely time-consuming task. Moreover, there would only be a very small number of bubbles to compare in each group. This would lead to a large level of uncertainty in the results. In the absence of more data, all that can be said about the cause of the discrepancy in attachment probabilities between both days must remain speculation.

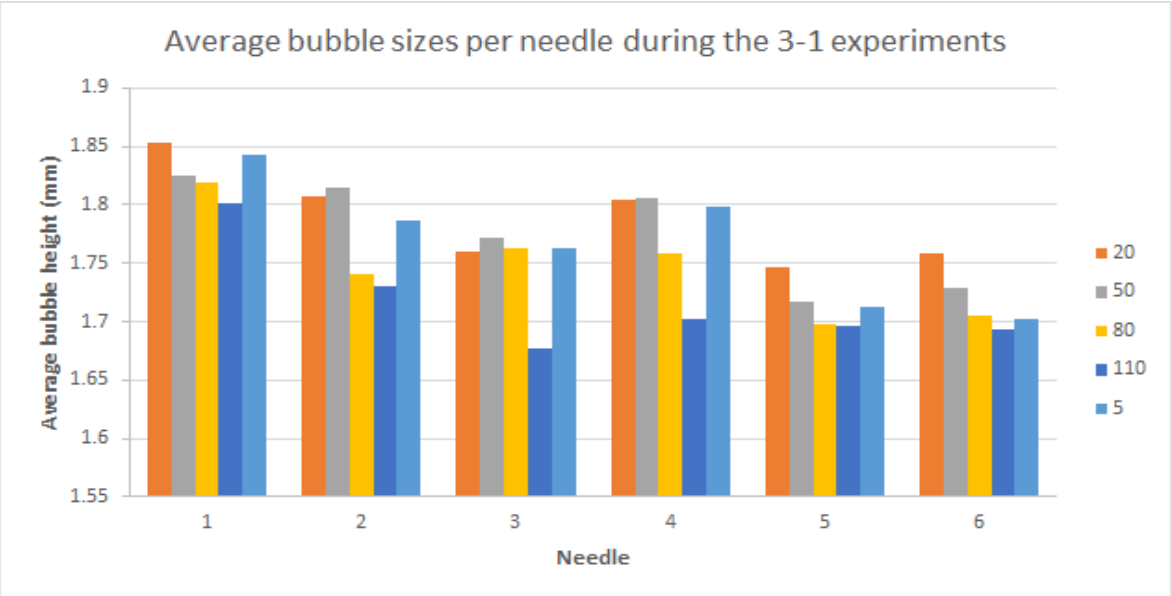


*Figure 79: The average sizes of the created bubbles divided per needle per measurement for the 3-1 experiment. This includes all created bubbles, no boundaries were set. The needles are ordered from left to right. The measurements are ordered from left to right in the order they were performed in.*

# 7. Conclusions

The first prototype of the ACTA experimental setup and its experimental method were developed for the measurement of attachment probability of particles to air bubbles. The instrument and the developed method serve as a tool to detect and predict changes in the floatability of particles in different liquid environments. The main aims of the work were improving the functionality and user friendliness of the first prototype of the instrument, developing the experimental methodology for performing particle-bubble attachment time studies with the device for different flotation related systems of interest, and providing proof of concept of the device and the experimental method.

The first aim was achieved by systematic testing and step-by-step changes to the device's operating software code, hardware components, and functionality. The experimental method for testing flotation related ore and mineral systems was also developed. This method includes the sample preparation and sample treatment both prior to measurements and after their completion. In addition, a procedure was developed for the processing of measurement results. The calculation and summarizing of values of interest from the measurement results was automated, saving future users both time and effort.

The proof of concept testing of the setup and the developed method were done by performing measurements on model systems, consisting of both pure and mixed samples of quartz and chalcopyrite particles. The expected trend of increasing attachment probability when the contact time between a bubble and hydrophobic particles increases, was observed in two of the experiments with chalcopyrite particles. The presence of these upwards trends indicates that the improvements made to the device and the experimental method have been a step in the right direction. For mixed solid samples, no increasing trend was observed, perhaps due to various issues with the homogeneity of the particle beds. Further studies will have to be performed to determine the reproducibility of the measurement results and to definitively validate the developed experimental method.

The work done during this thesis has resulted in many new insights into the limitations and the possibilities of ACTA. There can be no doubt that the device shows great potential for the gathering of significant amounts of data in short periods of time, to which no other currently available device can even come close. As this work comes to a close, it is now up to others to build on the foundations laid here and continue the work towards the eventual use of ACTA as a practical and reliable measurement tool in mineral flotation-related studies.

# 8. Recommendations

There is now a first indication that the expected trends in attachment probability can be obtained by measurements with ACTA. I have several recommendations on how to proceed with the ACTA development in the near future.

## 8.1 Future studies

There is not that much that can be deduced from the results presented in this work. Due to the many different types of conditions that were tested they can't effectively be compared. Even though during the 3rd round, 10 measurements were performed under the same conditions with the same samples, they are split over 5 contact times. The most comparable ones are the 4 measurements of that round that are within the 18-21 ms contact time range, but they do not paint a conclusive picture. It is impossible to pinpoint a reason for the lack of repeatability in the results. This is due to shifting bubble size distributions, different needle lengths, varied contact times, different measurement conditions. Adding to this there is a lack of knowledge about the influences of the moisture content of the surrounding air, solution pH, and the temperatures of the air and the liquid. I recommend the following approach.

1. Create a new array of needles in which the needles cannot move. Have the needles made as similar as possible and then cut them at the exact same length. Without this, none of the data regarding the size of the bubbles can be interpreted correctly.
2. Have the new holder of the needles be made of other material than Teflon. The material is too soft and the current one leaves far too much variation in the way it can be assembled as evidenced from the differing locations of the needles in the photographs. This will doubtless have affected the calibration of the shovel.
3. Ensure the shovel tube is glued in place so it cannot move anymore. Also make sure the shovel cannot twist beyond its intended 90° angle with respect to the pool wall. This removes uncertainty from the calibration procedure.
4. Make a new, wider calibration piece that is not made out of Teflon. Some of the needles are only barely touching the end of the piece. In addition the material is too soft to be certain about the height calibration.
5. When all this has been achieved, do a series of experiments on pure mineral samples prepared from the same stock, with one xanthate level (both g/t and g/L concentrations must be controlled) and one contact time. The moisture content, air and liquid temperatures, pH must all be recorded.

Such a systematic study is necessary for the identification and subsequent elimination of the measurement errors. From this we could hopefully learn the origins of the bubble size distribution shifts and perhaps quantify their impact on the attachment probability. Only in this way can we also conclude with certainty that the experimental method developed during this thesis is correct. Once this is known a good next step would be testing the device's sensitivity to different xanthate concentrations and slowly continue building to more complicated systems from there.

## 8.2 Coding

Another set of recommendations regards the code with which ACTA is operated.

1. I would suggest to make a project out of the creation of an automated particle detection system. The time and effort this would save in the interpretation of data should not be underestimated.
2. There could simultaneously be made improvements to the bubble size measurement code. If the measurements are more precise, smaller size classes can be used in the analysis of the data, which will allow for more precise interpretation of various trends.
3. There might be found better ways to automatically organise and save all the data. Now the data from ACTA is manually copied into one Excel template that calculates the values of interest. These files are saved separately for each experiment. However, the interesting trends can only be seen by combining the data obtained in several measurements. Currently that data is spread over several Excel files. Combining it takes time and leaves room for mistakes. Twenty-six measurements have been performed during this thesis, so the amount of data is still relatively small. When more experiments are performed, care must be taken that valuable time and oversight are not lost.

# References


Albijanic, B., Amini, E., Wightman, E., Ozdemir, O., Nguyen, A. V., Bradshaw, D.J., 2011. A relationship between the bubble–particle attachment time and the mineralogy of a copper–sulphide ore. Miner. Eng. 24, 1335–1339. doi:10.1016/j.mineng.2011.06.005

Albijanic, B., Bradshaw, D.J., Nguyen, A. V., 2012. The relationships between the bubble–particle attachment time, collector dosage and the mineralogy of a copper sulfide ore. Miner. Eng. 36, 309–313. doi:10.1016/j.mineng.2012.06.007

Albijanic, B., Nimal Subasinghe, G.K., Bradshaw, D.J., Nguyen, A. V., 2015. Influence of liberation on bubble–particle attachment time in flotation. Miner. Eng. 74, 156–162. doi:10.1016/j.mineng.2014.08.004

Albijanic, B., Ozdemir, O., Nguyen, A. V., Bradshaw, D., 2010. A review of induction and attachment times of wetting thin films between air bubbles and particles and its relevance in the separation of particles by flotation. Adv. Colloid Interface Sci. 159, 1–21. doi:10.1016/j.cis.2010.04.003

Anfruns, J.F., Kitchener, J.A., 1977. Rate of capture of small particles in flotation, Transactions of the Institution of Mining and Metallurgy. Trans. Inst. Min. Met. Sect. C 86, 9–15.

Aspiala, M., Schreithofer, N., Serna, R., 2017. A NEW PARTICLE-BUBBLE ATTACHMENT TIMER AS QUICK DIAGNOSTIC TOOL FOR MINERAL FLOATABILITY TESTING, to be submitted for publication to Miner. Eng.

Ball, B., Fuerstenau, D.W., 1971. Thermodynamics and adsorption behaviour in the quartz/aqueous surfactant system. Discuss. Faraday Soc. 52, 361. doi:10.1039/df9715200361

Bıçak, Ö., Ekmekçi, Z., Can, M., Öztürk, Y., 2012. The effect of water chemistry on froth stability and surface chemistry of the flotation of a Cu–Zn sulfide ore. Int. J. Miner. Process. 102–103, 32–37. doi:10.1016/j.minpro.2011.09.005

Butt, H.-J., 1994. A Technique for Measuring the Force between a Colloidal Particle in Water and a Bubble. J. Colloid Interface Sci. 166, 109–117. doi:10.1006/jcis.1994.1277

Chau, T.T., Bruckard, W.J., Koh, P.T.L., Nguyen, A.V., 2009. A review of factors that affect contact angle and implications for flotation practice. Adv. Colloid Interface Sci. 150, 106–115. doi:10.1016/j.cis.2009.07.003

Clift, R., Grace, J.R., Weber, M.E., 1978. Bubbles, Drops, and Particles. Academic Press, New York/London.

Crawford, R., Ralston, J., 1988. The influence of particle size and contact angle in mineral flotation. Int. J. Miner. Process. 23, 1–24. doi:10.1016/0301-7516(88)90002-6

Dai, Z., Dukhin, S., Fornasiero, D., Ralston, J., 1998. The Inertial Hydrodynamic Interaction of Particles and Rising Bubbles with Mobile Surfaces. J. Colloid Interface Sci. 197, 275–292. doi:10.1006/jcis.1997.5280

Dai, Z., Fornasiero, D., Ralston, J., 1999. Particle–Bubble Attachment in Mineral Flotation. J. Colloid Interface Sci. 217, 70–76. doi:10.1006/jcis.1999.6319

Derjaguin, B., Kusakov, M., 1937. Experimental investigation of solvation of surfaces and its application to the development of a mathematical theory of the stability of lyophile colloids

(Anomalous properties of thin liquid films, V). Izv. Akad. Nauk SSSR (Ser. Khim.) 5, 1119–1152 (in Russian).

Derjaguin, B.V., Dukhin, S.S., 1960. Theory of flotation of small and medium-size particles. Trans. Inst. Min. Met. 70, 221. doi:10.1016/0079-6816(93)90034-S

Dippenaar, A., 1982. The destabilization of froth by solids. I. The mechanism of film rupture. Int. J. Miner. Process. 9, 1–14. doi:10.1016/0301-7516(82)90002-3

Dobby, G.S., Finch, J.A., 1987. Particle size dependence in flotation derived from a fundamental model of the capture process. Int. J. Miner. Process. 21, 241–260. doi:10.1016/0301-7516(87)90057-3

Dobby, G.S., Finch, J.A., 1986. A model of particle sliding time for flotation size bubbles. J. Colloid Interface Sci. 109, 493–498. doi:10.1016/0021-9797(86)90327-9

Drzymala, J., 2007. Part III Separation Processes, in: Mineral Processing, Foundations of Theory and Practice of Minerallurgy. Oficyna Wydawnicza PWr., Wroclaw, pp. 121–492.

Ducker, W.A., Xu, Z., Israelachvili, J.N., 1994. Measurements of hydrophobic and DLVO forces in bubble–surface interactions in aqueous solutions. Langmuir 10, 3279–3289.

Eigeles, Volova, 1960. Kinetic investigation of effect of contact time, temperature and surface condition on the adhesion of bubbles to mineral surfaces. Proceedings, 5th Int. Miner. Process. Congr. Inst. Min. Metall. London 271–284.

Evans, L.F., 1954. Bubble-mineral attachment in flotation. Ind. Eng. Chem. 46, 2420–2424.

Finch, J.A., Dobby, G.S., 1990. Column flotation. Pergamon Press, Sydney.

Finch, J.A., Smith, G.W., 1972. Dynamic surface tension of alkaline dodecylamine acetate solution in oxide flotation. Trans. Inst. Min. Met. 81, C213–C281.

Fisher, L.R., Hewitt, D., Mitchell, E.E., Ralston, J., Wolfe, J., 1992. The drainage of an aqueous film between a solid plane and an air bubble. Adv. Colloid Interface Sci. 39, 397–416. doi:10.1016/0001-8686(92)80067-8

Frumkin, A., 1933. Physico-chemical fundamentals of flotation. Usp. Khim. 2, (in Russian).

Fuerstenau, M.C., Jameson, G.J., Yoon, R.-H., EBSCOhost., 2007. Froth flotation : a century of innovation. Society for Mining, Metallurgy, and Exploration.

Glembotsky, V.A., 1953. The time of attachment of bubbles to solid particles in flotation and its measurement. Lzv. Akad. Nauk SSSR, Otd. Tckhn. Nauk. 11, 1524–1531.

Gu, G., Sanders, R.S., Nandakumar, K., Xu, Z., Masliyah, J.H., 2004a. A novel experimental technique to study single bubble–bitumen attachment in flotation. Int. J. Miner. Process. 74, 15–29. doi:10.1016/j.minpro.2003.08.002

Gu, G., Sanders, R.S., Nandakumar, K., Xu, Z., Masliyah, J.H., 2004b. Hydrogen and Oxygen Bubble Attachment to a Bitumen Drop. Can. J. Chem. Eng. 82, 846–849. doi:10.1002/cjce.5450820426

Gu, G., Xu, Z., Nandakumar, K., Masliyah, J., 2003. Effects of physical environment on induction time of air–bitumen attachment. Int. J. Miner. Process. 69, 235–250. doi:10.1016/S0301-7516(02)00128-X

Hewitt, D., Fornasiero, D., Ralston, J., 1995. Bubble–particle attachment. J. Chem. Soc., Faraday Trans. 91, 1997–2001. doi:10.1039/FT9959101997

Hubbard, A.T., 2002. Encyclopedia of surface and colloid science. Marcel Dekker.

Ives, K.J., 2001. – Coagulation and flocculation: Part II—Orthokinetic flocculation, in: Solid-Liquid Separation. pp. 130–165. doi:10.1016/B978-075064568-3/50029-8

Iwasaki, I., Cooke, S.R.B., Colombo, A.F., 1960. Flotation characteristics of goethite.

Javor, Z., Aspiala, M., Schreithofer, N., Heiskanen, K., Serna, R., 2016. The development of a new attachment timer for predicting the change in ore floatability., in: Poster Session Presented at: XXVIII International Mineral Processing Congress, Quebec City, Canada.

Jiang, L., Krasowska, M., Fornasiero, D., Koh, P., Ralston, J., 2010. Electrostatic attraction between a hydrophilic solid and a bubble. Phys. Chem. Chem. Phys. 12, 14527. doi:10.1039/c0cp01367f

Jowett, A., 1980. Formation and disruption of particle-bubble aggregates in flotation, in: Fine Particle Processing, Proceedings of the International Symposium, Las Vegas, Nevada Vol. 1. pp. 720–754.

Kawatra, S.K., 2011. Fundamental principles of froth flotation, in: Darling, P. (Ed.), SME Mining Engineering Handbook. Littleton, CO, SME, pp. 1517–1531.

Koh, P.T.L., Hao, F.P., Smith, L.K., Chau, T.T., Bruckard, W.J., 2009. The effect of particle shape and hydrophobicity in flotation. Int. J. Miner. Process. 93, 128–134. doi:10.1016/j.minpro.2009.07.007

Krasowska, M., Carnie, S.L., Fornasiero, D., Ralston, J., 2011. Ultrathin Wetting Films on Hydrophilic Titania Surfaces: Equilibrium and Dynamic Behavior. J. Phys. Chem. C 115, 11065–11076. doi:10.1021/jp200387w

Krasowska, M., Malysa, K., 2007a. Wetting films in attachment of the colliding bubble. Adv. Colloid Interface Sci. 134, 138–150. doi:10.1016/j.cis.2007.04.010

Krasowska, M., Malysa, K., 2007b. Kinetics of bubble collision and attachment to hydrophobic solids: I. Effect of surface roughness. Int. J. Miner. Process. 81, 205–216. doi:10.1016/j.minpro.2006.05.003

Lai, R.W.M., Smith, R.W., 1966. On the relationship between contact angle and flotation behavior. Trans. Am. Inst. Min. Eng. 235, 413.

Laskowski, J.S., Miller, J.D., 1984. New reagents in coal flotation, in: M.J. Jones and R. Oblatt (Editors), Reagents in the Minerals Industry, Inst. Min. Metall. pp. 145–154.

Lazarov, D., Alexandrova, L., Nishkov, I., 1994. Effect of temperature on the kinetics of froth flotation. Miner. Eng. 7, 503–509. doi:10.1016/0892-6875(94)90163-5

Levay, G., Smart, R., Skinner, W., 2001. The impact of water quality on flotation performance. … South African Inst. … 1, 69–76.

Li, D., Fitzpatrick, J.A., Slattery, J.C., 1987. Industrial & engineering chemistry research., Industrial & engineering chemistry research. American Chemical Society.

Manor, O., Vakarelski, I.U., Stevens, G.W., Grieser, F., Dagastine, R.R., Chan, D.Y.C., 2008. Dynamic Forces between Bubbles and Surfaces and Hydrodynamic Boundary Conditions. Langmuir 24, 11533–11543. doi:10.1021/la802206q

Miklavcic, S.J., Horn, R.G., Bachmann, D.J., 1995. Colloidal interaction between a rigid solid and a fluid drop. J. Phys. Chem. 99, 16357–16364.

Miller, J.D., Laskowski, J.S., Chang, S.S., 1983. Dextrin adsorption by oxidized coal. Colloids and Surfaces 8, 137–151. doi:10.1016/0166-6622(83)80081-X

Miller, J.D., Lin, C.L., Chang, S.S., 1984. Coadsorption Phenomena in the Separation of Pyrite from Coal by Reserve Flotation. Coal Prep. 1, 21–38. doi:10.1080/07349348408945537

Newcombe, G., Ralston, J., 1994. Bubble spreading kinetics and mineral flotation. Miner. Eng. 7, 889–903. doi:10.1016/0892-6875(94)90131-7

Nguyen, A.V., Nalaskowski, J., Miller, J.D., 2003. A study of bubble–particle interaction using atomic force microscopy. Miner. Eng. 16, 1173–1181. doi:10.1016/j.mineng.2003.07.013

Nguyen, A.V., Schulze, H.J., Ralston, J., 1997. Elementary steps in particle—bubble attachment. Int. J. Miner. Process. 51, 183–195. doi:10.1016/S0301-7516(97)00030-6

Nguyen, A. V., 1999. Hydrodynamics of liquid flows around air bubbles in flotation: a review. Int. J. Miner. Process. 56, 165–205. doi:10.1016/S0301-7516(98)00047-7

Nguyen, A. V., Schulze, H.J., 2004. Colloidal science of flotation. Marcel Dekker.

Nguyen, A. V, Ralston, J., Schulze, H.J., 1998. On modelling of bubble–particle attachment probability in flotation. Int. J. Miner. Process. 53, 225–249. doi:10.1016/S0301-7516(97)00073-2

Nguyen Van, A., 1993. On the sliding time in flotation. Int. J. Miner. Process. 37, 1–25. doi:10.1016/0301-7516(93)90002-R

Oliver, J.., Mason, S.., 1977. Microspreading studies on rough surfaces by scanning electron microscopy. J. Colloid Interface Sci. 60, 480–487. doi:10.1016/0021-9797(77)90312-5

Ozdemir, O., Taran, E., Hampton, M.A., Karakashev, S.I., Nguyen, A.V., 2009. Surface chemistry aspects of coal flotation in bore water. Int. J. Miner. Process. 92, 177–183. doi:10.1016/j.minpro.2009.04.001

Pease, J.D., Curry, D.C., Young, M.F., 2006. Designing flotation circuits for high fines recovery. Miner. Eng. 19, 831–840. doi:10.1016/j.mineng.2005.09.056

Radoev, B.P., Alexandrova, L.B., Tchaljovska, S.D., 1990. On the kinetics of froth flotation. Int. J. Miner. Process. 28, 127–138. doi:10.1016/0301-7516(90)90031-S

Ralston, J., Dukhin, S.S., Mishchuk, N.A., 1999a. Inertial hydrodynamic particle–bubble interaction in flotation. Int. J. Miner. Process. 56, 207–256. doi:10.1016/S0301-7516(98)00049-0

Ralston, J., Fornasiero, D., Hayes, R., 1999b. Bubble–particle attachment and detachment in flotation. Int. J. Miner. Process. 56, 133–164. doi:10.1016/S0301-7516(98)00046-5

Rao, S.R., Leja, J., 2004. Surface chemistry of froth flotation. Volume 1, Fundamentals.

Rasemann, W., 1988. On the attachment probability of bubble/particle contacts in solid/liquid suspensions. Int. J. Miner. Process. 24, 247–267. doi:10.1016/0301-7516(88)90044-0

Rubinstein, J.B., 1995. Column flotation : process, designs and practices. Gordon and Breach.

Scheludko, A., Toshev, B. V., Bojadjiev, D.T., 1976. Attachment of particles to a liquid surface (capillary theory of flotation). J. Chem. Soc. Faraday Trans. 1 Phys. Chem. Condens. Phases 72, 2815. doi:10.1039/f19767202815

Scheludko, A., Tschaljowska, S., Fabrikant, A., 1970. Contact between a gas bubble and a solid surface and froth flotation. Spec. Discuss. Faraday Soc. 1, 112. doi:10.1039/sd9700100112

Schulze, H.J., 1992. Probability of particle attachment on gas bubbles by sliding. Adv. Colloid Interface Sci. 40, 283–305. doi:10.1016/0001-8686(92)80079-D

Schulze, H.J., 1984. Physico-chemical elementary processes in flotation : an analysis from the point of view of colloid science including process engineering considerations. Elsevier.

Schulze, H.J., Radoev, B., Geidel, T., Stechemesser, H., Töpfer, E., 1989. Investigations of the collision process between particles and gas bubbles in flotation — A theoretical analysis. Int. J. Miner. Process. 27, 263–278. doi:10.1016/0301-7516(89)90068-9

Smith, R.W., 1963. Coadsorption of dodecylamine ion and molecule on quartz. Trans. Am. Inst. Min. Eng 226, 427.

Snyder, B.A., Aston, D.E., Berg, J.C., 1997. Particle−Drop Interactions Examined with an Atomic Force Microscope. doi:10.1021/LA960903Z

Somasundaran, P., Zhang, L., Fuerstenau, D.., 2000. The effect of environment, oxidation and dissolved metal species on the chemistry of coal flotation. Int. J. Miner. Process. 58, 85–97. doi:10.1016/S0301-7516(99)00022-8

Stechemesser, H., Nguyen, A. V., 1999. Time of gas–solid–liquid three-phase contact expansion in flotation. Int. J. Miner. Process. 56, 117–132. doi:10.1016/S0301-7516(98)00045-3

Su, L., Xu, Z., Masliyah, J., 2006. Role of oily bubbles in enhancing bitumen flotation. Miner. Eng. 19, 641–650. doi:10.1016/j.mineng.2005.09.016

Sutherland, K.L., 1948. Physical Chemistry of Flotation. XI. Kinetics of the Flotation Process. J. Phys. Colloid Chem. 52, 394–425. doi:10.1021/j150458a013

Sven-Nilsson, I., 1934. Einfluß der Berührungszeit zwischen Mineral und Luftblase bei der Flotation. Kolloid-Zeitschrift 69, 230–232. doi:10.1007/BF01433238

Verrelli, D.I., Albijanic, B., 2015. A comparison of methods for measuring the induction time for bubble–particle attachment. Miner. Eng. 80, 8–13. doi:10.1016/j.mineng.2015.06.011

Verrelli, D.I., Bruckard, W.J., Koh, P.T.L., Schwarz, M.P., Follink, B., 2014. Particle shape effects in flotation. Part 1: Microscale experimental observations. Miner. Eng. 58, 80–89. doi:10.1016/j.mineng.2014.01.004

Verrelli, D.I., Koh, P.T.L., Nguyen, A. V., 2011. Particle–bubble interaction and attachment in flotation. Chem. Eng. Sci. 66, 5910–5921. doi:10.1016/j.ces.2011.08.016

Vizcarra, T.G., Harmer, S.L., Wightman, E.M., Johnson, N.W., Manlapig, E.V., 2011. The influence of particle shape properties and associated surface chemistry on the flotation kinetics of chalcopyrite. Miner. Eng. 24, 807–816. doi:10.1016/j.mineng.2011.02.019

Wang, L., Sharp, D., Masliyah, J., Xu, Z., 2013. Measurement of Interactions between Solid Particles, Liquid Droplets, and/or Gas Bubbles in a Liquid using an Integrated Thin Film Drainage Apparatus. Langmuir 29, 3594–3603. doi:10.1021/la304490e

Wang, W., Zhou, Z., Nandakumar, K., Masliyah, J.H., Xu, Z., 2005. An induction time model for the attachment of an air bubble to a hydrophobic sphere in aqueous solutions. Int. J. Miner. Process. 75, 69–82. doi:10.1016/j.minpro.2004.04.009

Wills, B.A., Finch, J.A., 2016. Wills' Mineral Processing Technology: An introduction to the Practical Aspects of Ore Treatment and Mineral Recovery, Eighth. ed. Butterworth-Heinemann, Oxford.

Ye, Y., Khandrika, S.M., Miller, J.D., 1989. Induction-time measurements at a particle bed. Int. J.

Miner. Process. 25, 221–240. doi:10.1016/0301-7516(89)90019-7

Ye, Y., Miller, J.D., 1989. The significance of bubble/particle contact time during collision in the analysis of flotation phenomena. Int. J. Miner. Process. 25, 199–219. doi:10.1016/0301-7516(89)90018-5

Ye, Y., Miller, J.D., 1988. Bubble/Particle Contact Time in the Analysis of Coal Flotation. Coal Prep. 5, 147–166. doi:10.1080/07349348808945563

Yoon, R.-H., 2000. The role of hydrodynamic and surface forces in bubble–particle interaction. Int. J. Miner. Process. 58, 129–143. doi:10.1016/S0301-7516(99)00071-X

Yoon, R.-H., 1991. Hydrodynamic and surface forces in bubble–particle interactions, in: Proc. 17th Int. Mineral Processing Congr. (Dresden, Germany), Vol. II. Fine Particle Processing (Flotation). pp. 17–31.

Yoon, R.-H., Mao, L., 1996. Application of Extended DLVO Theory, IV. J. Colloid Interface Sci. 181, 613–626. doi:10.1006/jcis.1996.0419

Yoon, R.-H., Yordan, J.L., 1991. Induction time measurements for the quartz—amine flotation system. J. Colloid Interface Sci. 141, 374–383. doi:10.1016/0021-9797(91)90333-4

Yoon, R.H., Luttrell, G.H., 1989. The Effect of Bubble Size on Fine Particle Flotation. Miner. Process. Extr. Metall. Rev. 5, 101–122. doi:10.1080/08827508908952646

Young, T., 1805. An Essay on the Cohesion of Fluids. Philos. Trans. R. Soc. London 95, 65–87.

Zawala, J., Drzymala, J., Malysa, K., 2008. An investigation into the mechanism of the three-phase contact formation at fluorite surface by colliding bubble. Int. J. Miner. Process. 88, 72–79. doi:10.1016/j.minpro.2008.06.006